CFD Analysis of Pressure and Flow Characteristics of the Human Nose

BJS - NC08

A Major Qualifying Project Report:

Submitted to the faculty

of the

WORCESTER POLYTECHNIC INSTITUTE

In partial fulfillment of the requirements for the

Degree of Bachelor of Science

by

Kalen Smith

March 17th

_____

Prof. Brian James Savilonis, Advisor

Table of Contents

Acknowledgements

I would like to extend my appreciation to the following individuals without whom this project would not have been possible.

Professor Brian James Savilonis – Professor at Worcester Polytechnic Institute

Dr. David B. Wexler, M.D. – Otolaryngologist at Fallon Clinic

Abstract

CFD analysis is an alternative method to the construction of an experimental model for modeling airflow through human nasal cavities. In this study, a mesh was created from an MRI, and imported into Fluent for analysis. Simulations were run with various steady and unsteady models, which were then compared with each other. Steady state models were also run with both laminar and k-epsilon turbulence models. For this patient and these particular flow patterns and geometry, the flow was determined to be quasi-steady since the steady and unsteady models correlated well with each other. Also, it was found that the choice of which viscous model to use (in this case, k-epsilon vs. laminar) was found not to play a significant role in the outputs. Finally, the results of this study were somewhat different from the results determined experimentally.

Table of Graphs

Chapter 1: Introduction:

Developing an understanding of the pressure and flow behavior that take place during normal breathing conditions has been a subject of much discussion and research. Traditionally, this has been accomplished by building a model based on the nose of a human cadaver or CAT scan or MRI images of a human nose, and making a fluid pass through the model in a manner such that it resembles the flow conditions exhibited during the normal breathing cycle. Measurements are made, and the empirical data are analyzed to estimate the flow characteristics. Performing such an experiment is believed to yield fairly accurate results, provided that the experiment is properly constructed. However, due to the complexity of such an experiment, there are a number of things that could go wrong, and therefore the results may not accurately reflect the actual breathing conditions that the researchers are trying to emulate.

An alternative to constructing a physical experiment is to perform a Computational Fluid Dynamics (CFD) analysis. This involves taking a meshed geometry, and using a CFD software package to create a simulation resembling the real world flow. There are several differences between using CFD Analysis and a physical experiment to analyze any type of flow. First of all, the CFD approach relies on computer tomography (CT) scans, which can yield consistent results whenever a simulation is run. However, no matter how advanced the CFD package is, the CFD approach is limited in that it cannot take into account all the physical variables that play a role in a real world simulation. The CFD results tend to give results that suggest how the flow is expected to behave, rather than how it actually does behave in a real world simulation. As a result, there is often a discrepancy between the results found in a physical experiment and those found during a CFD analysis. Therefore, in order to determine the validity of CFD

analysis, it is often necessary to compare the results from CFD simulations with those found experimentally.

However, CFD analysis has many benefits. It is much cheaper and faster to create a CFD simulation than to complete an experiment. Therefore, it is possible to run many more CFD models in the cost and time frame of a project than would be possible by running a physical experiment. Because of the time and cost savings, using the CFD approach allows the possibility to analyze problems or research questions which require substantial amounts of data. CFD results can also be easier to analyze than experimental data. With CFD, it is possible to observe detailed physical behavior taking place at any location within the flow, which makes it easy to determine the effects of geometry on flow behavior. CFD can also analyze physical properties which would be difficult to analyze experimentally, such as turbulence, shear stress and the flow patterns of streamlines.

Chapter 2: Background

In a study by Croce [2], the experimenters sought to determine pressure-flow relationships for airflow through a subject's nasal passages. This was done by creating an in vitro experiment as well as a numerical (CFD) analysis, and the results from each of these approaches were compared with those of the other and the literature from previous experiments. The most important purpose of this study was to determine the validity of using CFD software to monitor or analyze nasal airflow.

The first step in conducting the experiment was the creation of a plastinated model. After the model had been constructed, the next step for the researchers was to determine the types of gases that needed to be used and begin simulating the flow through the model. During the process of inspiration, a potentiometer was used to control flow rates, and a pneumotograph was used to measure pressure. Expiration was studied by connecting the compressed air tap to a valve.

The numerical study was conducted by taking 3-D scanned images of the plasticized model. During a process known as segmentation, the experimenters could isolate the various parts of the model that they were interested in. This involved tracking every individual pixel and making sure that each pixel could be identified with the location it refers to in the actual geometry. After this, the mesh was created with about 100,000 triangular faces and 830,000 tetrahedral cells. This mesh was tested, but it was found that due to large pressure gradients in the flow fields, a finer mesh of 1,350,000 tetrahedral cells was needed.

After the mesh was created, the experimenters were ready to begin the simulation. It was predicted that they would have flow that was steady, incompressible and laminar. The FLUENT software

package was used for this purpose. Because of the way that the mesh was segmented, a segregation solver was applied. A pressure difference was applied and standard no-slip conditions were assumed at the boundaries. Boundary conditions were established at the front of the nose and outlet of the model. Finally, the simulation was ready to begin and data collected which is shown in Figure 1.

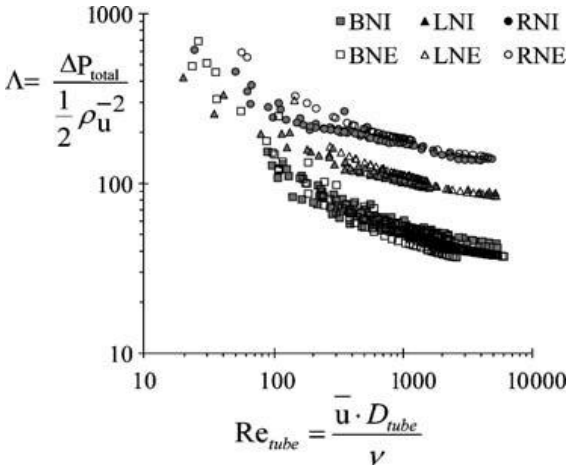

Figure 1: Pressure drops vs. Reynolds Number for both nostrils.[1]

After data was collected from both the experimental and numerical models, the data from the two models were compared with each other. The data from the experiments and numerical models were very similar, except when analyzing very high flows. Even at these high flow rates, the data between the two experiments did not differ by more than 17%. The fact that the data of the two models corresponded well together seemed to justify that a numerical model could yield results in sync with those of similarly constructed experimental models.

When analyzing the data relating to the pressure changes, it was observed that the right nostril displayed more negative pressure than the left nostril, which can be a result of the fact that there was a larger flow rate on the left side of the nose. This can be shown by the contours in Figure 2.

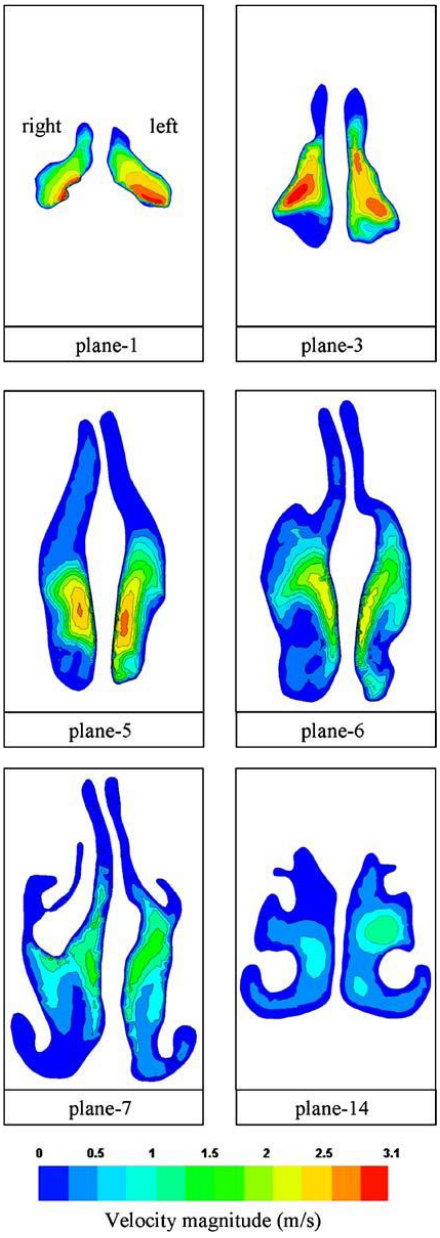

Figure 2: Contour plots of Croce study[1]

The reason for the discrepancy between the experimental and numerical models at high flow rates may be due to the higher turbulence level while the numerical model was based on laminar flow calculations. This study suggests that flow becomes turbulent when a flow rate of 250 ml/s is exceeded. This transition value is slightly smaller than the one the experimenters were comparing to in the literature. One possible explanation to this difference lies in the fact that in the computerized model the researchers were able to look at "cuts" spaced 0.5 mm away from each other, while those of the physical models were spaced 2 to 4 mm apart. The velocities that were obtained in this research were similar to those of the experiment conducted by other researchers. The maximum velocity of this experiment was about 3.1 m/s, and those of several other researchers were approximately 4 m/s, but this is to be expected since the areas they were calculating over were slightly larger (quantitative values for these areas are not described in the article).

Until the development of CFD analysis, it was very difficult to analyze the effects of sniffing on nasal airflow. In a study by Zhao [3], a CFD approach was taken to determine the effects of sniffing on both airflow and odorant transport in nasal passages of both human and rat noses, however in critiquing this article, emphasis was placed on the analysis of nasal airflow. A 3D nasal model was constructed from a CT scan which included both nostrils and the nasopharynx. Inspiratory steady-state airflows were simulated with both laminar and turbulent models. In this study, one of the main objectives was to estimate the amount of turbulence in the airflow. The turbulence was approximated by computing the turbulence intensity.

A three dimensional mesh was created from an axial 3D CT scan from both sides of a woman's nose. Inspiratory flows were modeled with Fluent. The flows were all modeled as steady state, but different models were used to describe turbulence. In addition to a model that assumed laminar flow, the turbulence models that were used were the k–ω, the k–ε, and the Spalart–Allmaras models.

After the simulation was run, velocity contours were compared among the various turbulence models, and the differences between the models were found to be rather subtle. After comparing velocity contours, the researchers analyzed the pathlines. The pathlines were found to be tangent to velocity vectors. The pathlines for the various models were less uniform among the various models than those of the velocity contours, but the patterns were overall fairly consistent between the different turbulence models. Next, contours were developed to represent the turbulence intensity in the regions of interest. The actual turbulence intensity values were larger for the CFD values than those found experimentally, however, the areas where high and low turbulence occurred corresponded well with those found experimentally. The conclusion that can be drawn from this evidence is that for this particular model, the choice of which turbulence model to use was not a crucial factor. However, there is no discussion about the use of laminar models, so this study cannot conclude whether or not a laminar model would yield appropriate results.

A study conducted by Ishikawa Arch Otolaryngol Head Neck Surg, was similar to those conducted by other research groups that used CFD software to model airflow through the human nose [4]. However, there are two important features of this study that differentiate it from most others. First of all, this simulation used a model for unsteady flow. Secondly, this study analyzed vorticity as well as velocity, while other studies only took velocity into consideration. Also, the flow patterns were compared between inspiration and expiration. The researchers claim that to the best of their knowledge, they are(or were) the first group to study this flow behavior.

The first step the researchers took was to create a three-dimensional model of the subject's nasal geometry. This was accomplished by taking DICOM data from a computed tomographic image. This data was retrieved through a software program known as INTAGE. After this three-dimensional

image was extracted, the geometry was meshed with GAMBIT. After a meshed geometry was completed, the researchers were ready to import the meshed file into FLUENT.

The numerical simulation required the use of Navier-Stokes and continuity equations. Because of the complexities involved in solving this type of problem, the researchers found it necessary to simplify the problem. These assumptions were that the fluid was Newtonian, incompressible, and holds uniform properties throughout the substance. The unsteady-state condition was defined so that both stages of inspiration and expiration could be modeled. Additional assumptions that the researchers made were that the tidal volume was 500 ml, and that 12 breaths were taken per minute (i.e. each breath lasting 5 seconds, approximately 2.5 seconds for inspiration, 2.5 seconds for expiration, and has a very brief resting period between). This pattern could be represented by a sinuisoidal function as shown in Figure 3.

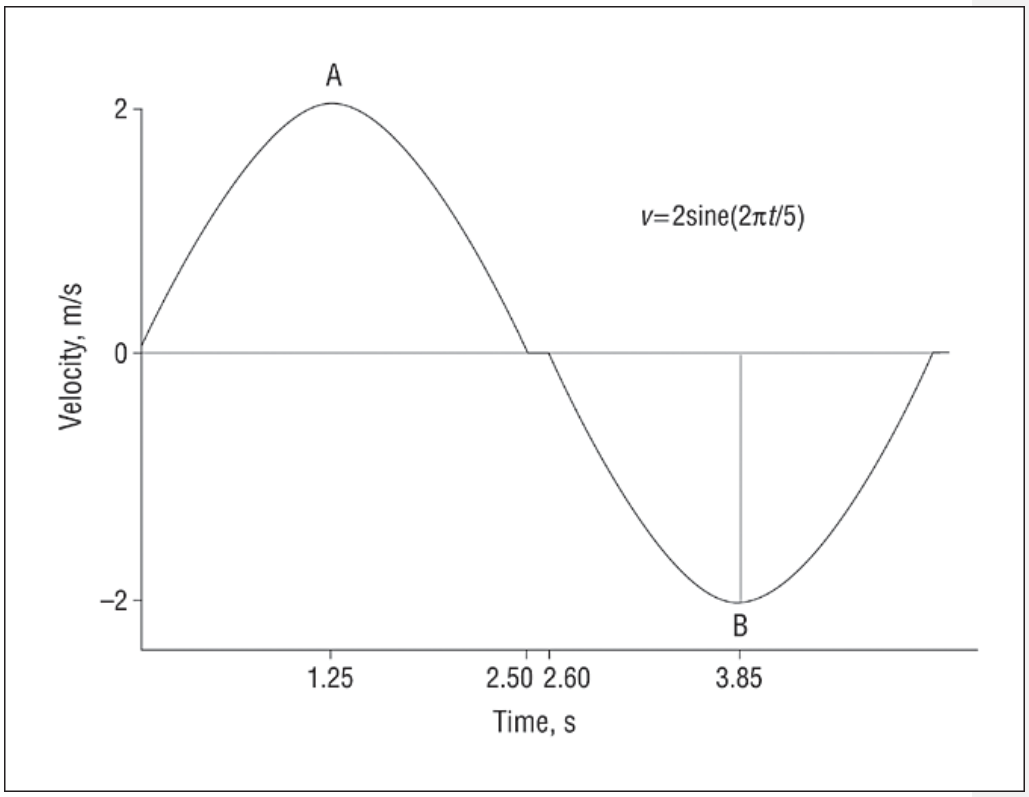

Figure 3: Plot over entire breathing cycle[4]

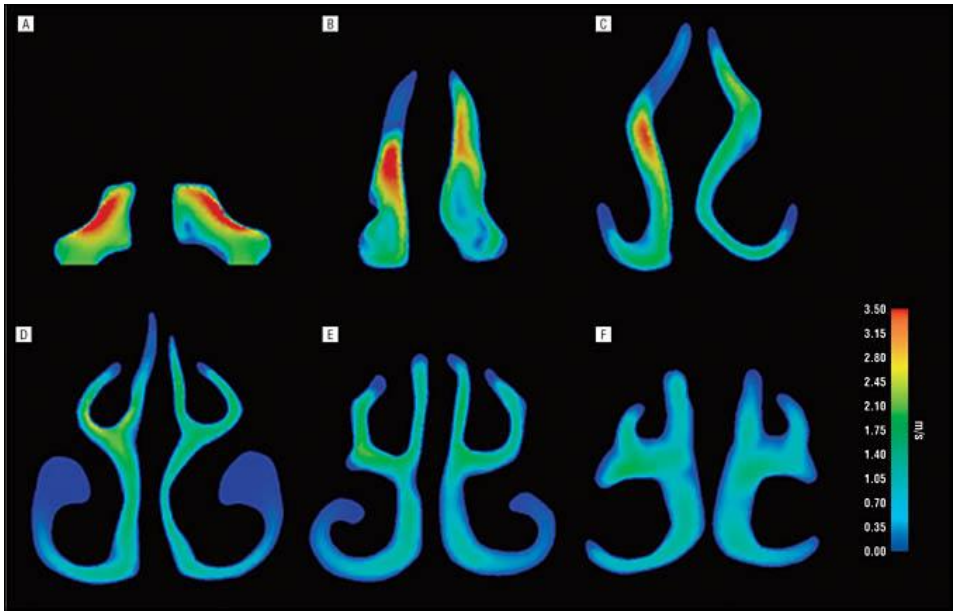

Figure 4: Results seen at mid-inspiration state,
time = 1.25 seconds. The researchers state (as can also be seen by these contours) that the maximum velocities steadily decrease away from the front of the nose.[4]

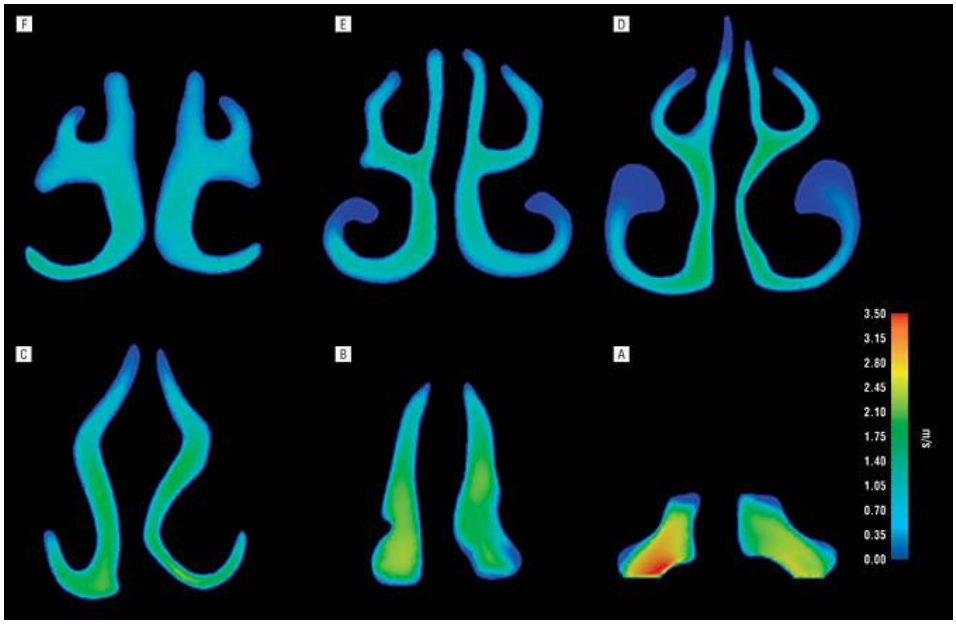

Figure 5: Results seen at mid-inspiration state, time = 3.85 seconds. The researchers state (as can also be seen by these contours) that the maximum velocities steadily decrease away from the front of the nose.[4]

After this data was entered into FLUENT, the researchers analyzed the results at the two peak points. From the graph above, it is clear that these peak points occur at 1.25 and 3.85 seconds. The above contours describe velocity magnitude at mid-inspiration state, time = 1.25 seconds in Figure 4 and time = 3.85 seconds in Figure 5. The researchers state (as can also be seen by these contours) that the maximum velocities steadily decrease away from the front of the nose.

T.K. et al, conducted a similar study to many previous experiments [5]. However, while other studies sought primarily to find general conclusions about the velocity magnitudes and pressure differences at different locations within the nasal cavity, the main objective of this

particular study was to develop a more detailed understanding of velocity profiles within the nose. Despite having a more narrowly defined objective, the experimenters faced the same challenges as other experimenters performing similar experiments. These challenges include:

- Developing a geometry that closely resembles that of the subject's nasal cavities
- Making appropriate assumptions to simplify the problem
- Understanding the limitations of the model, whatever form that model may take
- Deciding on the level of detail that would got into the experiment (the inclusion of nasal hairs, mucous membranes, etc)

After a model was constructed, the experimenters used Particle Image Velocimetry to obtain the two dimensional velocity vector fields that existed throughout the model.

After this experiment was conducted, the velocity fields were compared at different locations within the nasal geometry. Several important conclusions were drawn from the data. First of all, velocity vectors were plotted on four different planes, which were spaced a millimeter away from each other. These vector plots show that the velocity fields become more strongly pronounced further away from the septum. When the velocity fields are studied close to the inferior turbinate, the flow beneath the inferior turbinate is shown to have a much higher velocity because it yields a much smaller area than that above the inferior turbinate. The meatuses (spongy tissue near the turbinate region) have almost no flow passing through them. Also, it is possible to recognize the formation of an eddy when studying the velocity fields far enough away from the septum. This eddy can be explained by the presence of an adverse pressure gradient caused by the sudden increase in cross-sectional area from the nasal valve to the main nasal passage. The researchers site another experiment conducted by another group which found two

smaller eddies, and suggest that the discrepancy in these results is probably due to differences in the anatomical details of the two models.

The goal of Horschler was to analyze how changes in nasal geometry may affect airflow [6]. One observation that seems clear from other literature is that the CFD results from various studies conflict with one another, and the researchers conducting these studies often hypothesize that these discrepancies may be due to differences in the anatomy of various models. This study decided to address this issue, and determine whether this is a valid theory.

Like other studies, this experiment was constructed by developing a three dimensional model of a nose based on an actual model (this particular study used a CT scan of a subject's nose). However, this study also relied upon a technique known as Digital Particle Image-Velocimetry to better observe velocity profiles. The use of this technique required the experimenters to have an unobstructed view of the fluid as it flowed through the model, therefore it was necessary to make sure the model was transparent. In addition to the model that was designed to closely resemble the anatomical detail of the CT scans, two other models were constructed. One of these models only included an upper turbinate, while the other only had a lower turbinate. By studying each of these models, the researchers felt they could better understand the effects that each turbinate had on the airflow, both individually and collectively.

Several important observations were made after this experiment was conducted. Before going into detail about results pertaining to the effects of the geometry within the nasal cavity, a couple general observations were made. First of all, after carefully studying the velocity profiles the researchers concluded that the flow could be considered laminar, since the velocity profiles

were clearly not fully developed. Secondly, it was clear that at all locations within the geometry the maximum velocity was of greater magnitude during expiration than inspiration.

In regards to the effects to the effects of geometrical features, the researchers predominantly studied velocity fields and pressure contours at various "cuts", which were taken in both the horizontal and vertical planes. The pressure contours show that in the model where only a lower turbinate is present, there is a smaller pressure gradient, which the researchers say indicates that the upper turbinate is responsible for most of the pressure gradient. However, neither of the turbinates has a significant impact on the pressure gradients or flow behavior. Sudden velocity changes and large pressure gradients exist at locations where there is a sudden expansion region, indicating that such an expansion region is of greater consequence than either of the turbinates.

T. Elad studied airflow through the human nose both by experiment and CFD analysis [7] Two anatomically correct, transparent resin models of human nasal cavities were cast and CAD models were developed based on computed tomography scans. One of these models represented a healthy human nose, while the other represented an abnormal one. Finally, velocity and pressure fields were computed for all models using CFD software. The main objective of this study was not to conduct new research regarding airflow, but rather to establish whether or not the results of CFD analysis match those of experimental data, which would indicate whether or not CFD analysis is reliable for this type of problem.

Unfortunately, recent research shows that numerical simulations for nasal airflow are limited in that it is impossible to include all of the thousands of variables and conditions that would play a part in real applications. Such variables may include varying pressure, density, viscosity, temperature difference, as well as obstructions from mucous, hair and small particles. A particularly important

limitation is that most CFD programs have difficulty modeling both laminar and turbulent flow at the same time.

In order to mitigate these limitations, there are some standards that Weihold and Mlynski[14] suggest need to be met. First, medical images should be used from various medical imaging devices, such as those used to create CAT scans, CT scans and MRI's. Secondly, the complex anatomical details of these nose and the three dimensional laminar, turbulent and transitional characteristics should be met. The simulation had to be able to take into account a large number of physical variations. The computations must be reliable and capable of performing complex, detailed analysis. Finally, the simulation must yield quality results and show visual models that are descriptive and detailed.

Two transparent resin models of nasal cavities were created with sufficient anatomical detail. These models were based on computer tomography scans (CT). Geometric models were developed with CAD models. Finally, these models were analyzed with computational fluid dynamic software. After the models were developed and the experiments were performed, their results were used to investigate the breathing patterns on two patients. A pressure drop-volume flow rate curve was developed for a patient with a normal nasal anatomy, and another was developed for the patient with a deviated septum. In addition to the numerical results, the two models were also qualitatively compared at various flow rates, and the qualitative and quantitative results showed good accordance.

There were several assumptions that needed to be made on the part of the experimenters, which could limit the accuracy of the results of the study. Namely, the flow was assumed to be steady-state, incompressible, and isothermal. Also, it was in the inspiration direction and had no gravitational effects. Also, there was no change in the nasal mucous membranes.

After the four models were created, rhinoresistometric curves were created using the CFD package, FloWorks. Each of these curves consisted of 8 to 17 points. Graphs were made which plotted

pressure drops relative to volumetric flow rate. Points were plotted on the graph for volumetric flow rate values of 50 ml/s, 100 ml/s, 150 ml/s, 200 ml/s, and then 100 ml/s intervals beyond that point. These plots included the results from both the experiment and the simulation. As can be seen from Figure 6, these results compared well with each other, so we can conclude that if the experiment was well constructed, the numerical simulation is also valid.

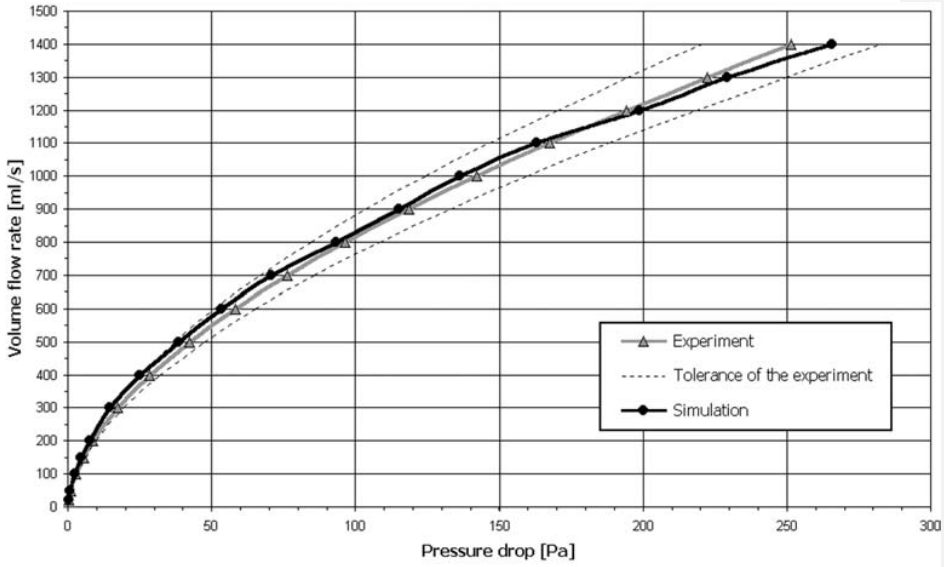

Figure 6: Experimental Results vs. Numerical Results [7]

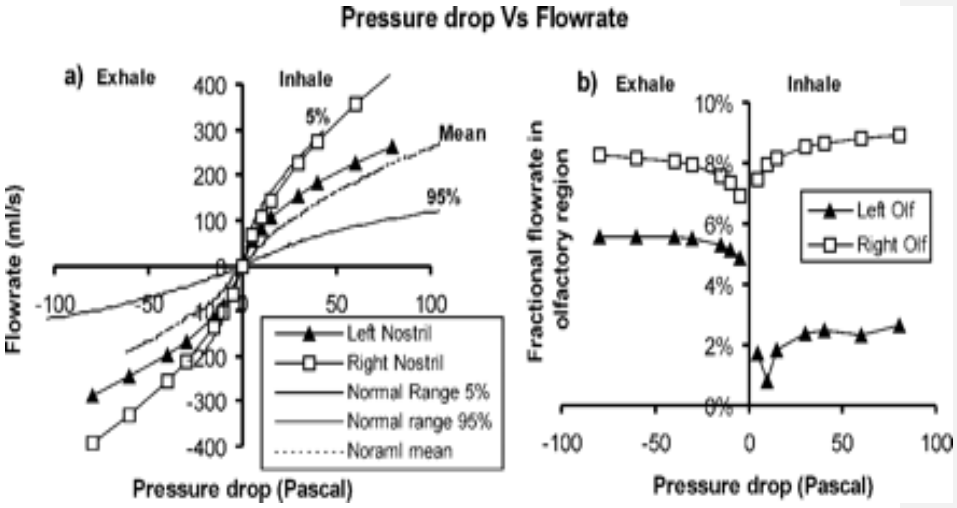

Figure 7: Pressure Drops seen over both nostrils for Zhao study[8]

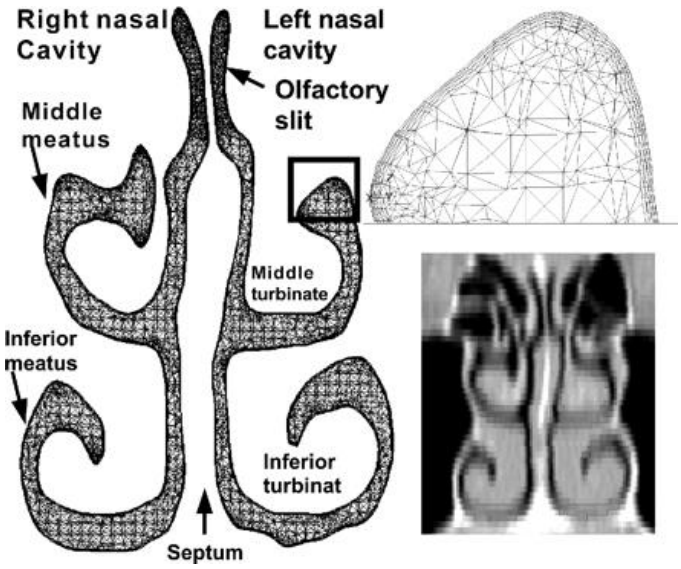

Figure 8: Nasal Anatomy seen near Turbinates[8]

In one of his other studies, Zhao focused on how changes in the anatomy affect the data from an experiment with nasal flow [8]. The researchers took a number of two dimensional images, and meshed them to get an approximation of a three dimensional geometry. Most of the findings in this article were consistent with the results from other articles (i.e. there is no flow through meatuses, and there should be vortex formation near turbinate regions). However, this article provided a pressure drop versus flow rate curve which shows how the pressure drops over the left and right nostril differ from each other. This article claims that for both inspiratory and expiratory flow there is a greater pressure drop over the left nostril for any given flow rate.

Turbulence Modeling

When dealing with turbulence, the variables are decomposed into both their mean and fluctuating components (i.e. mean velocity and fluctuating velocity components). After the Navier Stokes Equation has been simplified by assuming it to be incompressible, we substitute the total velocity (both fluctuating and mean components) into the simplified Navier-Stokes equation[5].

When performing turbulence modeling, one of the most important decisions that one can make is whether or not they believe the Boussinesq assumption to hold[8]. The Boussinesq assumption states that the apparent turbulent shearing stresses are related to the mean strain through the turbulent viscosity. The Boussinesq assumption states that the Reynolds stress tensor, τ_{ij} , is proportional to the mean strain rate tensor, S_{ij} , and can be written in the following way ():

$$\tau_{ij} = 2\,\mu_t\,S_{ij}$$

k here is represented by the turbulent kinetic energy, $K = 1/2u_i * u_i$. So, the turbulent kinetic energy depends on the fluctuating velocity components without regard to the mean velocity. This quantity is derived from the Navier-Stokes equations.

Since the Boussinesq assumption states that the turbulent shearing stresses are related to the turbulent viscosity, it is necessary to find a numerical means of modeling the turbulent viscosity [8]. This is done by solving an equation of a form similar to one below:

$\mu_T = \rho v_T l$

The biggest obstacle here is that we need to find a means of expressing the kinematic viscosity (v_T) and the characteristic length scale (l). The difference between the various turbulence models which operate under the Boussinesq assumption lies in how these two variables are found.

The simplest type of turbulence modeling method is known as the simple algebraic method. In such an equation, neither the characteristic length nor the turbulent kinematic viscosity is represented by a differential equation, but rather a simple algebraic equation. The dynamic viscosity is then solved by solving a single ordinary differential equation. One of the most classic models can be shown through the expression:

$\mu = \rho l^2 (du/dy)$ [8]

One of the most successful algebraic models is the Cebeci-Smith model, which is shown as:

$\mu = \alpha \rho u \xi$

The Cebeci-Smith model seems to yield good results because it takes into account effects from pressure variations, pressure gradients, blowing and surface roughness. This model has had good results for many high speed flows, and hence has been applied to many aerodynamic applications. However, its applications are limited to those in which there are low levels of curvature or rotation, as well as those in which there are large variations in properties due to flow separation [8].

Despite their simplicity, algebraic equations on the whole have yielded less than desirable results. The largest criticism of algebraic models is that they only take into account the local flow parameters, even though it is clear that the effects of pressure/velocity fields upstream may a significant impact on downstream turbulence. Also, while Cebeci-Smith models have shown good results in experiments dealing with high speed flows, algebraic equations as a whole seem to only offer good results for problems with low Reynolds numbers. Consequently, while algebraic equations may be the easiest to work with, they are not ideal. Also, from the equation for dynamic viscosity shown above, the viscosity is equal to zero whenever the velocity gradient is zero. Obviously, this does not correspond well with results in the real world [8].

Another class of equations is known as the one equation model [8]. In such a system, the turbulent kinematic viscosity is calculated from an equation of similar form to the format used with the algebraic method. However, the difference is that one of the variables in the equation is found by solving a partial differential equation. Most commonly, this variable is the turbulent kinetic energy (k). A common form is:

$\mu_T = C_k \rho l (k)^{1/2}$

Now, k is solved with a partial differential equation, typically taking the form of:

$$\frac{\partial k}{\partial t} + U_j \frac{\partial k}{\partial x_j} = \tau_{ij} \frac{\partial U_i}{\partial x_j} - C_D \frac{k^{\frac{3}{2}}}{l} + \frac{\partial}{\partial x_j} \left[\left(\nu + \frac{\nu_T}{\sigma_k} \right) \frac{\partial k}{\partial x_j} \right]$$

A common turbulence model which is not based on turbulent kinetic energy is known as the Spallart Allmaras model [8], which find the turbulent viscosity based on a parameter which is proportional to turbulent viscosity is shown by:

$v_T = v'f$

The Spalart Allmaras model has some distinct strengths. First of all, it is a good method for analyzing convergence of velocity, or other parameters. Secondly, it is exceptional for handling

the effects of pressure gradients. Also, experimental data suggests that it does a better job handling some flow separation problems than the algebraic models[8]. However, Spalart Allmaras modeling is still relatively new, so it is not known how suitable it is for many applications, for example high speed flows. One experiment is currently underway to determine the suitability for Spalart Allmaras modeling for MACH Numbers greater than 5[8]. In what experiments have been conducted, the Spalart-Allmaras method shows better results than the older one equation methods and the algebraic models. On the whole, however, the results of one equation models have proven disappointing.

Because algebraic and one equation models do not seem to yield fair results, researchers decided a new means of turbulent modeling needed to be developed. Consequently, two equation models were born. In contrast with the one equation models where the turbulent viscosity was derived from an equation where one variable varied with a partial differential equation and the length scale was evaluated with an algebraic expression, a two equation model has a second transport equation for the length scale[8].

The two most commonly used two equation models are the k-ε and the k-ω models. In the k-ε model, the two varying properties are the turbulent kinetic energy and the turbulent dissipation. The k-ω model uses the turbulent kinetic energy and the specific dissipation. The length scales for these models are, respectively:

$l = C_D k^{3/2}/\varepsilon$ [8] and $l = C_D k^{1/2}/\omega$ [8]

Standard k-ε model

For turbulent kinetic energy k

$$\frac{\partial}{\partial t}(\rho k) + \frac{\partial}{\partial x_i}(\rho k u_i) = \frac{\partial}{\partial x_j}\left[\left(\mu + \frac{\mu_t}{\sigma_k}\right)\frac{\partial k}{\partial x_j}\right] + P_k + P_b - \rho\epsilon - Y_M + S_k$$

For dissipation ϵ

$$\frac{\partial}{\partial t}(\rho\epsilon) + \frac{\partial}{\partial x_i}(\rho\epsilon u_i) = \frac{\partial}{\partial x_j}\left[\left(\mu + \frac{\mu_t}{\sigma_\epsilon}\right)\frac{\partial \epsilon}{\partial x_j}\right] + C_{1\epsilon}\frac{\epsilon}{k}\left(P_k + C_{3\epsilon}P_b\right) - C_{2\epsilon}\rho\frac{\epsilon^2}{k} + S_\epsilon$$

K-ω model

Turbulence Kinetic Energy

$$\frac{\partial k}{\partial t} + U_j\frac{\partial k}{\partial x_j} = \tau_{ij}\frac{\partial U_i}{\partial x_j} - \beta^* k\omega + \frac{\partial}{\partial x_j}\left[\left(\nu + \sigma^*\nu_T\right)\frac{\partial k}{\partial x_j}\right]$$

Specific Dissipation Rate

$$\frac{\partial \omega}{\partial t} + U_j\frac{\partial \omega}{\partial x_j} = \alpha\frac{\omega}{k}\tau_{ij}\frac{\partial U_i}{\partial x_j} - \beta\omega^2 + \frac{\partial}{\partial x_j}\left[\left(\nu + \sigma\nu_T\right)\frac{\partial \omega}{\partial x_j}\right]$$

The k-ε model is probably the most commonly used model for modeling turbulence. It is probably the simplest model to complete relative to the other models which yield good results. It is robust, economical, and it yields results with reasonable accuracy for many different types of turbulent flow. However, a primary drawback of the k-ε method is that it does not work very well within the viscous sublayer. The Standard equation does not take buoyancy or streamline curvature effects into account, although some suggestions have been made to account for these effects.

The k-ω is not as commonly used as the k-ε model, however, it does have several distinct advantages. Experimental data suggests that it performs better in transitional regions, as well as in flows with pressure gradients that are strongly affecting the flow. Also, from a numerical perspective it is very stable, and tends to produce converged solutions more rapidly than the k-ε model. Finally, when dealing with low Reynolds numbers, it is more economical and elegant than

the k- ε models, in that it does not require the calculation of wall distances, additional source terms and/or damping functions based on the friction velocity.

Reynolds Stress Models are a means of modeling turbulence that are unlike any of the proceeding methods. All of the other turbulent modeling methods described above operate under the Boussinesq assumption. Reynolds stress models, on the other hand, do not assume that the turbulent shearing stresses are proportional to the rate of mean strain [8]. Therefore, these models can be expected to provide better predictions when there is a sudden change in the mean strain rate or when effects such as streamline curvature and large gradients need to be taken into account. Because Reynolds equations are unstable, it is difficult to compare this model with k-epsilon without stabilizing factor.

An example of when this may be desirable is when considering turbulent flow through a channel with a noncircular cross-section. Reynolds Stress Models are also good for helicopter fuselages, where there is three dimensional flow over complex geometries [13] .

Mathematically, this is accomplished by multiplying the ith momentum equation by the fluctuating by the fluctuating velocity component u'_j and adding this to the jth momentum equation and the u'_i. This is then time averaged. This creates new transport equations, but also introduces new unknowns, thus showing in turbulence modeling that transport equations cannot be solved exactly. Furthermore, they are not widely used because of their overall complexity. However, many predict that the Reynold's Stress Models have the best chance of becoming the "ultimate" turbulence model because they do not rely on the Boussinesq assumption and they contain the largest number of PDEs [8].

Based on this research, it is possible to decide which turbulence model would be most appropriate for CFD analysis of nasal airflow. Ideally, it would be best to either use a two equation model or a Reynold's Stress Model. However, because a Reynold's Stress Model is so sophisticated,

it would probably take too long to run. Therefore, the most logical alternatives would be either a k-ε or k-ω model. Since the k-ε model tends to be more robust and economical, it is the model that was selected as being most appropriate for this project.

Chapter 3: Methodology:

Steady State:

All CFD analysis was conducted with the Fluent software package. After opening Fluent, the first step in conducting the steady state nasal flow simulations was to read the mesh file of the geometry to be analyzed. This is done by clicking the File tab, selecting Read, and then choosing the mesh file from the list provided. The mesh was then checked for errors and displayed across the screen in order to develop an understanding of the geometry. After the mesh was loaded, the units of the grid were checked to ensure that they were consistent with the units that were going to be provided in the simulation. In this case, the metric (SI) system was used.

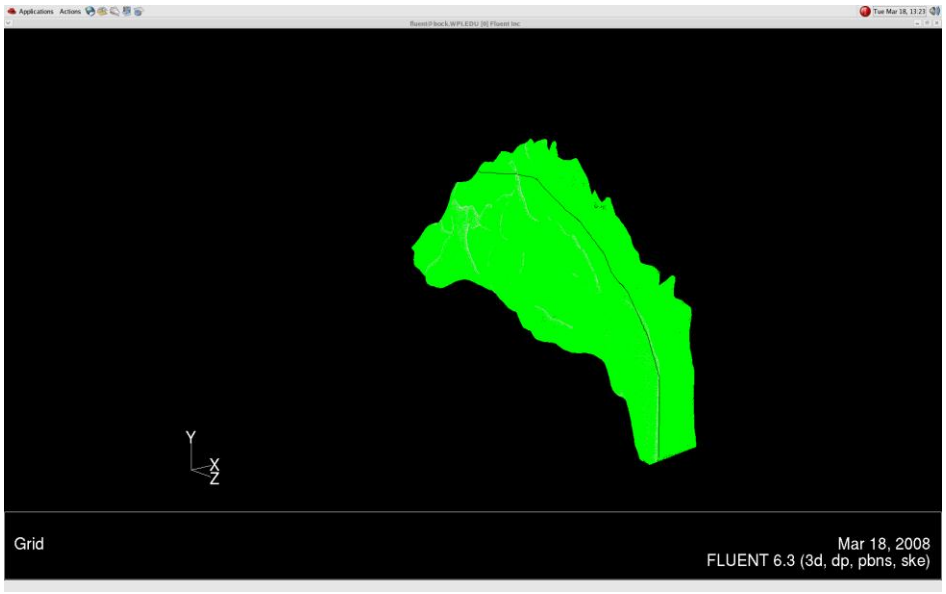

Figure 9: Side View Cutting plane shown in Nasal Geometry

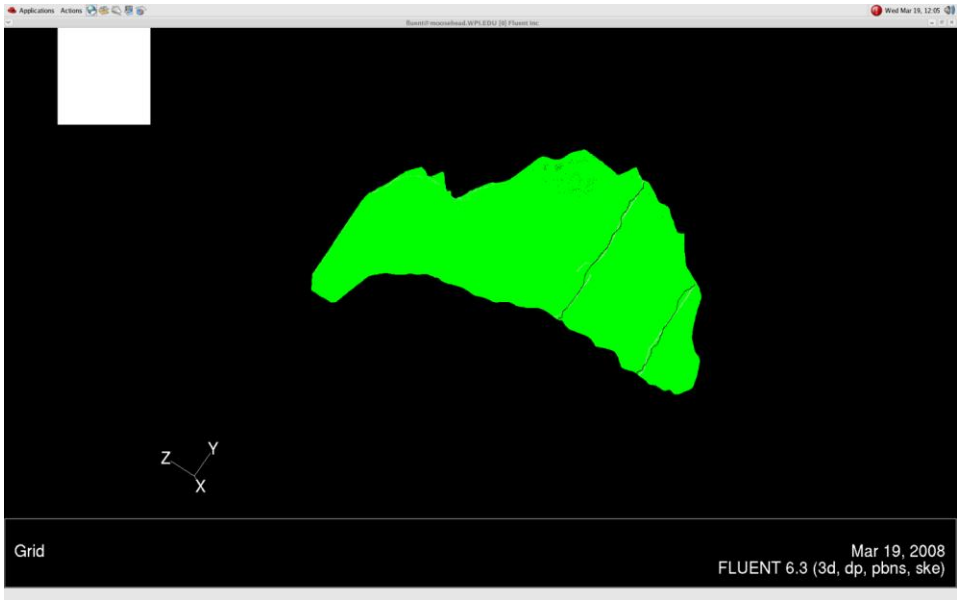

Figure 10: Frontal Cutting Planes shown in Nasal Geometry

After defining the mesh and unit systems for the problem, the next step was to define the models that were to be used for the simulation. First, the solver model was chosen. In Fluent, the solver model can be chosen to be either pressure based or density based. The density model is typically used only for problems involving compressible flow, while the pressure based model is used for the majority of simulations. Since one of the assumptions for this problem was that the density of air was constant throughout the geometry, the pressure based model was selected. Within the solver based model it was also necessary to define how the model varies with time; in other words whether it is steady or unsteady. For the first series of simulations, the steady state model was selected.

The final determinations that needed to be made were whether or not the energy equation was to be used, and what type of viscous model was to be selected. Because there was no heat transfer or work being performed, the energy model was not used. Two steady state models were run each for a low flow rate, a medium flow rate, and a high flow rate respectively. For each flow rate, one simulation was run using the laminar model and the other was run using the k-epsilon turbulence model.

After defining the models that were to be implemented in running the simulations, the next step was to define the material properties that would be used. The default material was air with standard properties at room temperature. These default properties were retained.

At this time, it was necessary to define the boundary conditions to serve as a basis for the computations that would be used to analyze the problem. The conditions that were defined in the mesh included the wall of the nose, all solid material within the nose, the outlet and the nostrils. The meatuses are not given their own boundary condition, but are probably part of the wall, which explains why the flow passing through them is forced to zero. No heat transfer was defined passing through the nose, and because we did not have any significant source of friction, the roughness constant was taken as the default. Also, the wall of the nose was defined as stationary. By convention, the nostrils serve as the source of airflow. Therefore, the nostrils were the only boundary condition that needed to have an input. In the dialogue box for the nostril boundary conditions it was necessary to input the flow velocity and turbulence intensity entering the nostrils. The turbulent intensity at the inlet was defined as being less than one.

After defining the boundary conditions, the system had all the data necessary to begin running the simulation. The first step in running the simulation was to define the boundary conditions from the nostrils as the basis for the computations. Next, convergence criteria were set to specify how accurate the results should be. In this case, convergence criteria were set at the level of E-03, which typically gives good convergence without requiring excessive computation times. Finally, the computations were performed. This was achieved by specifying the number of iterations that needed to be performed. Typically, about 2,000 iterations were specified, and the solution would converge within the first few hundred iterations.

After the necessary iterations were performed, it was possible to analyze the results. First, several planes were taken at various cuts over the meshed geometry. Contours and vector plots were then drawn over the cutting planes to get an idea of the physical properties over different locations within the geometry, most notably the velocity fields, pressure distribution, and turbulence intensities. The cutting planes are seen in Figures 11, 12, and 13. Also, by plotting pressures at points on the nostrils and outlet, it was possible to see how pressure changed across the line, and make an estimation of the pressure drop from nostril to within the geometry. These cutting planes can also be seen by the black lines in figures 9 and 10.

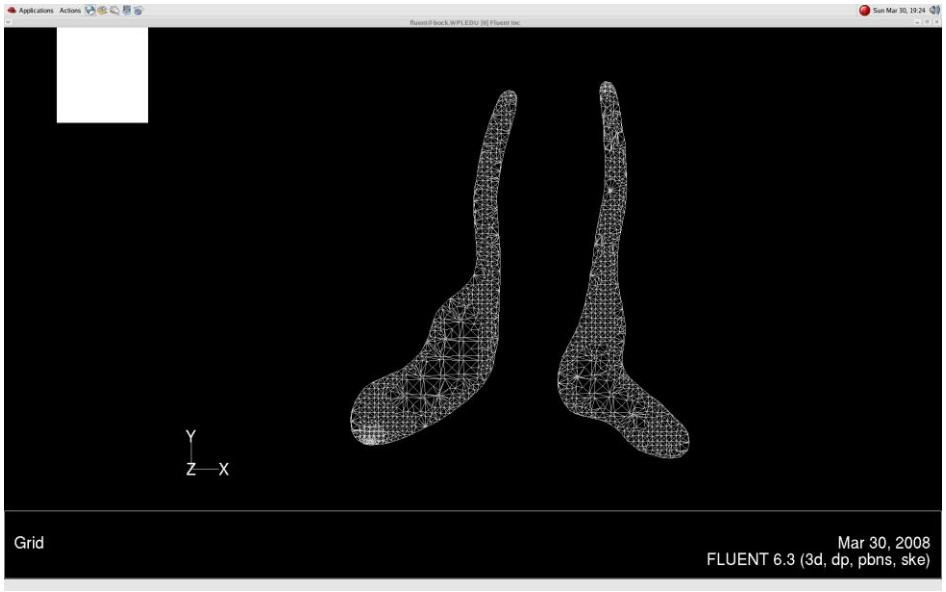

Figure 11: Cutting Plane Taken Near the Front of the Nose

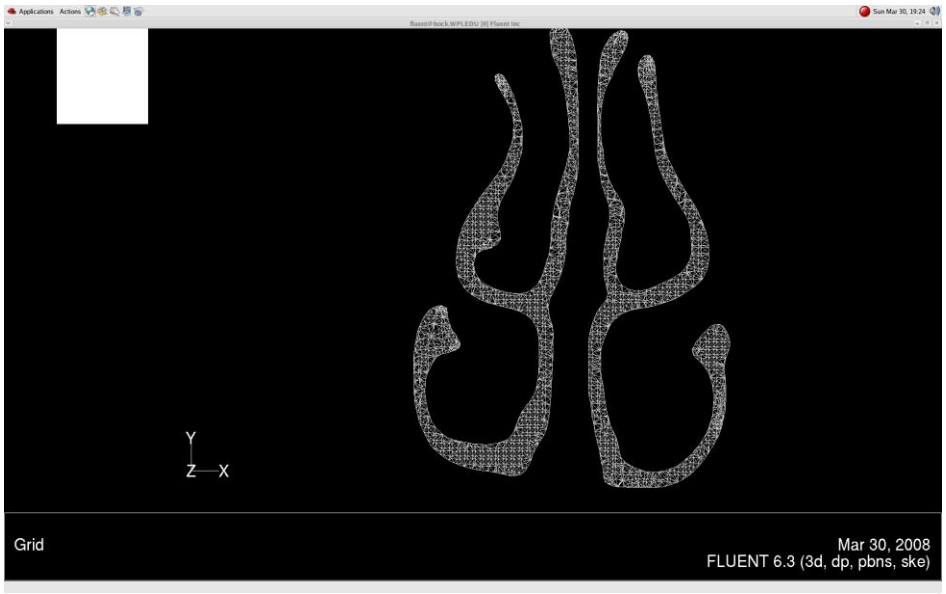

Figure 12: Cutting Plane Taken Near the Turbinates

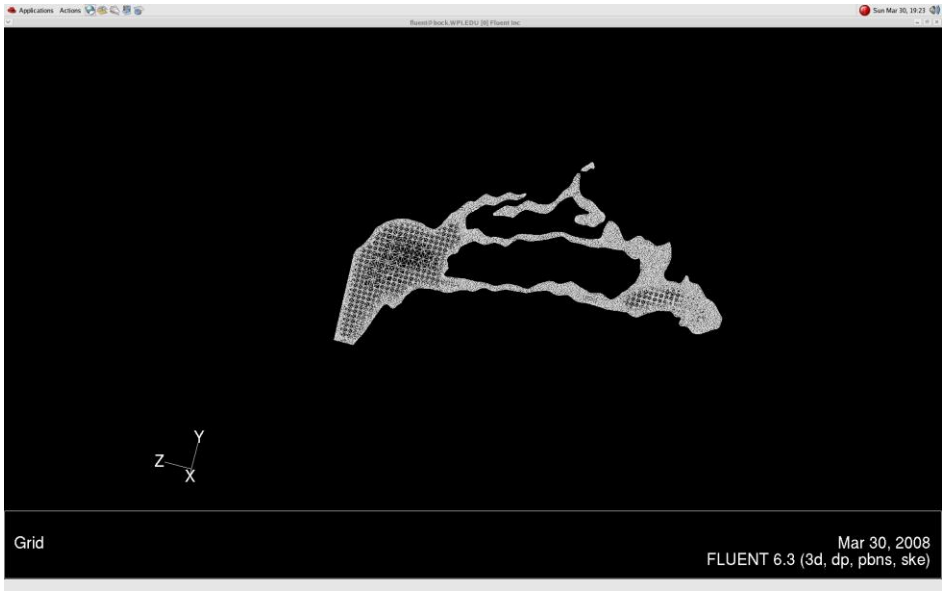

Figure 13: Cutting Plane Taken From the Side

Unsteady State:

The first step in creating an unsteady flow simulation was to determine an equation which represented the flow behavior of an unsteady model. Based on experimental data, a function that relates the volumetric flow rate, in liters per second, was given to be:

$Q(t) = -0.0077t^6 + 0.1224t^5 - 0.699t^4 + 1.6366t^3 - 1.0651t^2 - 0.5387t$

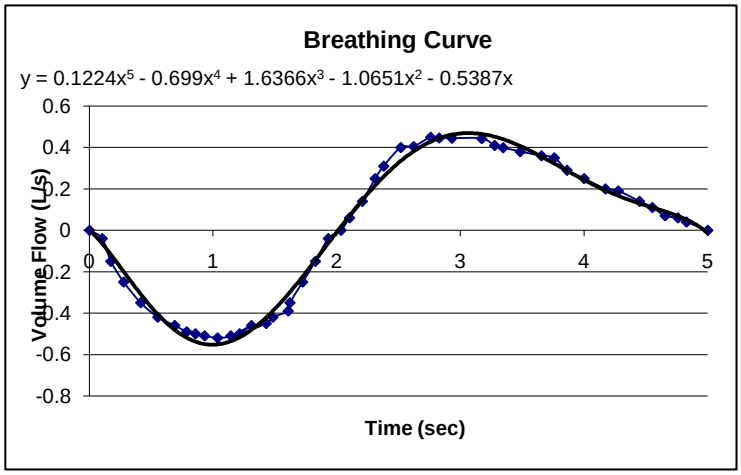

Figure 14: Plot of Breathing Curve

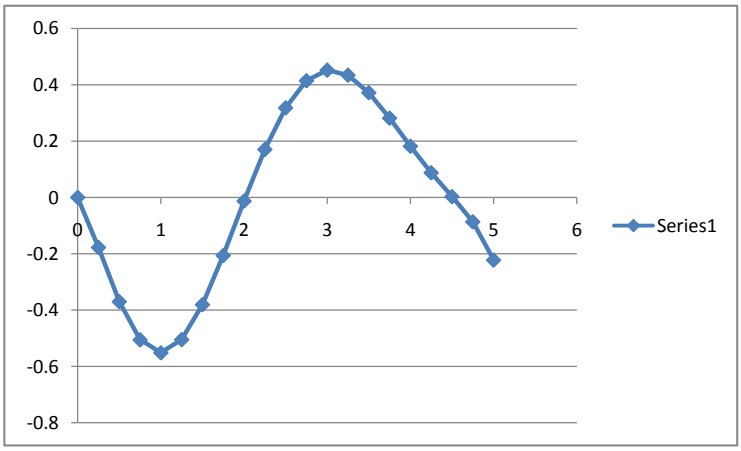

Figure 15: Plot of Volumetric Flow Rate with Respect to Time Obtained from Breathing Curve

This function was defined as velocity input in the dialogue box for the boundary conditions of the nostrils. Next, it was necessary to choose which times were to be output and steady state models were run for each these velocities so that the steady state and unsteady state models could be

compared with each other in order to determine whether the flow could be expected to be quasi-steady or unsteady.

However, since Fluent requires a velocity input, the volumetric flow rate had to be converted from liters per second to meters per second. First, the units of the above function were converted from liters to cubic meters, which involved dividing the equation by 1000. Next, the velocity function was solved for by dividing the volumetric flow rate by the area over the nostrils. Since the area solver in Fluent determined that the area over the nostrils was approximately 0.0001 square meters, this had the same effect as multiplying the function by 10,000. After performing these unit conversions, a velocity function in terms of meters per second was found to be:

$$V(t) = -0.077t^6 + 1.224t^5 - 6.99t^4 + 16.366t^3 - 10.651t^2 - 5.387t$$

At this point, all necessary information was available to derive an unsteady solution. First, a steady state model was run to convergence, as described above. After convergence was reached, the solver model window was reopened, and the time solver option was changed from steady to unsteady. All other solver options remained the same.

Next, a user defined function was loaded which reflected the nature of the unsteady state flow conditions. This program was written using the C programming language, and is shown below:

```
#include "udf.h"

DEFINE_PROFILE(inlet_xv_sinisoidal, thread, nv)
{
face_t f;
real t = RP_GET_REAL("flow-time");

begin_f_loop (f, thread)
{
F_PROFILE(f, thread, nv) = 10*(-0.0077*t*t*t*t*t*t*t) + 10*(0.1224*t*t*t*t*t*t) +
10*(-0.699*t*t*t*t) + 10*(1.6366*t*t*t) + 10*(-1.0651*t*t) + 10*(-0.5387*t);
```

```
}
end_f_loop(f, thread)
}
```

After the user defined function was compiled, the unsteady state boundary conditions were set. The user defined function was selected as the input for the flow velocity across the nostrils. The rest of the boundary conditions remained the same.

At this point all necessary information was inputed in order to successfully run the unsteady simulation. In the iteration task panel, it was necessary to specify three important parameters: the time step size, the number of iterations that were to be computed during each time step, and the number of time steps that were needed. Based on the results from steady state models of a similar geometry, it was reasonable to assume that the computation may take several thousand iterations to reach convergence. Therefore, a time step size of 0.001 seconds was selected. For most Fluent problems, 15-20 iterations per time step are specified, which is typically enough to reach convergence within each time step. After deciding which times were needed for analysis, it was easy to compute the number of time steps that were needed. Whenever a desired time was reached, the simulation would stop, and all case and data files would be saved. The process was then repeated by specifying the number of time steps needed to reach the next desired time.

After the data were retrieved for all of the desired times, it was possible to analyze the graphs, contours, and vector plots as was done in the steady state analysis. After determining the maximum values of pressure, velocity magnitude, and turbulence intensity, these values were plotted in Excel. After plotting this data, it was possible to derive equations which approximate how these properties change with time. Also, it was possible to compare the values obtained from the various time with those from steady-state models to determine whether a quasi-steady or unsteady flow behavior is exhibited. Finally, the data was then compared with the data derived experimentally.

Chapter 5: Results:

Steady State Results:

The numerical data which was used for this simulation was based on physiological data found in the literature. An average steady flowrate was calculated by multiplying the tidal volume (in cubic meters) by the average number of breaths taken per minute. This flow rate was then divided by the cross-sectional area over the nostrils, to yield the average velocity at which the air could be expected to be passing through both nostrils.

- *Volume of Air breathed per minute = 14 breaths per minute * Tidal Volume of 0.0005 cubic meters (per breath)= 0.007 cubic meters per minute (or 0.0001 cubic meters per second or 100 cc/s)*
- *Velocity = (0.0001 cubic meters per second)/(0.0001 square meters) = 1 meter per second*

While Fluent requires a velocity as an input, the results are described in flow rates, which is the standard used in these studies.

Based on these calculations, it was estimated that when an average individual is at rest, the air passes through their nostrils at a flow rate of about 100 cc/s. The first two simulations that were run with Fluent used this velocity. Four other simulations were run at higher flow rates. The literature suggests that fully turbulent flow takes place when the air passes through the nose at about 250 cc/s, and so for the third and fourth models we used a flow rate of 270 cc/s to make sure that we were not

looking at flow that was within the transition period. The last two models used 500 cc/s as a flow rate, which is the highest flow rate that we would typically expect to find in a subject during normal breathing conditions.

Model 1:

The purpose of the first model was to analyze the airflow conditions while the individual is at rest (using the calculated flow rate of 100 cc/s passing through both nostrils). Because most available research suggests that this flow rate results in laminar behavior, the laminar viscous model was chosen. After the procedure was completed as outlined in the Methodology, data were and the results were reviewed to analyze the following:

- Pressure magnitude and variation throughout the model
- Velocity vectors and magnitude

Pressure:

The static pressure was the first variable to be analyzed. Contours were taken at various sections along the geometry, which were then compared with one another. Also, a graph was plotted to show how pressure changed in the "axial" direction (i.e. the distance from the nostrils to the outlet). This graph is shown in Figure 16.

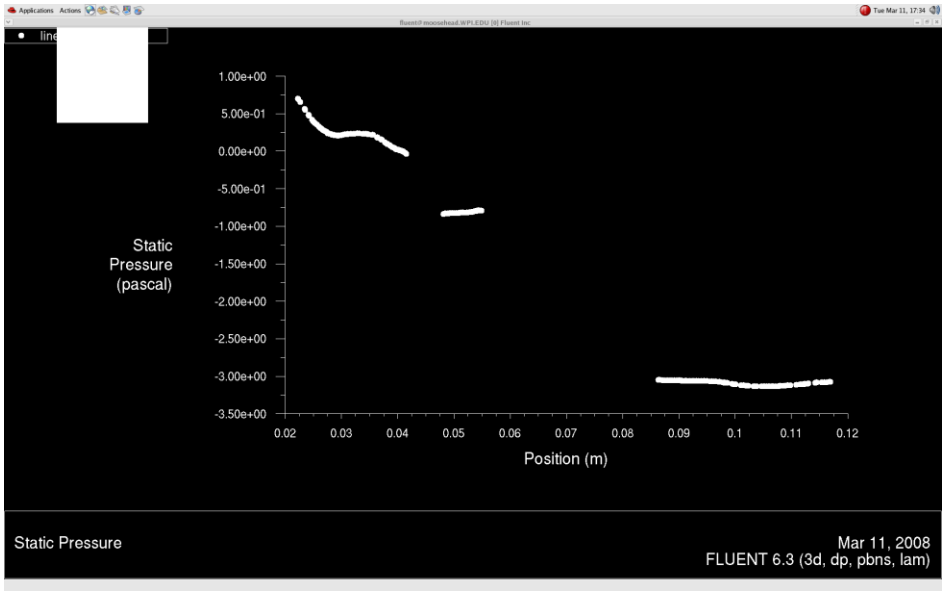

Figure 16: Pressure Drop Seen From Nostrils to Nasal Outlet at Flow Rate of 100cc/s with Laminar Model

By analyzing this graph, it is clear that the pressure at the outlet is approximately 4 Pa lower than that near the nostrils. This phenomenon is similar to the one discussed in the flow through a straight tube. A pressure drop of 4 Pa is generally considered very small, which seems logical given the small length over which the flow takes place. This is roughly the pressure drop that was predicted from experimental data.

In addition to the difference in pressure between the nostrils and the outlet at the back of the nose, another important factor to consider was the difference between the pressure over the right and left nostrils. According to the article by Zhao, for any given flow rate, the pressure drop over the left nostril is expected to be greater than that over the right. According to the graph shown in this article,

the pressure drop for small velocities such as the one used in this model is expected to be only a couple of pascals. The contour shown in Figure 17 indicates that the pressure over the left nostril is about 1 pascal, and the pressure over the right nostril is close to zero. While the contours over the two nostrils are represented with contrasting colors, the difference between them in terms of magnitude is very small. However, it is still evident that there is a slight difference between the pressures in the two nostrils,

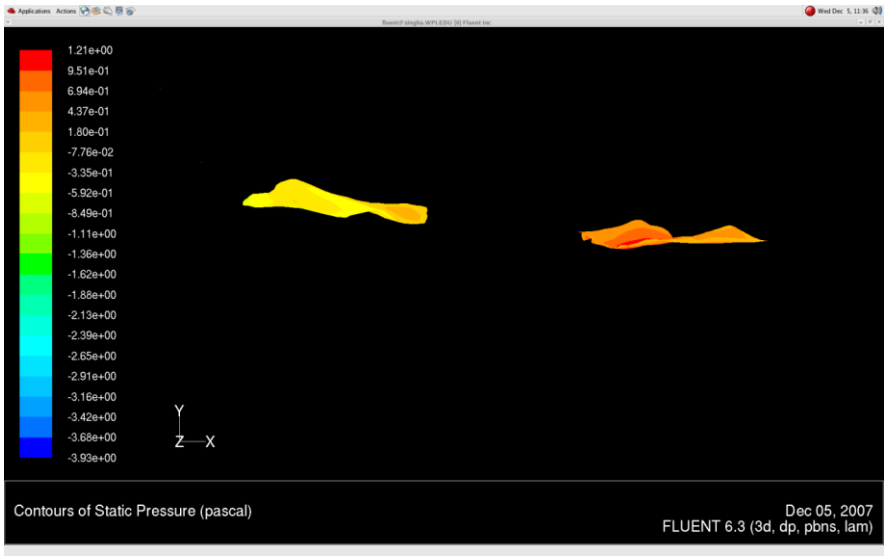

Figure 17: Pressure Contours of Nostrils at 100 cc/s from Laminar Model

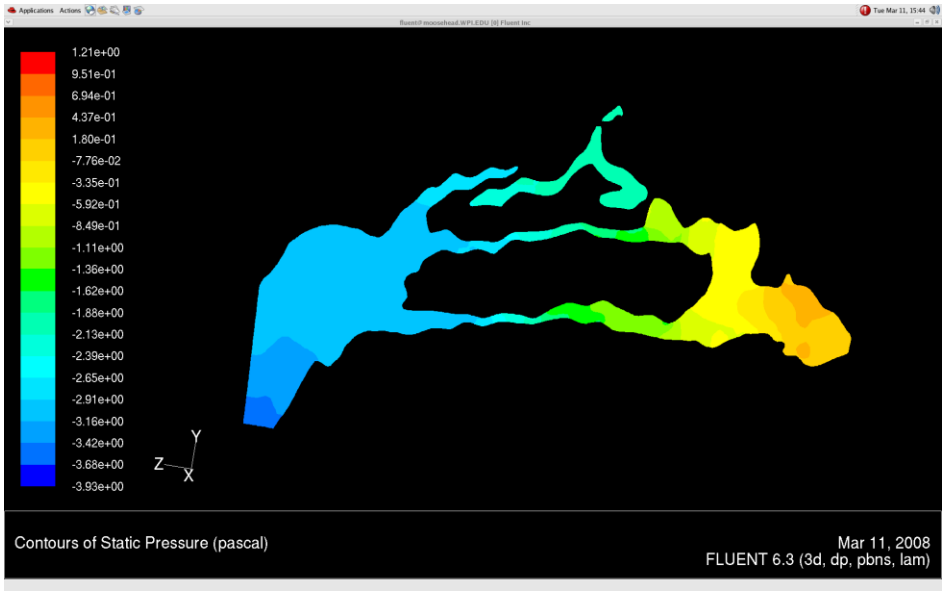

Figure 18: Pressure Contours Seen over Side View Cutting Plane at 100 cc/s and Laminar Model

Velocity Profiles:

While analyzing the velocity behavior at the nostril inlets, outlet, and the cavities between them, there were a number of issues that needed to taken into consideration. First of all, it was helpful to view both the vector and contour plots individually. While the vector plots gave a better indication of the direction the air was flowing, the contours gave a better presentation of the overall magnitude at various stages throughout the flow. Because it was important to make sure that the no-slip condition held at all solid boundaries, it was necessary to observe the contour plots at all physical boundaries, and make sure that the value there was zero.

We wanted to see if the velocity fields were roughly symmetric, as shown by previous studies. It was also important to compare the effects of anatomical parts such as the septum, meatuses and turbinates with the effects as predicted in the literature. Identifying the areas where vortices appeared and the number of vortices that were present was also an important observation. Finally, it was important to establish whether or not the velocity profile at the outlet was fully-developed.

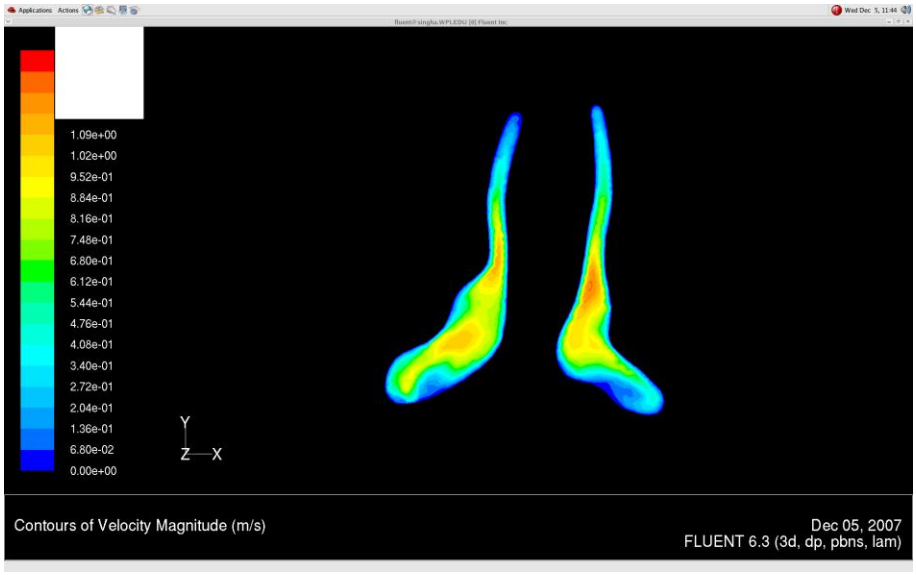

Figure 19: Velocity Contours Near the Entry Region at 100cc/s for Laminar Model

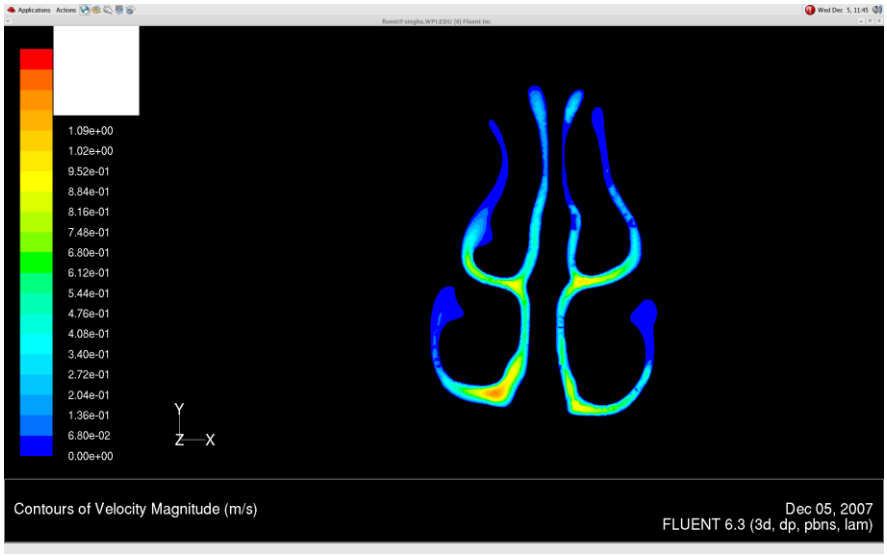

Figure 20: Velocity contour Near Turbinate Region for 100 cc/s Laminar Model

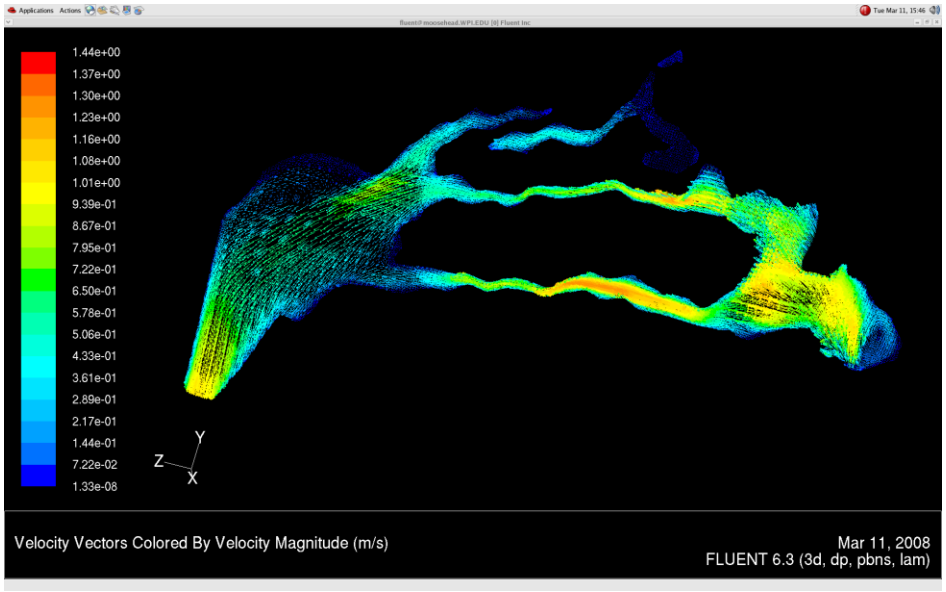

Figure 21: Velocity Vector Plots from Side View for 100 cc/s Laminar Model

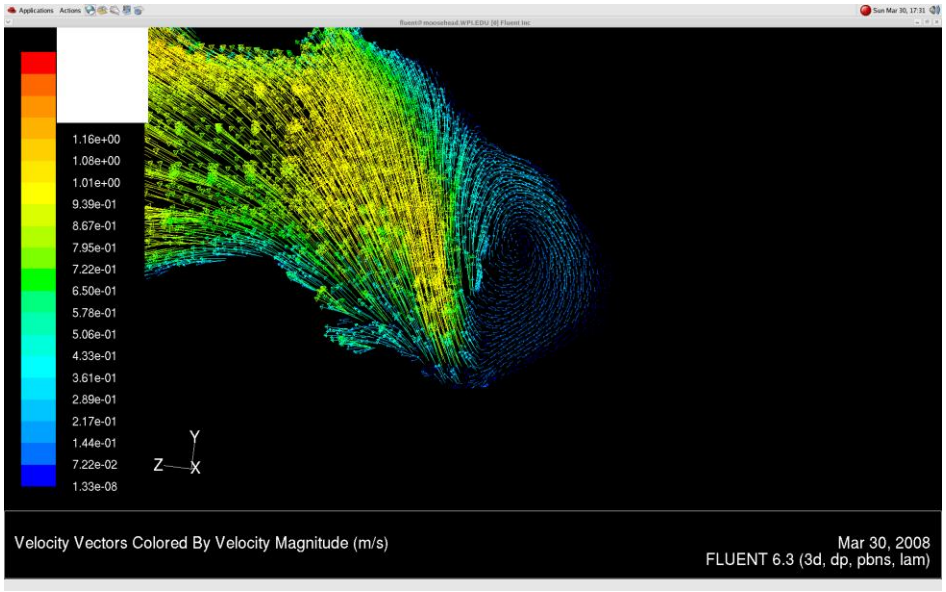

Figure 22: Vortex Plot for 100 cc/s Laminar Model

According to our plots, the velocity profiles follow roughly the same behavior in both the left and right sides of the nose, thus affirming the results found in the literature. The literature also suggests that velocity fields increase in magnitude at locations further away from the septum. It is not clearly established in the literature why this happens, but this is most likely a result of the no-slip condition. As points are analyzed closer to the wall of the nose, it would be expected that the velocity magnitudes would begin to decrease again. This is not described in the literature, because the velocity field plots shown in these articles only extend to the center of the nasal cavity. The phenomena we would expect to see would be analogous to the concept of pipe flow, where the septum and the wall of the nose would both represent the walls where the velocity would be lowest. By observing the contour plot in Figure 19, it is clear that this behavior occurs; the velocity is greatest in the center of the nasal cavity, and steadily decreases as either the septum or wall are approached.

Analyzing these contours and plots also can also give an idea of the flow behavior near the various turbinates. According to the experiment conducted by Kelly [5], there should be very little flow in the meatuses. On the velocity contours, almost all of the meatuses are represented as being dark blue, suggesting that there is no flow at all through them, except over a few small areas. Kelly also suggests that the areas near the inferior airway have the highest flow, which is evident from the contour plots in Figure 20. This seems to agree with the results seen in the vector plot shown in Figure 21. The flow velocity passing through the inferior airway seems to be about 25% higher than that through the middle airway, and has approximately twice the area. This suggests that about 70% of the flow is passing through the inferior turbinate.

From the vector plots in Figure 21, we can see that an eddy develops in the lower region of the nasal valve (i.e. the third vector plot shown). This is approximately where an eddy would be expected to develop based on the results outlined from previous experiments. However, the eddy is shown with blue vector lines, indicating that it is very small in magnitude. According to Kelly: "…this depicts an eddy in the anterior part of the cavity." Since the vector plot shows the area near the anterior section of the nasal cavity, this seems to coincide with our results. Looking at the plots in the areas adjacent to the turbinates, we do not see any noticeable eddies, which may be explained by the fact that the passages are very thin. The only vortices that appear in the vector plots are seen near the inlet of the nose. There are no vortices near the turbinate region, although the literature suggests that they may sometimes appear there.

While it was particularly important to study flow through the cavities, it was also important to analyze the flow over the inlet and outlet. One major objective was to compare the flow over the two nostrils, and in doing so it was clear that while the vectors were moving in different directions because the shape of the two inlets was not exactly the same, the magnitude itself was uniform between the two

nostrils. Another objective was to observe the flow through the outlet, and determine whether or not the flow seemed to be fully developed. Looking at the velocity vectors over the outlet, it was clear that the velocity shows a flat profile, so we may conclude that a fully developed profile has not been reached. This may be because the length over which the air flows is not sufficient for a fully developed profile to occur, or because the area is constantly changing, which may be constantly affecting the velocity profile.

Model 2:

This simulation was run using the k-ε turbulence model. The purpose of running this simulation was to determine the role that a turbulence model played in the results when the flow behavior was assumed to be laminar. Before running this simulation, it was predicted that results would show agreement with those obtained using the laminar model, which for the most part seemed to be the case, as evidenced by the following plots and data.

Pressure:

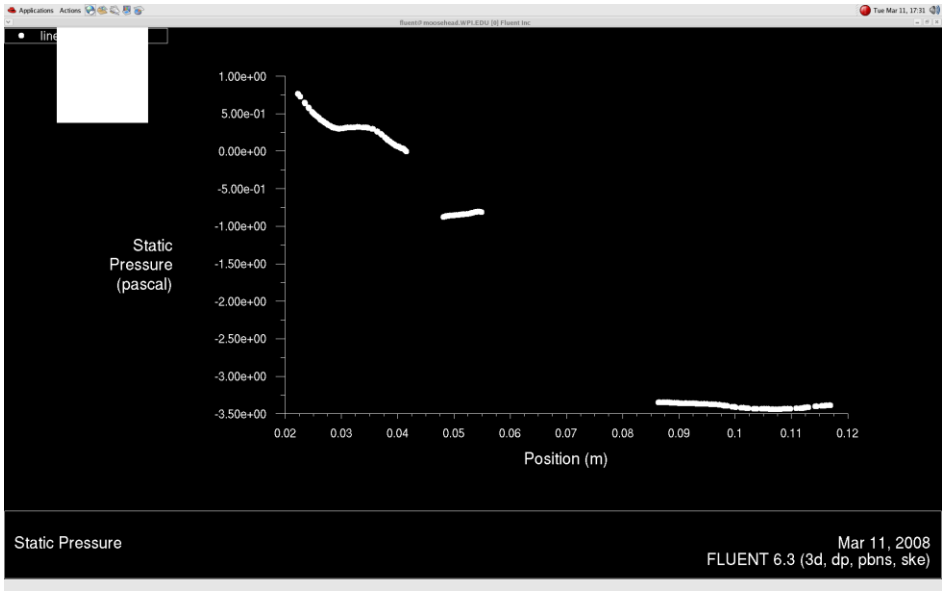

Figure 23: Pressure Drop from Nostrils to Outlet for 100 cc/s K-Epsilon Model

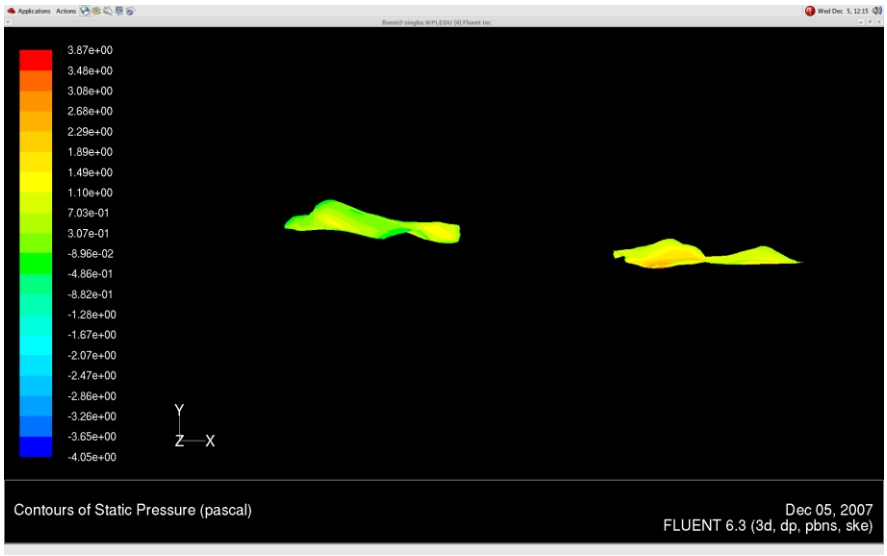

Figure 24: Pressure Contours Over Nostrils Seen at 100 cc/s K-Epsilon Model

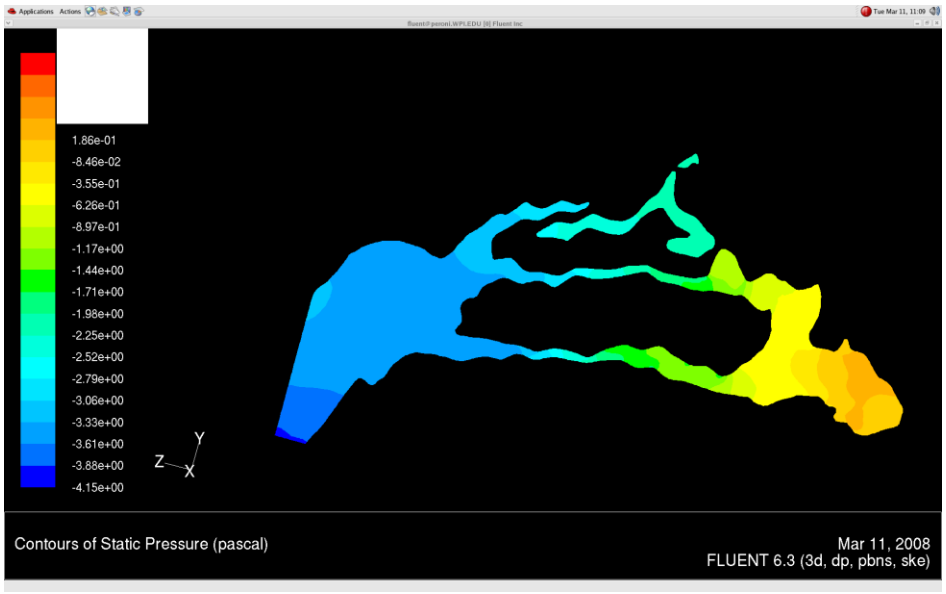

Figure 25: Pressure Contour Seen From Side View at 100 cc/s K-Epsilon Model

We can see from these contours that the pressure drop from the nostrils to the outlet in Figure 23 is approximately the same as the one observed in the laminar model, which is about 4 Pa. Since the flow in this model is expected to be fairly laminar, we would not expect that the choice of a k-epsilon model would have a significant effect on the pressure. After comparing the pressure over the two nostrils in Figure 24, we can find that the difference in pressure is about 4 Pa, which is once again approximately the same as the results from the previous simulation. The pressure over the outlet is about 0.2 Pa less than that seen in the previous model, showing that there is a very slight difference between the pressure contours of the laminar and turbulent models.

Velocity Profiles:

Figure 26: Velocity Contours Seen Near Entry-Region for 100 cc/s K-Epsilon Model

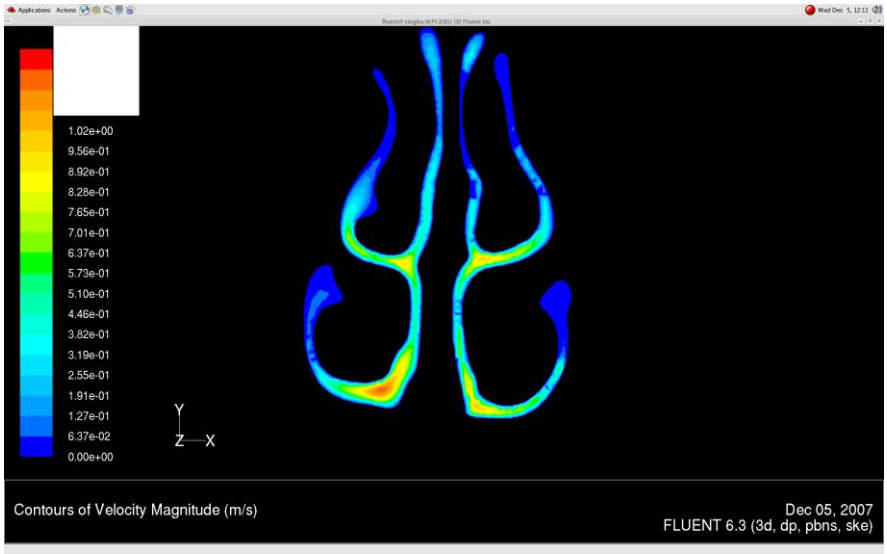

Figure 27: Velocity Contours Seen Near Turbinate Region for 100 cc/s K-Epsilon Model

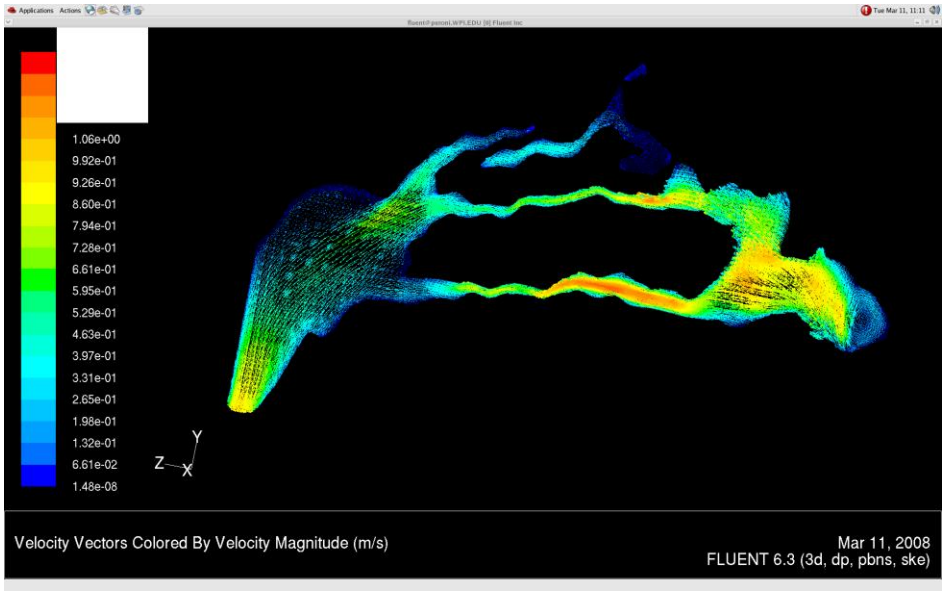

Figure 28: Velocity Vector Plot from Side View for 100 cc/s K-Epsilon Model

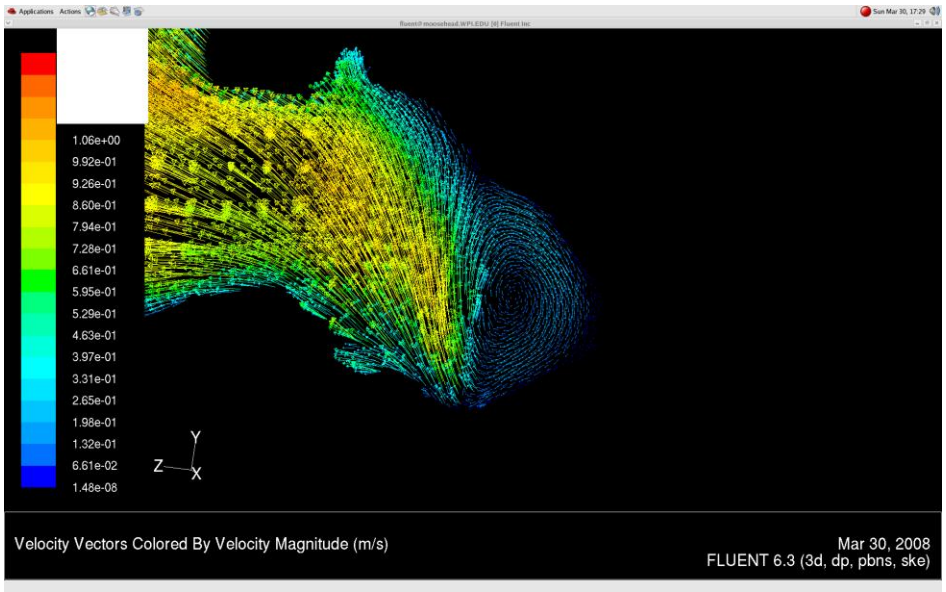

Figure 29: Vortex Plot for 100 cc/s K-Epsilon Model

For the most part, there are not too many differences in the velocity profiles between this model and the previous one. The flow rate seems to be the same through the various regions (i.e. the area near the inferior turbinate yields the highest flow). Also, the only visible eddy can be seen near the nostril inlet, in the same place as the previous model.

Turbulence:

Since the previous model was run under the laminar viscous model, it was not possible to analyze the turbulence of the flow. Since the k-ε model was selected for this simulation, turbulence was analyzed. The turbulence was quantified by studying the turbulence intensity over a selected side view plane, and is shown in Figure 30.

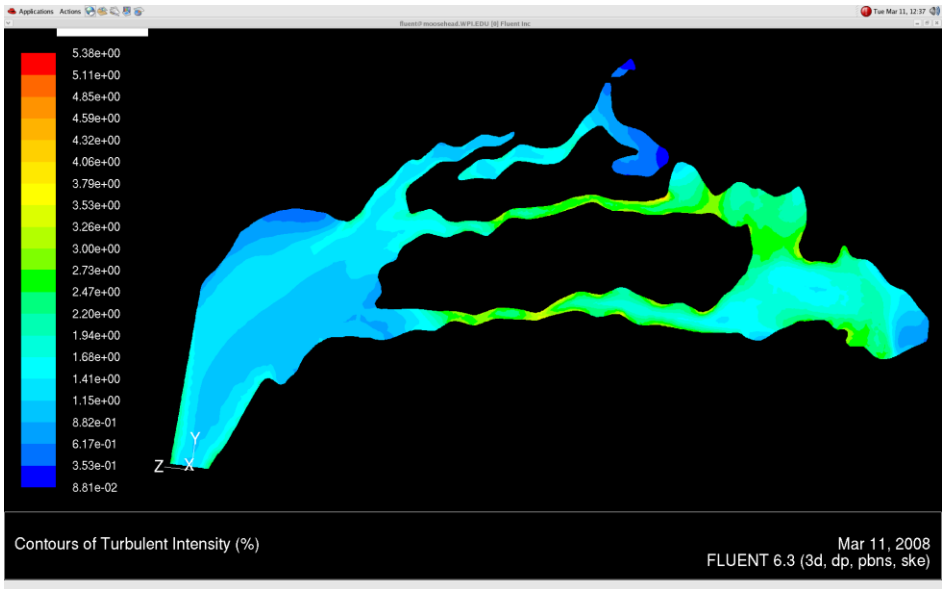

Figure 30: Turbulent Intensity Contour for 100 cc/s K-Epsilon Model

By studying the turbulence intensity contours, it is clear that the average turbulence intensity is between one and two percent. This turbulence seems somewhat higher than we would expect, since the literature suggests that at this flow rate the flow behavior should be expected to be laminar, and we might expect the turbulence intensity to be less than 1%. However, this value is still very small, and probably can be considered laminar or close to laminar. The turbulence seems to be highest while approaching the turbinates. This may be best explained by the complicated geometry and very small areas where flow can pass through.

Model 3:

According to the literature, air flowing through the nose typically can be considered to show laminar behavior, but after flowrates of about 250 ml/s or higher have been reached, the flow is typically considered turbulent. In this model, we ran a k-ε model with a flow rate of 270 cc/s at the inlet. Given that the area over the nostrils is about 1E-04 square meters, this would yield a volumetric flowrate of approximately 270 ml/s, which we would expect to be fully turbulent.

Pressure:

After carefully analyzing the graph in Figure 31, it seems that the pressure drop between the nostrils and the outlet is roughly 14 Pa. This value is significantly higher than that found in both of the previous models, however this is expected because since the velocity plays a very large role in the pressure drop. From the head loss function, we found that the head loss is roughly proportional to the square of the velocity. Therefore, a flow rate of 270 cc/s should yield a pressure drop much greater than one seen

with a flow of only 100 cc/s. The most important thing to be aware of is that the pressure drop will be significant as the velocity increases.

Observing the pressure contours over the two nostrils seems to differ by about 3 Pa, which is not far off from the values that we received from the other simulations.

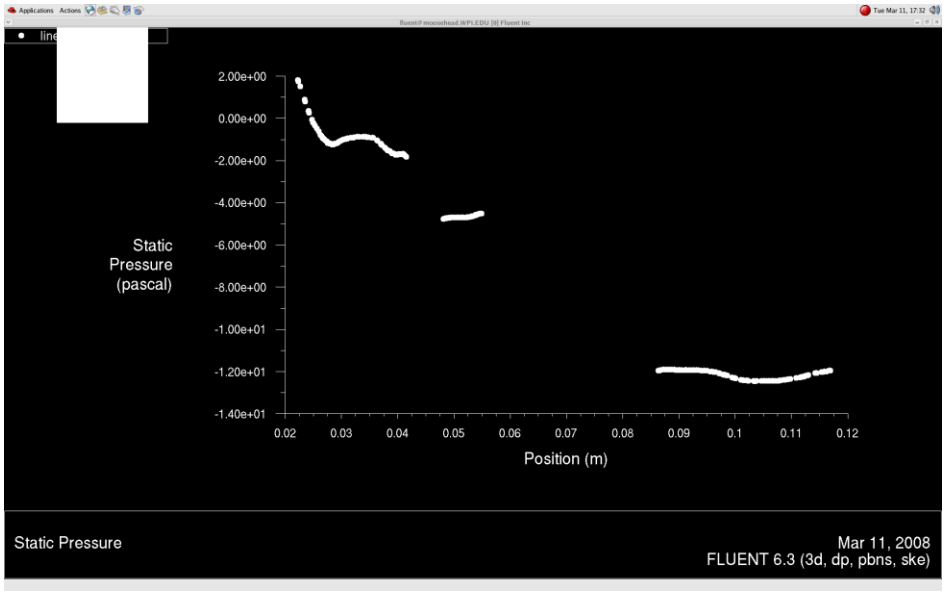

Figure 31: Pressure Drop from Nostrils to Outlet for 270 cc/s K-Epsilon Model

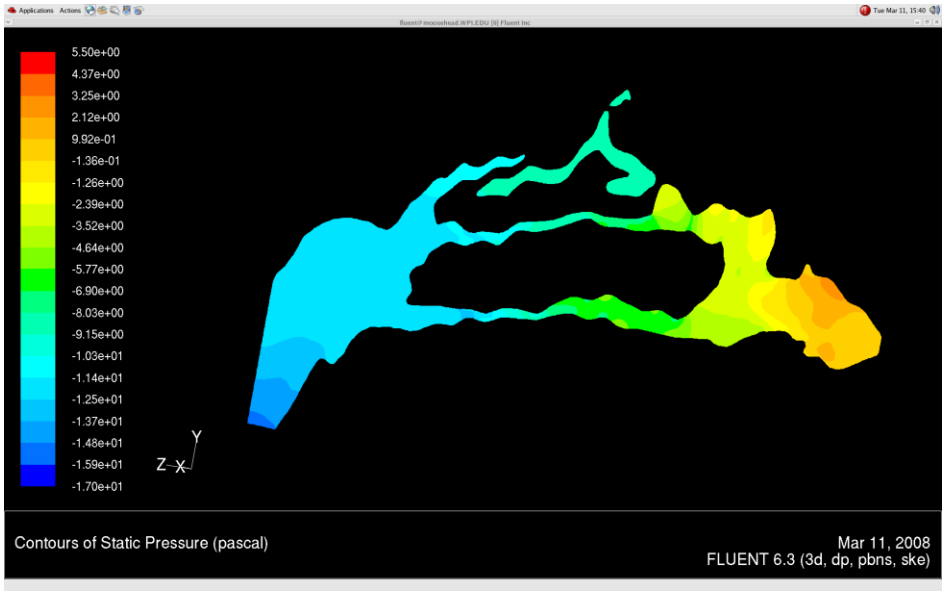

Figure 32: Pressure Contours Seen from Side View for 270 cc/s and K-Epsilon Model

Velocity Profiles:

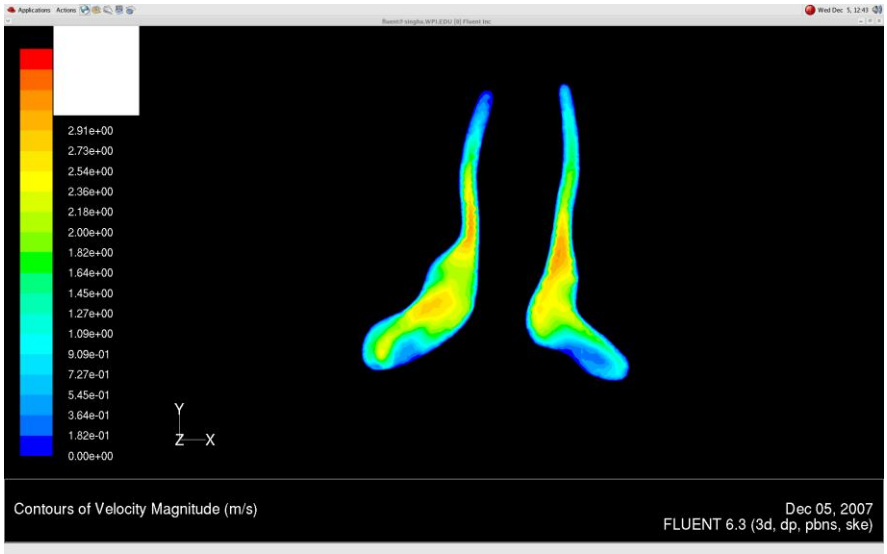

Figure 33: Velocity Contours Seen at Entry-Region for 270 cc/s K-Epsilon Model

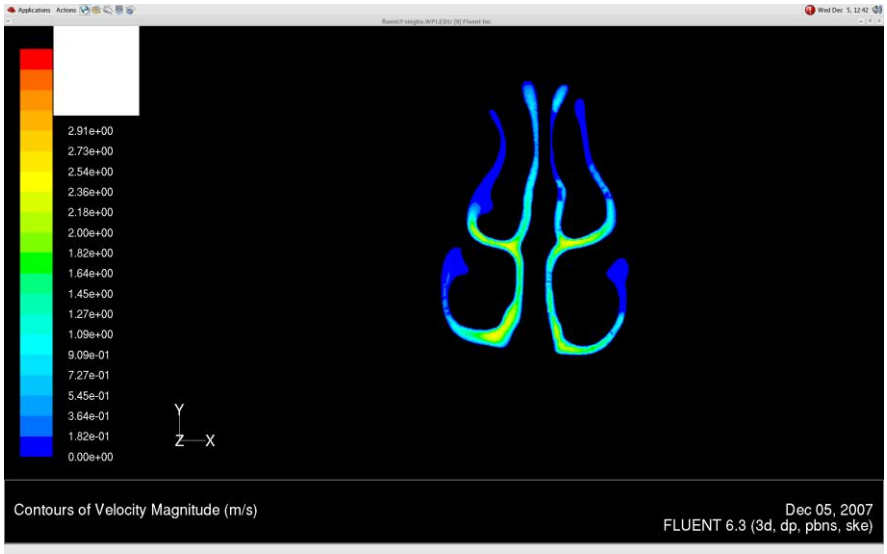

Figure 34: Velocity Contours Seen Near Turbinates for 270 cc/s K-Epsilon Model

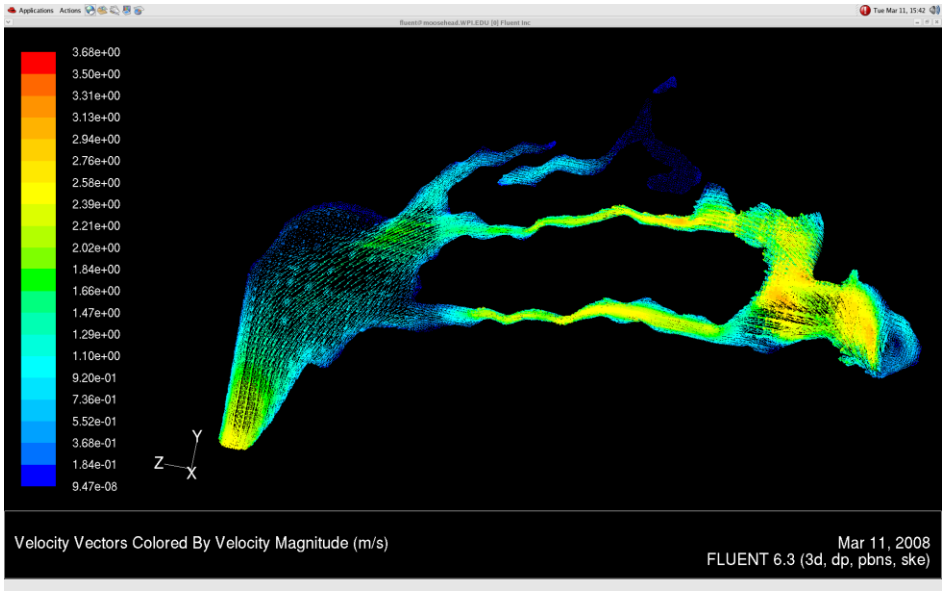

Figure 35: Velocity Vectors Seen at 270 cc/s K-Epsilon Model

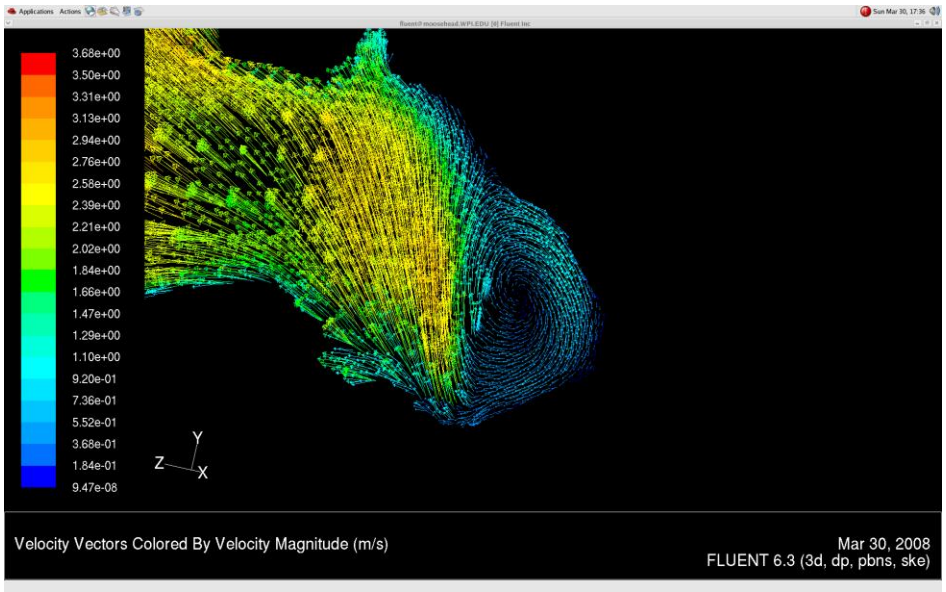

Figure 36: Vortex Vectors Seen at 270 cc/s K-Epsilon Model

The velocity behavior in this model seems to be similar to that of the previous two models. The vortex that appears in this simulation appears in the plot near the front of the nose, which is seen in Figure 36, at approximately the same place as the models with lower flow. The anatomy of the nose seems to have the same effects on the flow as the previous two models (i.e. there is no flow through the meatuses, the flow is highest through the inferior airway, and the velocity magnitudes are greatest away from both the septum and the wall of the nose). The only key difference is that that the proportion of flow passing through the inferior airway is lower (seen in Figure 35). Now, the velocity passing through the inferior airway is about 2 m/s, and the velocity passing through the middle airway is about 2.6 m/s. Since the inferior airway has probably twice the area of the middle airway, about 60% of the flow is passing through the inferior airway. Finally, the flow through the outlet still does not appear to have become fully developed.

Turbulence:

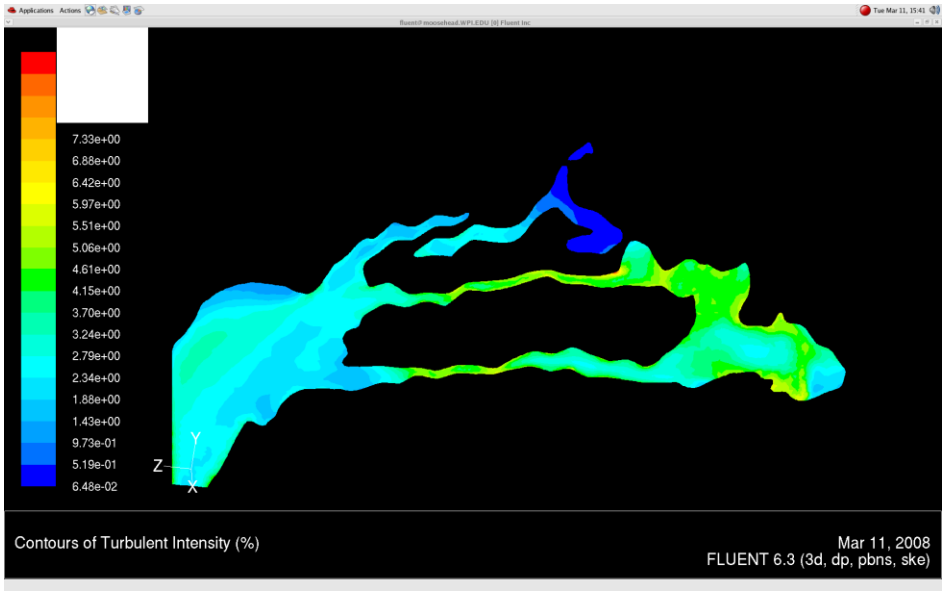

Figure 37: Turbulent Intensity Contours at 270 cc/s K-Epsilon Model

Analyses of these contours in Figure 37 show that the turbulence intensity can reach values up to 5%, which is significantly higher than the previous model, and indicates that turbulent conditions have been reached. Another observation is that the turbulence intensity seems to be highest near the turbinates, which is consistent with the observation made from the previous models.

Model 4:

This model was run as a laminar model with the same 270 cc/s flow rate as the previous k-epsilon model.

Pressure:

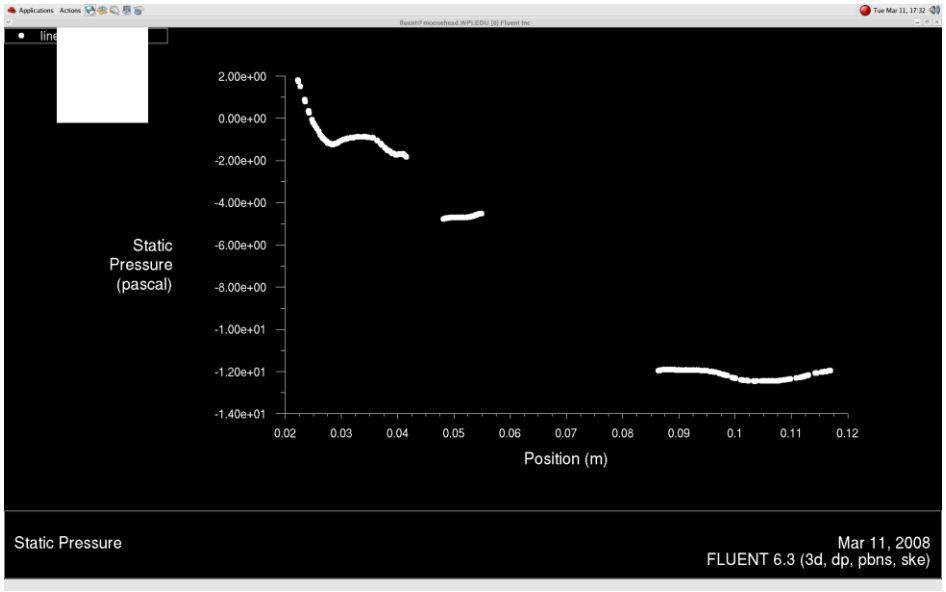

Figure 38: Pressure Drop Seen from Nostrils to Outlet for 270 cc/s Laminar Model

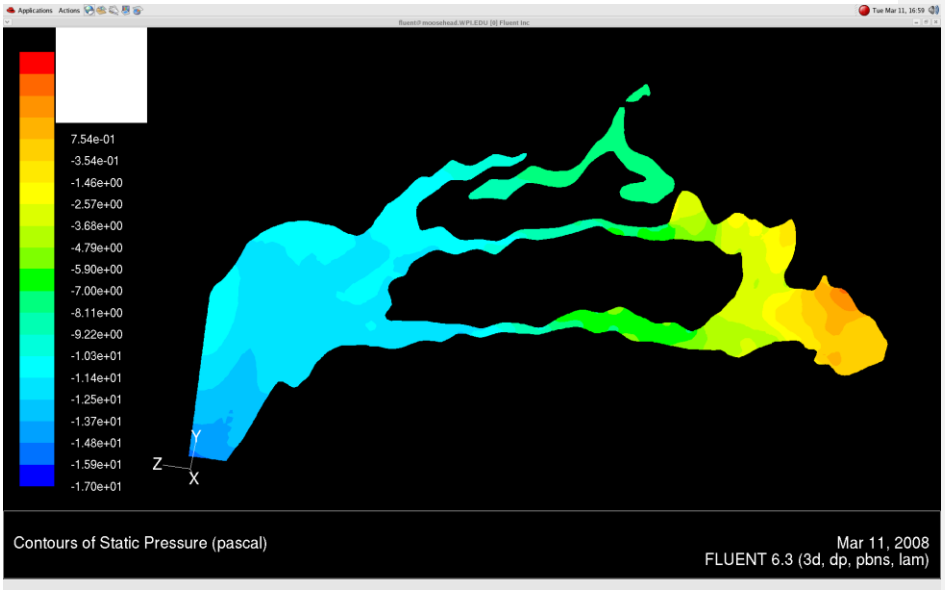

Figure 39: Pressure Contours of Side View for 270 cc/s Laminar Model

The pressure contours and graphs (Figures 37-39) show the same behavior in this model as the k-epsilon model.

Velocity:

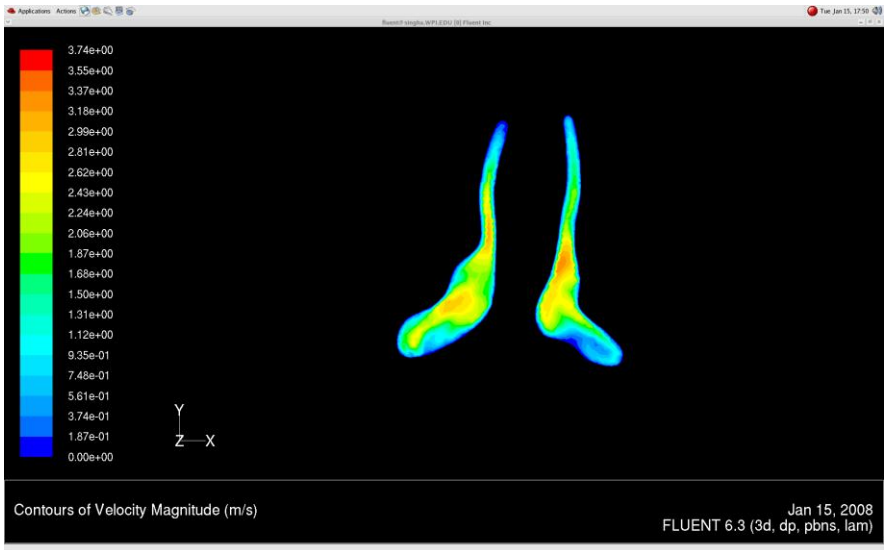

Figure 40: Velocity Contours Near Entry-Region for 270 cc/s Laminar Model

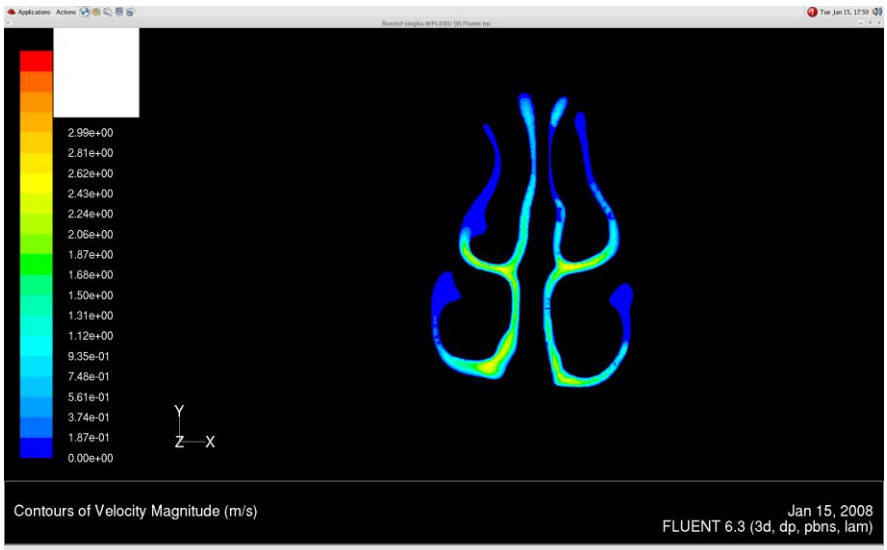

Figure 41: Velocity Contours Seen Near Turbinate Region for 270 cc/s Laminar Model

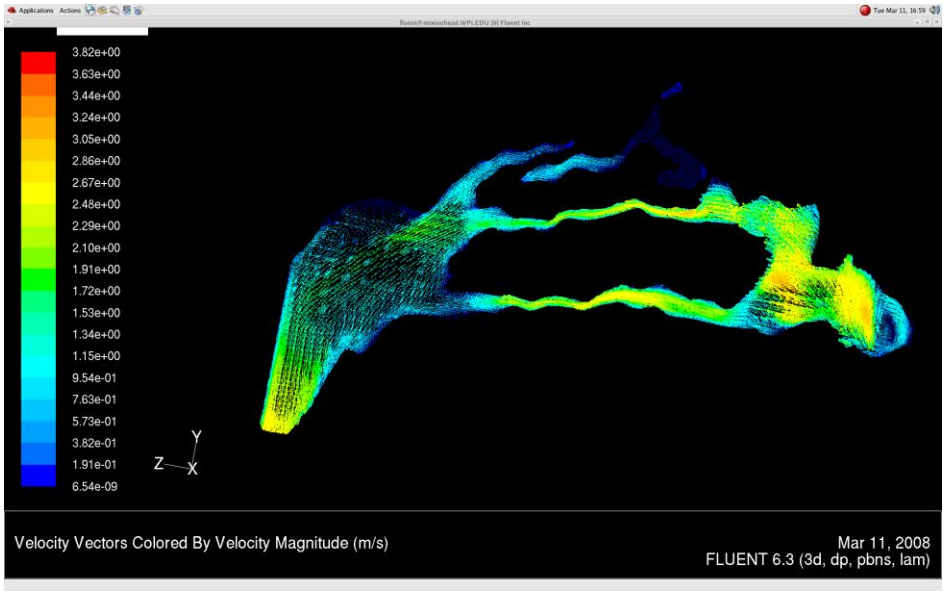

Figure 42: Velocity Vectors Seen for 270 cc/s Laminar Model

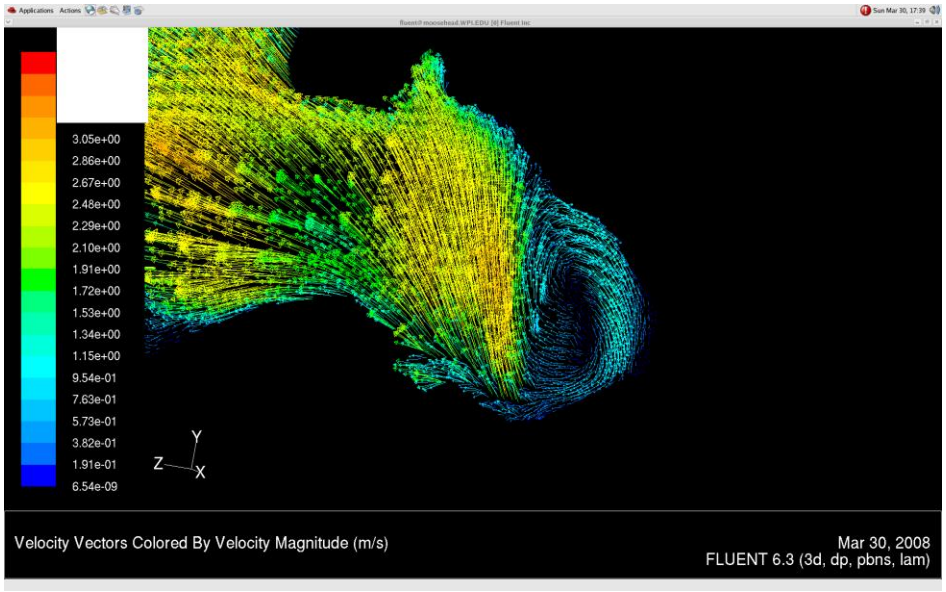

Figure 43: Vortex Vectors for 270 cc/s Laminar Model

The velocity contours and vectors show the same behavior and magnitudes as are seen with the previous model. The only key difference is that in this laminar model (Figure 43) the vortex seems to follow a less organized pattern than the vortex in the k-epsilon model (Figure 36).

Model 5:

This model was based on a high flow rate (500cc/s). High turbulence is expected to develop at this flow rate, and this model used the k-epsilon turbulence model.

Pressure:

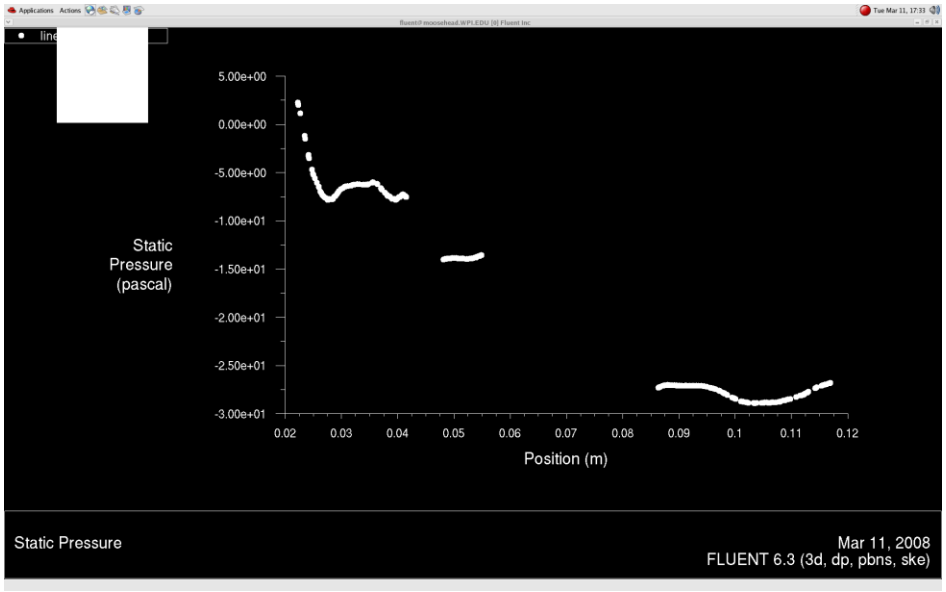

Figure 44: Pressure Drop from Nostrils to Outlet for 500 cc/s K-Epsilon Model

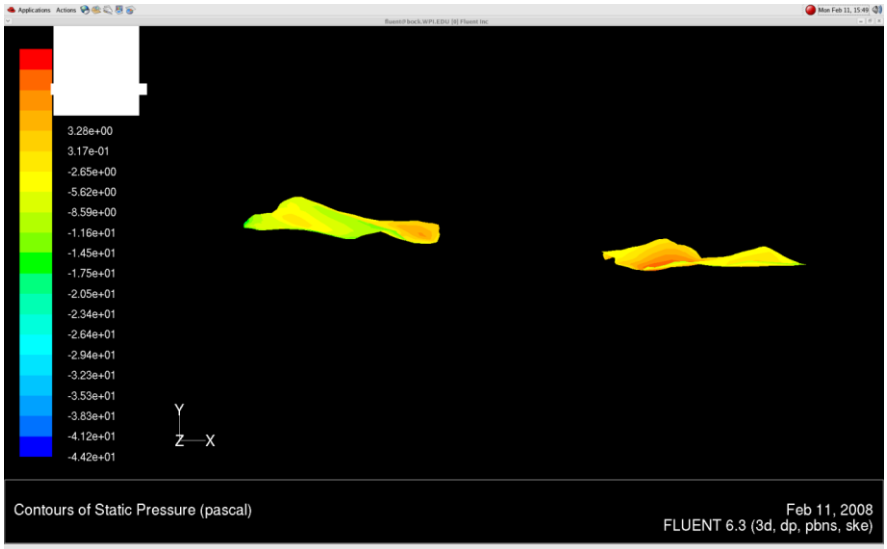

Figure 45: Pressure Contours Over Nostrils for 500 cc/s K-Epsilon Model

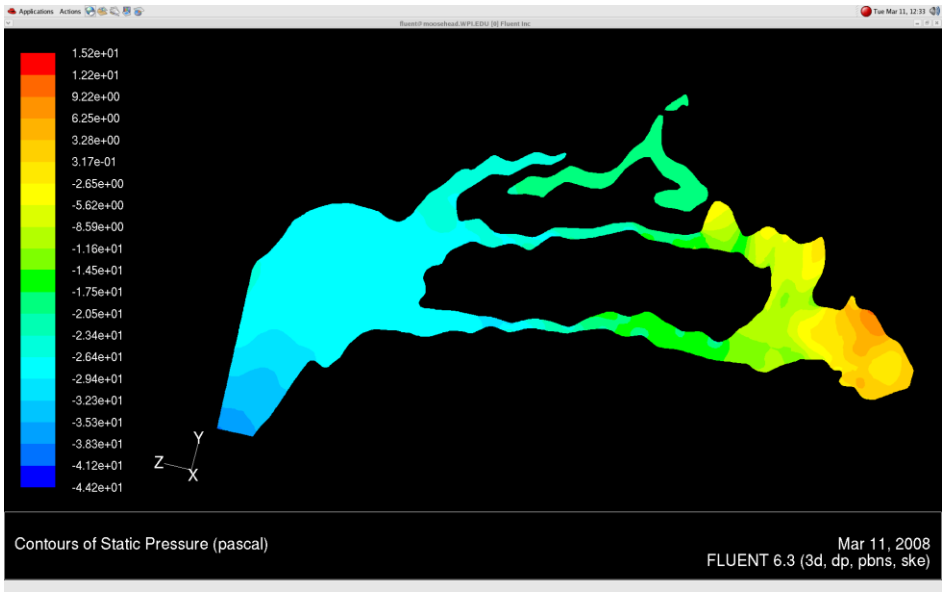

Figure 46: Side View Pressure Contour for 500 cc/s K-Epsilon Model

The pressure plot in this model shows a pressure drop of about 30 Pa in Figure 44. Also, in Figure 45 the pressure drop seen over the left nostril is about 8 Pa higher than that seen over the right nostril. This difference is significantly higher than that observed from the previous models, which is expected since this model relies on a much higher flow rate.

Velocity:

Figure 47: Velocity Contour Seen Near Entry Region for 500 cc/s K-Epsilon Model

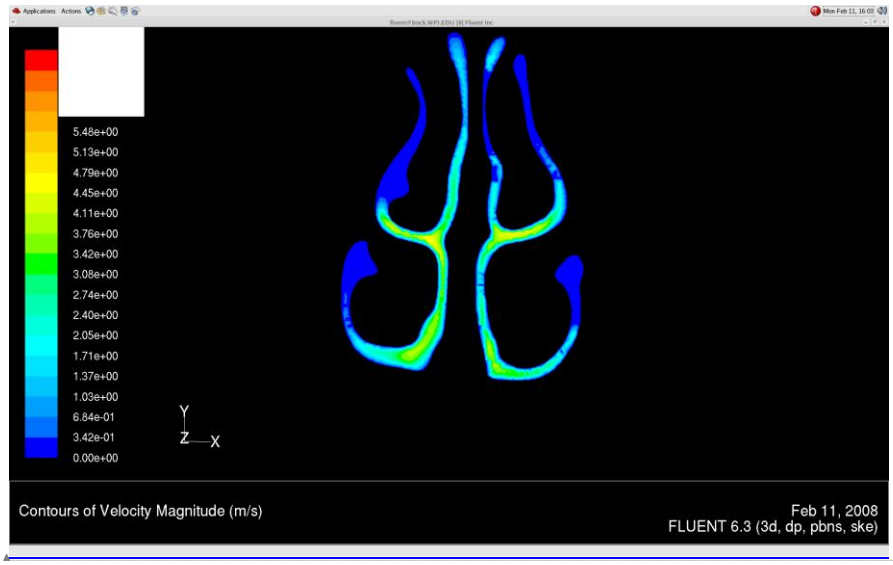

Figure 48: Velocity Contour Seen Near Turbinate Region for 500 cc/s K-Epsilon Model

Formatted: Font: 8 pt, Bold

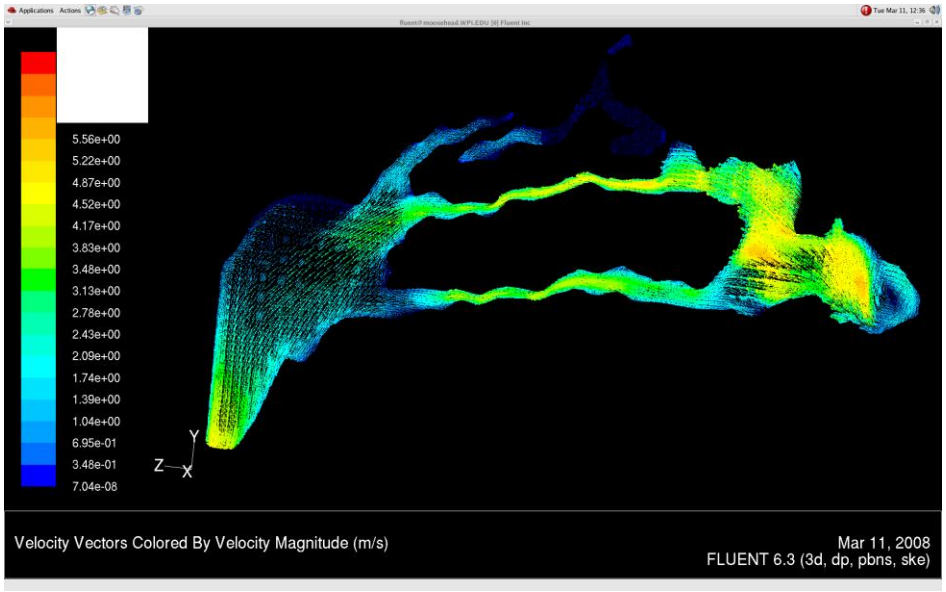

Figure 49: Velocity Vectors Seen for 500 cc/s K-Epsilon Model

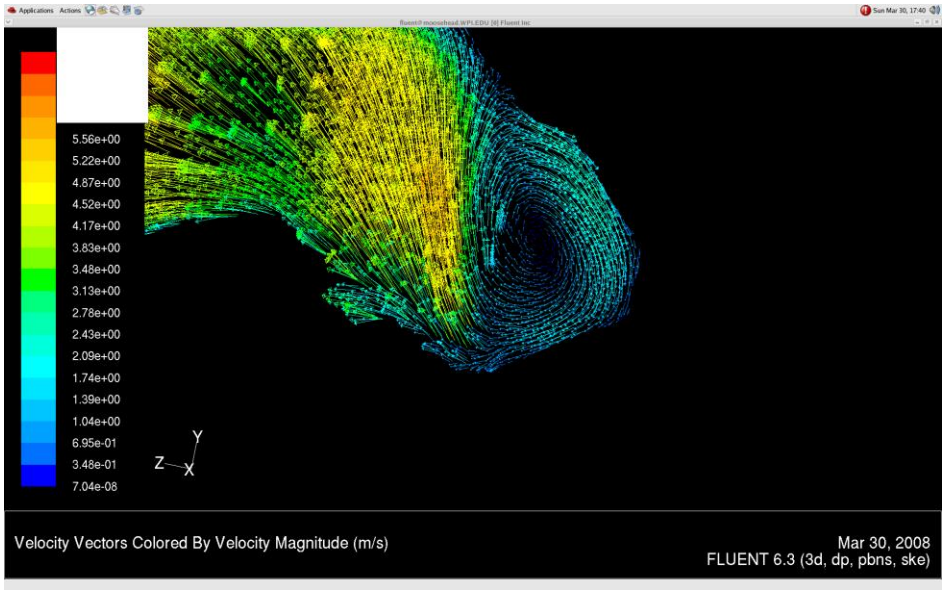

Figure 50: Vortex Vectors Seen for 500 cc/s K-Epsilon Model

The flow characteristics follow the same behavior that was observed in the previous models. However, the velocity magnitudes are much higher because of the higher flow rate. The percentage of flow passing through the inferior airway shown in Figure 49 is about the same as that in the medium flow models.

Turbulence:

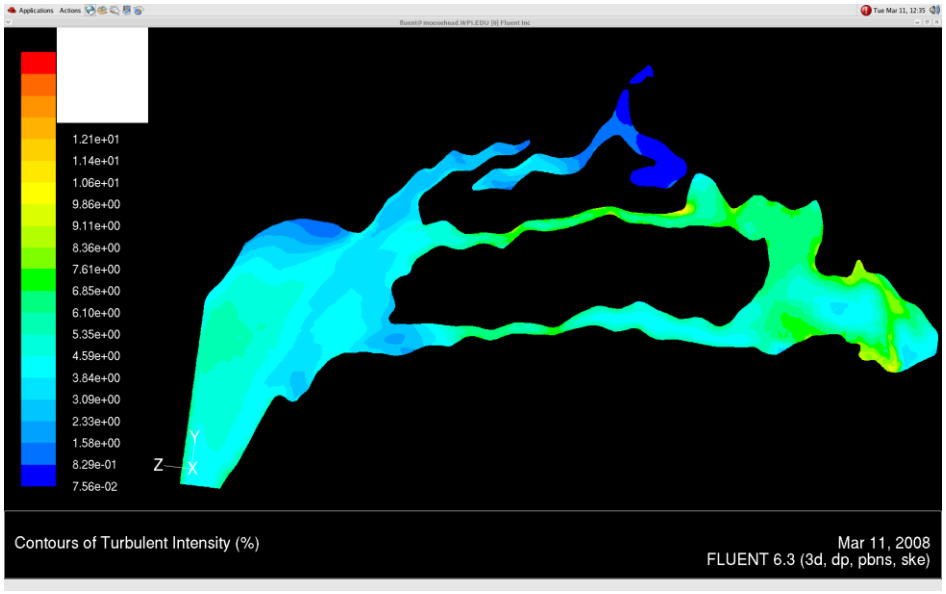

Figure 51: Turbulent Intensity Contours Seen for 500 cc/s K-Epsilon Model

The patterns seen in the turbulence intensity plot in Figure 51 is similar to those of the previous models, although the magnitudes are much higher. In this model, the turbulence intensity can reach values of almost 7%, which indicates that the flow is much more turbulent than laminar, in contrast with the model with a 100 cc/s, which observed a much more laminar flow.

Model 6:

This model used the same high flow rate (500 cc/s) as the previous model. However, this model used a laminar model. The results were then compared with those found in the k-epsilon model, so that we could observe the role that the viscous model played in our results.

Pressure:

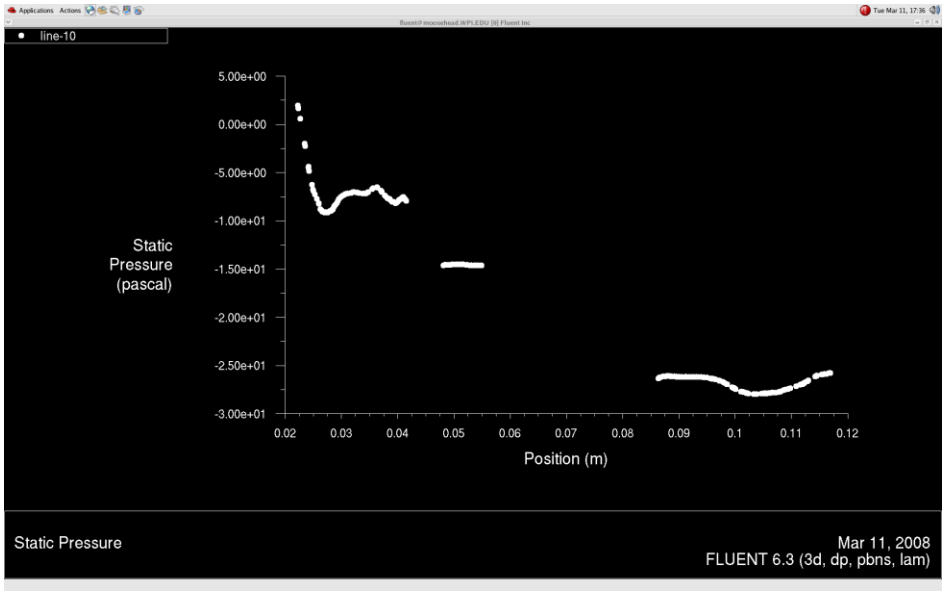

Figure 52: Pressure Drop Seen from Nostrils to Outlet for 500 cc/s Laminar Model

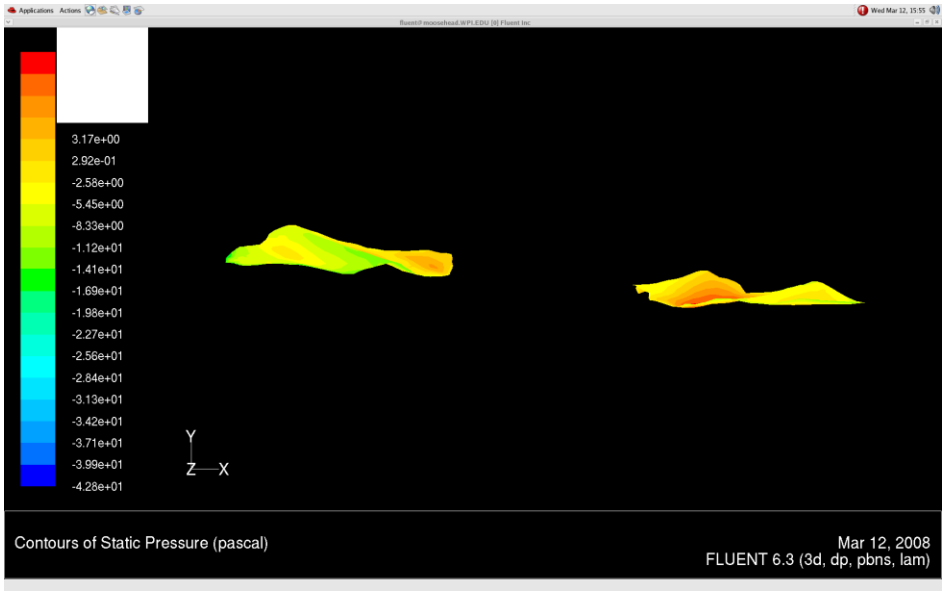

Figure 53: Pressure Contours Seen Over Nostril for 500 cc/s Laminar Model

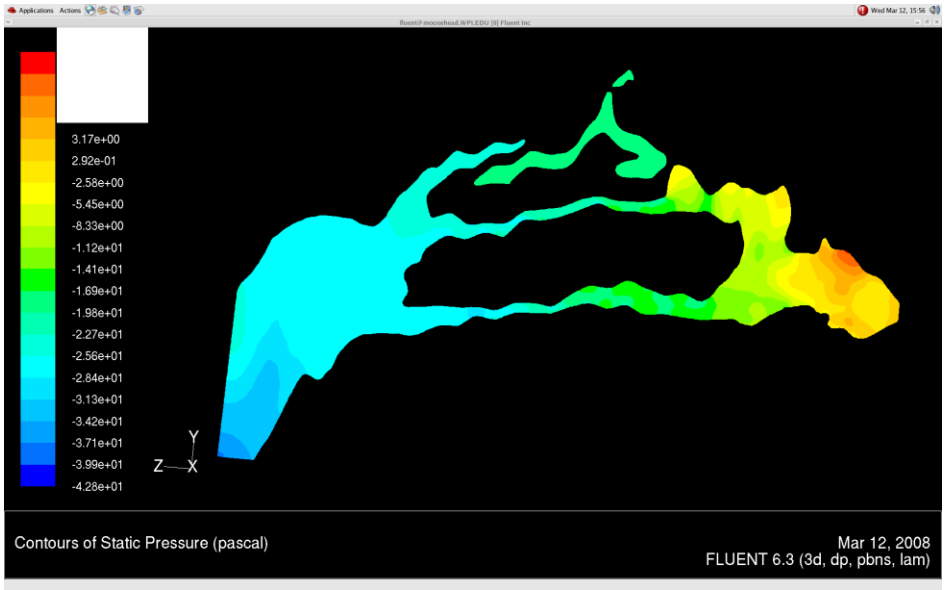

Figure 54: Pressure Contours from Side View for 500 cc/s Laminar Model

The pressure contours and graphs seen in this model are very close to those seen in the previous model. Once again, a 30 Pa drop is observed in the flow, as shown in Figure 52. The final pressure contour in Figure 54 seems to show results that are less than a couple percent smaller than those seen in the previous model.

Velocity:

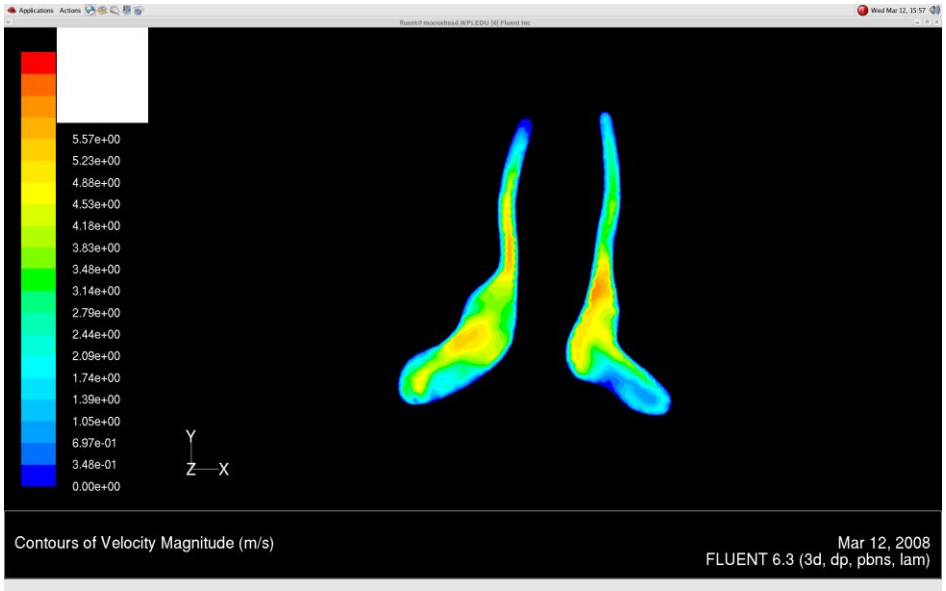

Figure 55: Velocity Contours Seen Near Entry-Region for 500 cc/s Laminar Model

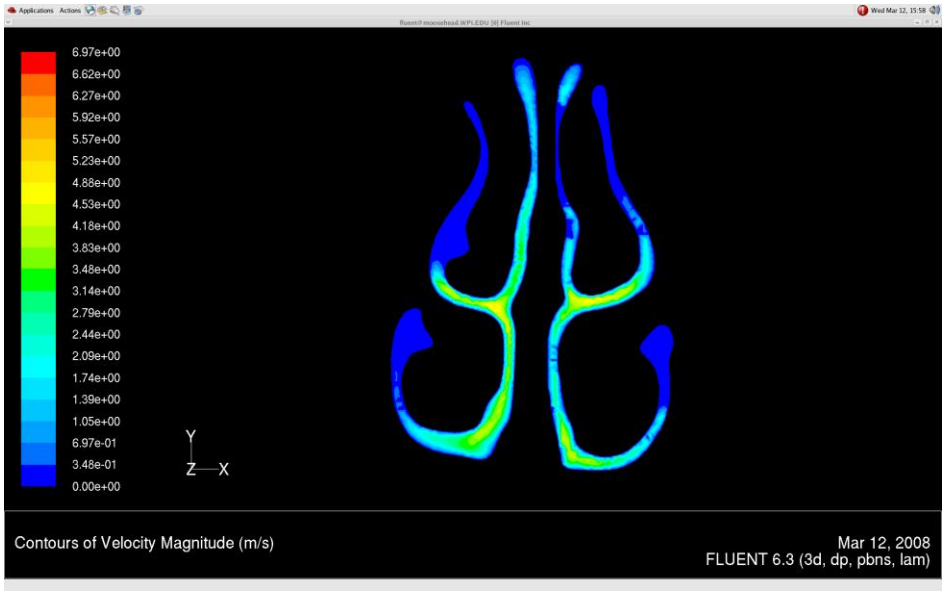

Figure 56: Velocity Contours Seen Near Turbinate Region for 500 cc/s Laminar Model

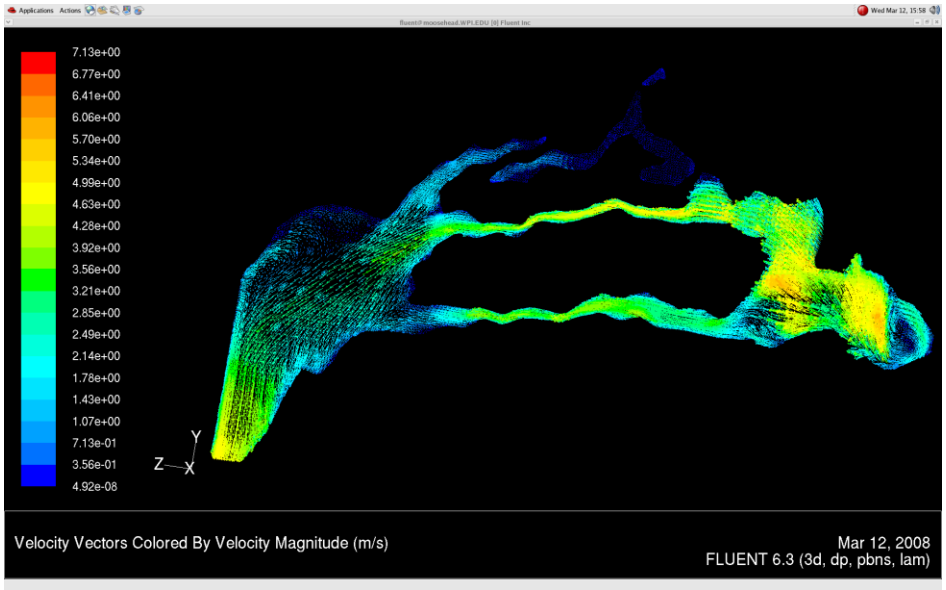

Figure 57: Velocity Vectors Seen for 500 cc/s Laminar Model

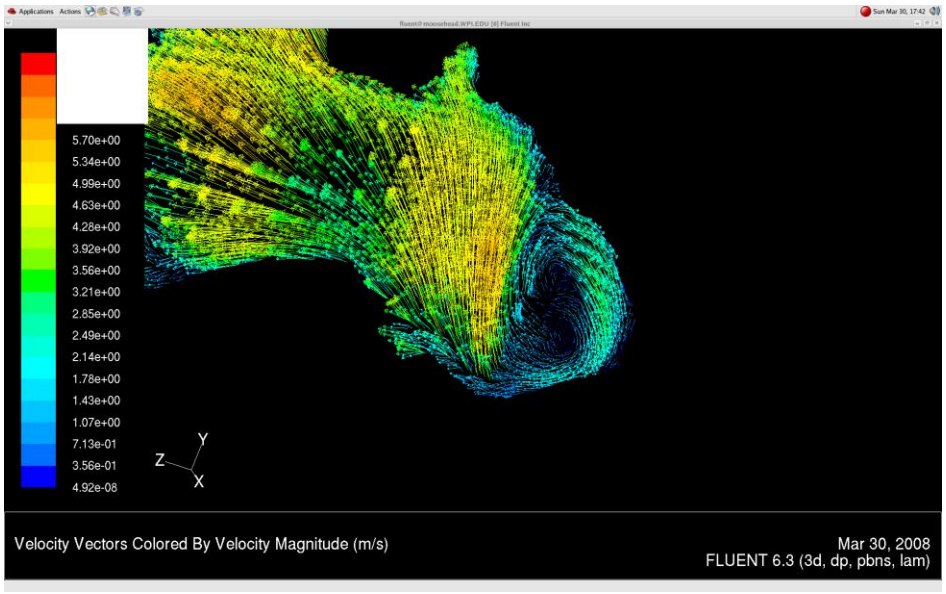

Figure 58: Vortex Vectors Seen for 500 cc/s Laminar Model

Studying the velocity vector and contour plots shows that the flow follows the same behavior observed in the k-epsilon model. The only distinction is that the vortex shown in Figure 58 does not show the same organized formation as the one in the k-epsilon model, shown in Figure 50.

Unsteady Results and Discussion

Table 1: Unsteady Results for Various Times and the Steady Flow Rates they Correspond to.

Time	Corresponding (Steady) Flow velocity(m/s)	Volumetric flow(cc/s)	Steady Flow Comparison
0.4	3	300	300 cc/s
0.8	5.2	520	500 cc/s

1.2	5.2	520	500 cc/s
1.6	3.15	315	300 cc/s
2.0	0.13	13	13 cc/s
3.5	3.7	370	370 cc/s

Table shows the outputs seen at various flow rates in the unsteady model, and what steady state flows they correspond with. Also, this table explains which steady state flow rates were used to compare to these unsteady results. The table explains that the steady state results were not exactly the same as the corresponding unsteady results, which can explain why there may be a discrepancy in the data collected.

Pressure:

Time = 0.4 s.

The first time that was output was 0.4 seconds. By observing the graph in Figure 59, it is clear that there is a pressure drop of about 16 Pa, and the corresponding steady state model in Figure 90 shows a pressure drop of 14 Pa, which is to be expected considering that the steady state flow is slightly smaller. This was determined by defining a line that traveled from the nostrils to the outlet, and calculating the pressure changes along this line. The unsteady model showed the same pressure drop as the steady state model. The fact that there is not a difference between the steady and unsteady models suggests that at this flow rate, the unsteady terms do not have a significant effect on the pressure drop. Also, observing the pressure contours, it is also obvious that the two models are similar, and would probably have the same magnitudes if they shared the same flow rate.

Time = 0.8 and 1.2 s. (Same flow rate)

After analyzing the pressure graphs and contours for the times 0.8 and 1.2 seconds into the breathing cycle (which have the same flow rates), we can see that for both of these times the steady and unsteady models corresponding to this time/flow rate are the same. We observe a pressure drop of approximately 32 Pa for the unsteady results in Figures 60 and 61, and 27 Pa for the steady state results

in Figure 97. Also, the contours of the two models show the same patterns, and also have very similar magnitudes. The small discrepancy is most likely caused by the fact that the steady state model relies on a slightly smaller flow.

Time = 1.6 s.

After looking at the values at the stage 1.6 seconds into the breathing cycle, the pressure drop seen in the unsteady model was about 16 Pa in Figure 62, and the pressure drop seen in the steady model of equivalent flow is the about the same. Again, there are no obvious differences between the steady and unsteady results.

Time = 2.0 s.

At a time of 2.0 seconds, we observe a pressure drop of less than half of a Pa for both models, shown in Figures 63 and 105. Close analysis of the pressure plots show that the pressure seen over the outlet in the unsteady model is about 5 times the magnitude of the pressure seen along the same point in the steady curve. Also, the contour plots between the two models are not nearly as uniform as is seen in the other stages in the breathing cycle. Therefore, at this time value, there seems to be a discrepancy in the data between the steady and unsteady model.

Time = 3.5 s.

The last stage of the breathing cycle that was analyzed was at 3.5 seconds, which was part of the expiratory stage of the breathing cycle. At this stage, both the unsteady and steady models correspond to a pressure drop of 25 Pa. These results are seen in Figures 64 and 117.

If the quasi-steady flow condition is valid, both the steady and unsteady models would indicate exactly the same pressure drop. Our results indicate that they are the same for every time for most flows. The only time that we observed where there was a discrepancy between the steady and

unsteady models was at 2.0 seconds, where the flow was transitioning from the inspiratory cycle to the expiratory cycle.

Velocity:

Carefully studying the contours and vector plots, we can see that there is almost no difference in the flow fields in between the unsteady results at this time and the steady state results. Because the flow rate in the steady state model is slightly smaller than that seen in the unsteady model, the magnitudes seen in the velocity fields is slightly lower. If the inlet velocity was identical between the two models, the graphs would probably be exactly the same.

In addition to the magnitudes being very similar, the vortice formation is also the same between the steady and unsteady models. In each model, the only vortices that appear are seen in the entry region, prior to reaching the turbinates. In these cases, the vortice is seen near the area near the boundary between the lower and middle airways, which is what was suggested in the literature.

The only case where the velocity behavior exhibited in the unsteady model did not match that seen in the corresponding steady state model was at the stage 2.0 seconds into the breathing cycle. The most logical explanation for this is that because this time corresponds to the shift from inspiratory flow to expiratory flow, in which case the unsteady terms may play more of a role in the computations.

Turbulence:

The turbulent intensity contours between the two models do not show any significant differences, except at a time of 2.0 seconds. This suggests that the unsteady conditions do that have a significant effect on the turbulent intensities at this flow rate.

Pressure Drops:

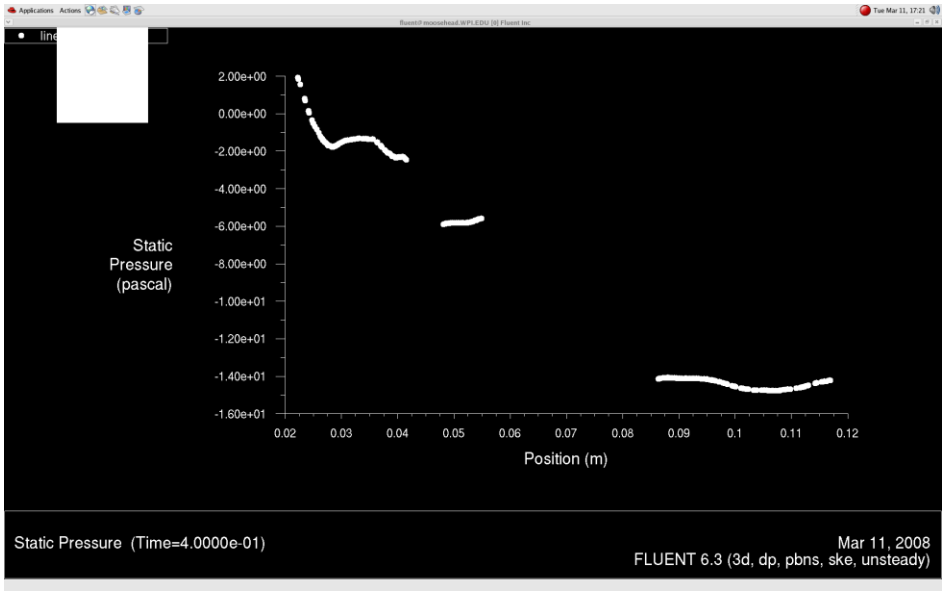

Figure 59: Pressure Drop Seen from Nostrils to Outlet at 0.4 seconds

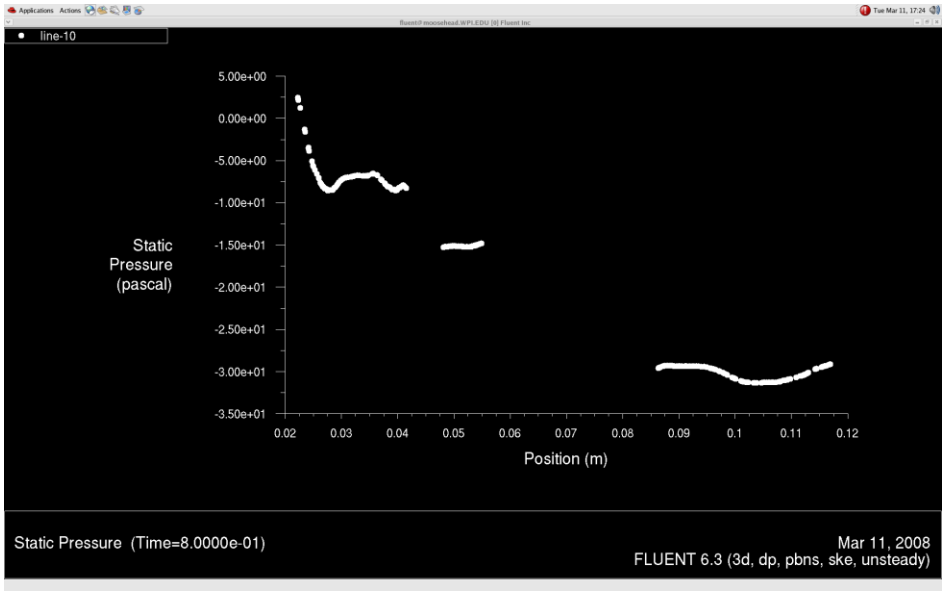

Figure 60: Pressure Drop Seen from Nostrils to Outlet at 0.8 seconds

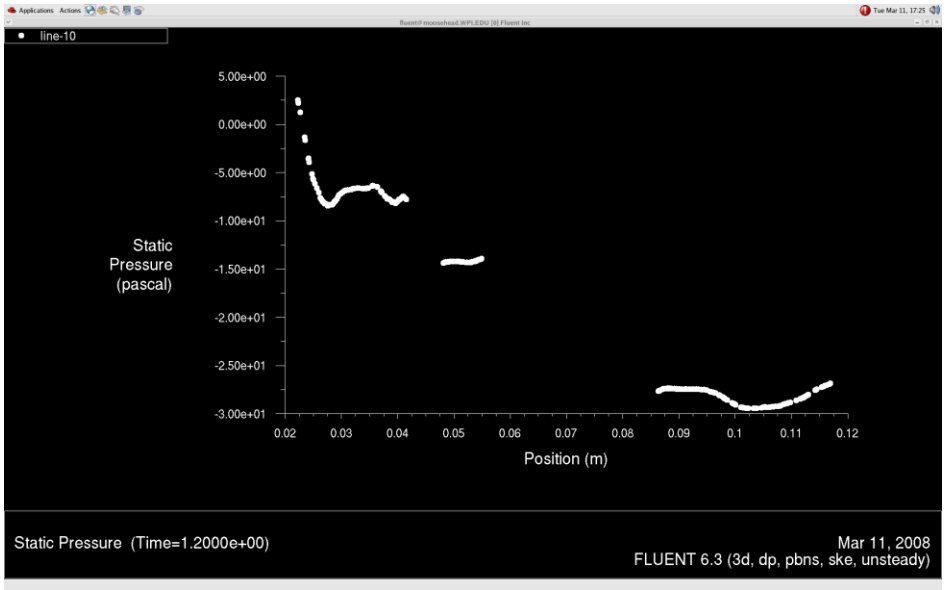

Figure 61: Pressure Drop Seen from Nostrils to Outlet at 1.2 seconds

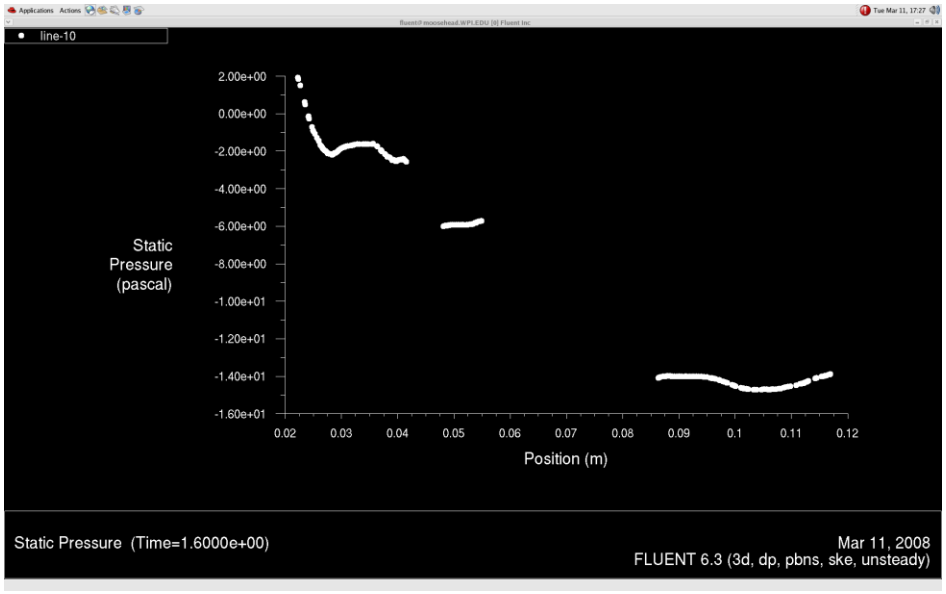

Figure 62: Pressure Drop Seen from Nostrils to Outlet at 1.6 seconds

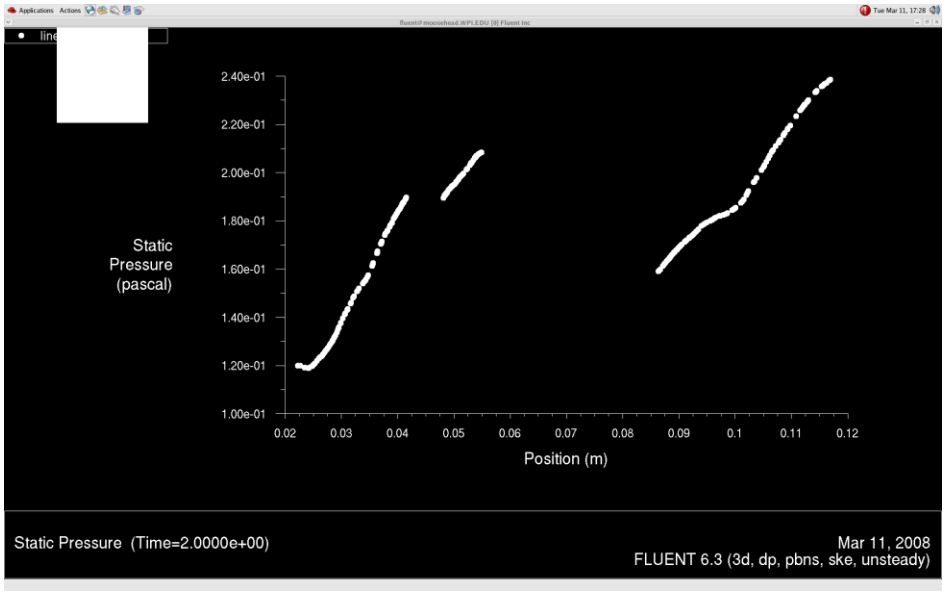

Figure 63: Pressure Drop Seen from Nostrils to Outlet at 2.0 seconds

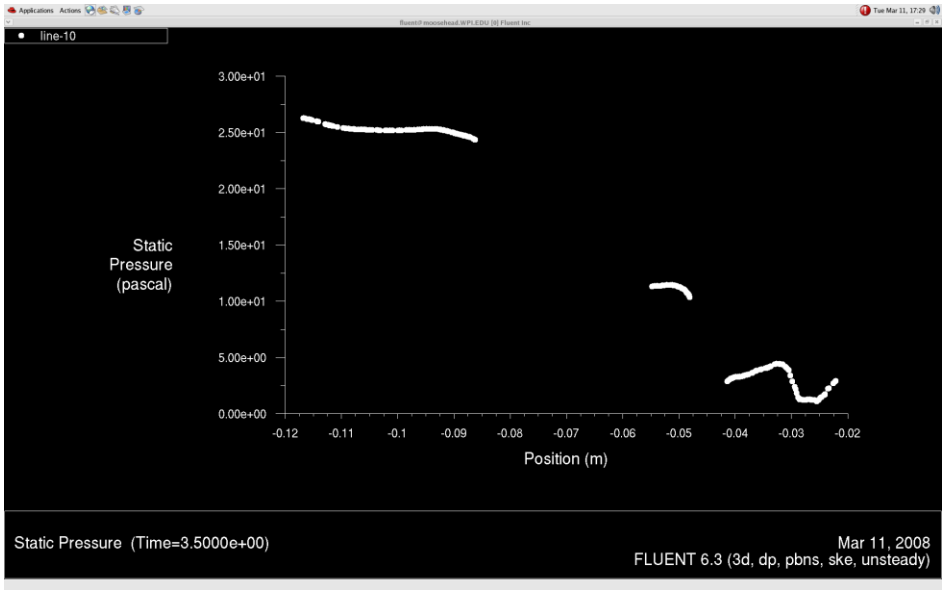

Figure 64: Pressure Drop Seen from Nostrils to Outlet at 3.5 seconds

Pressure Contours:

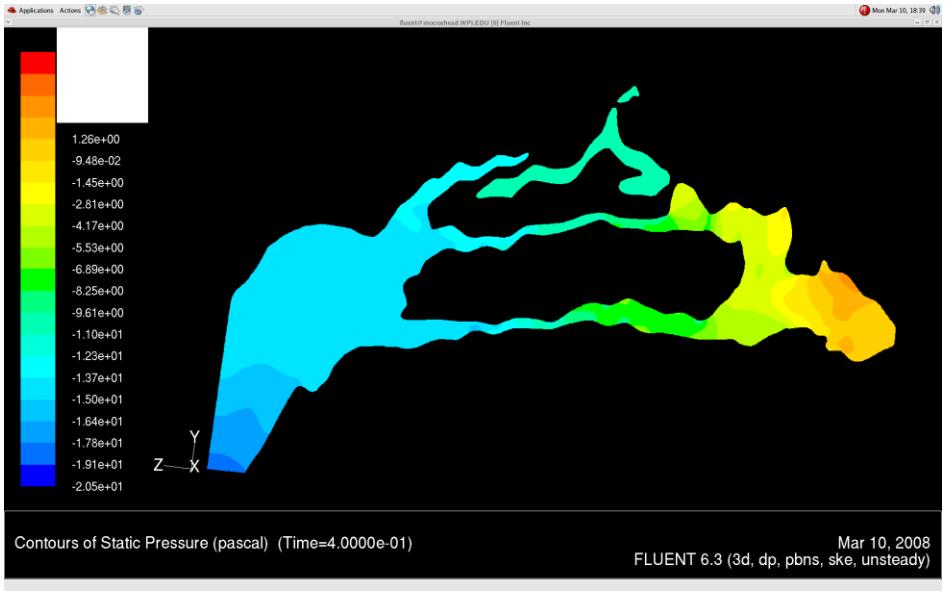

Figure 65: Pressure Contour Seen at 0.4 Seconds

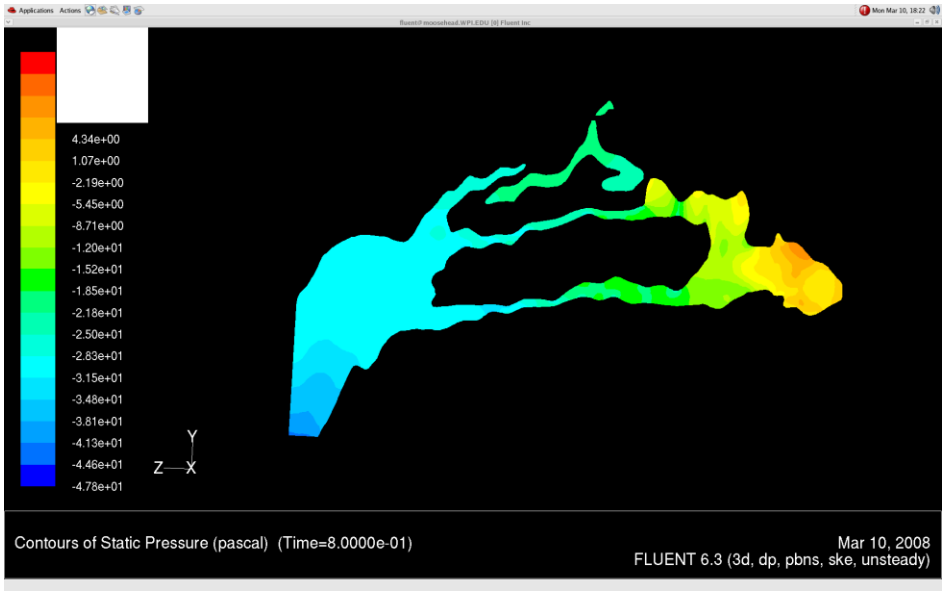

Figure 66: Pressure Contour Seen at 0.8 Seconds

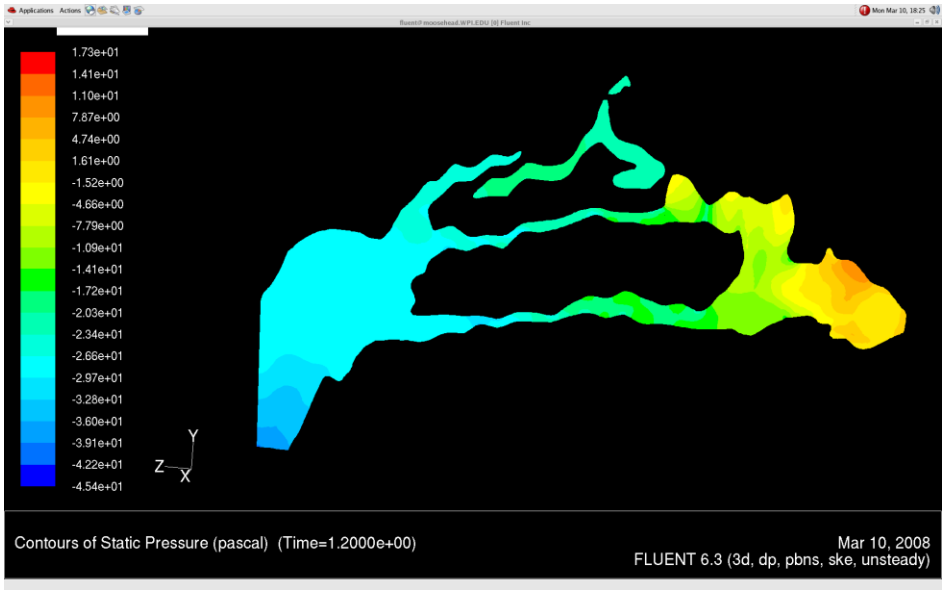

Figure 67: Pressure Contour Seen at 1.2 Seconds

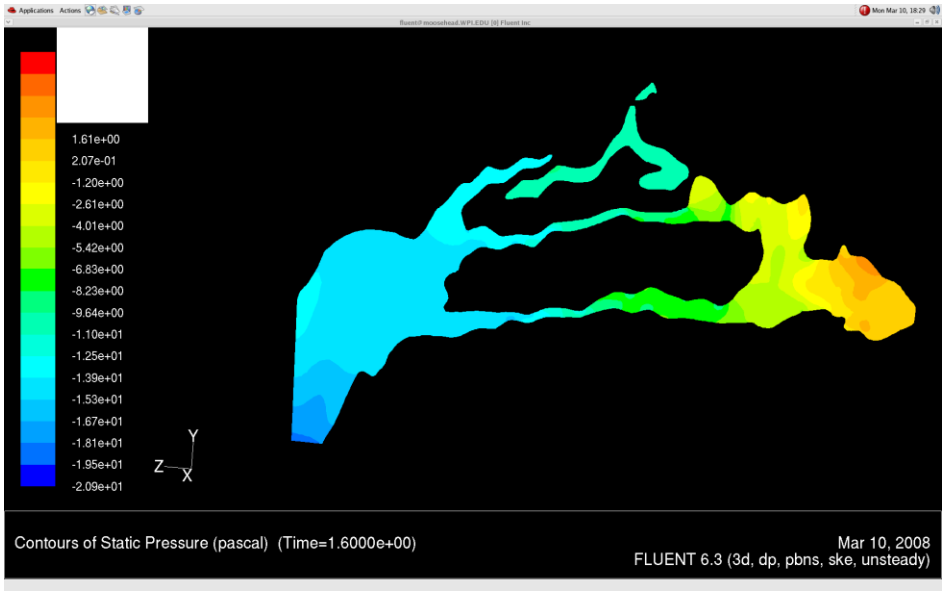

Figure 68: Pressure Contour Seen at 1.6 Seconds

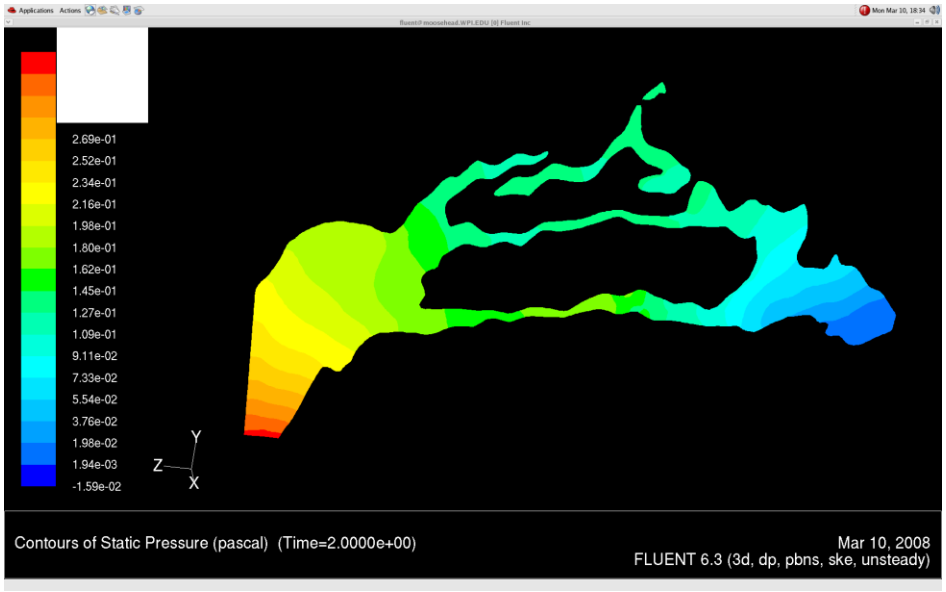

Figure 69: Pressure Contour Seen at 2.0 Seconds

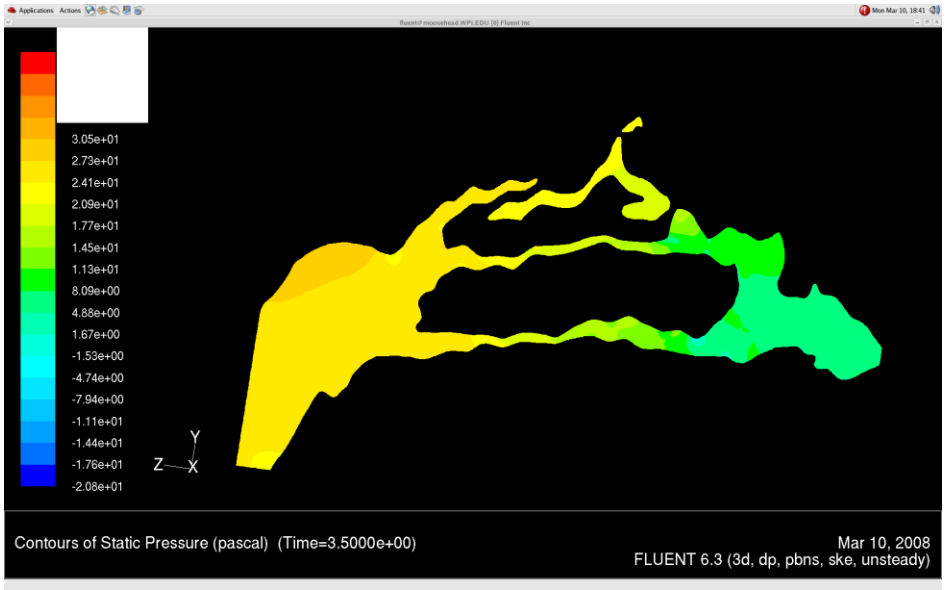

Figure 70: Pressure Contour Seen at 3.5 Seconds

Velocity:

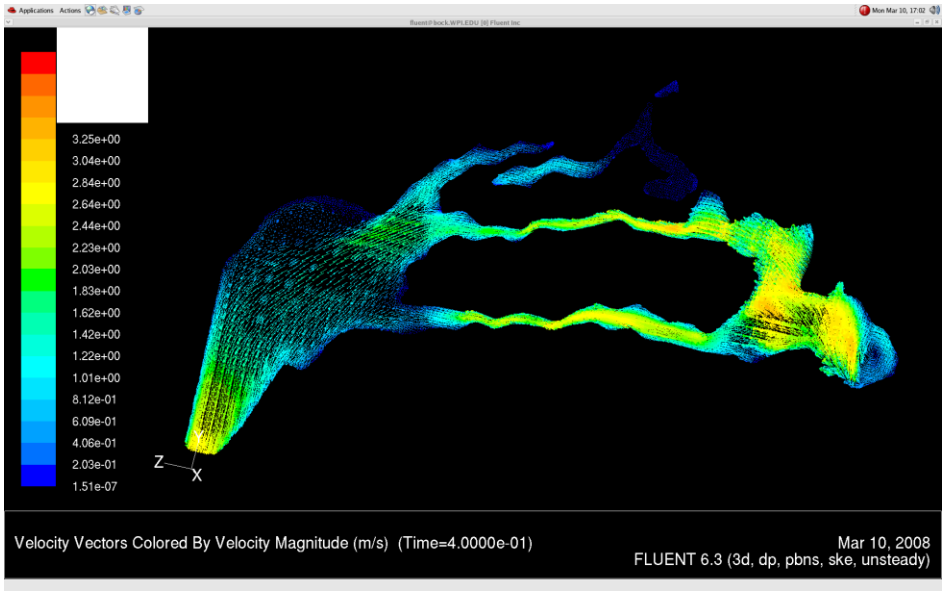

Figure 71: Velocity Vectors seen at 0.4 Seconds

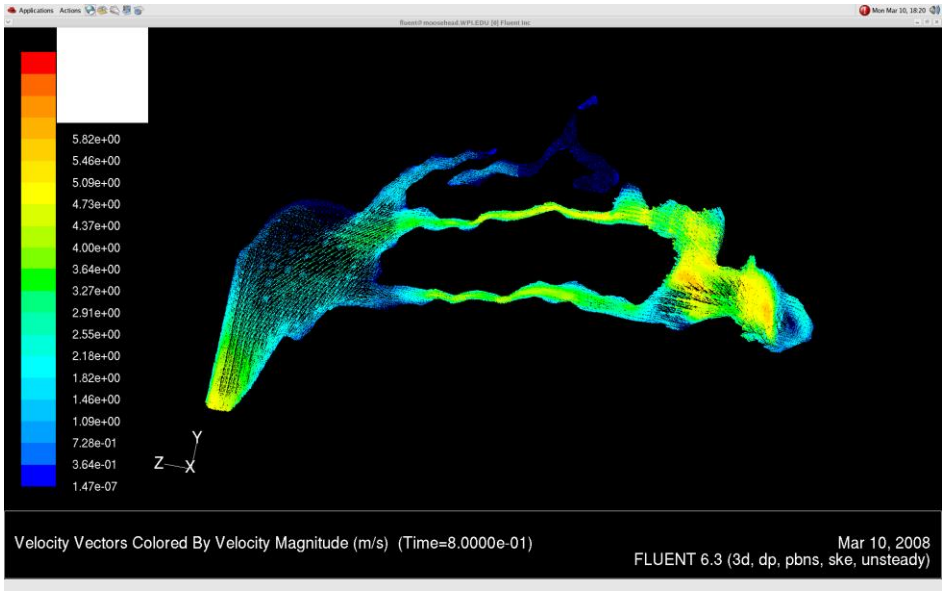

Figure 72: Velocity Vectors seen at 0.8 Seconds

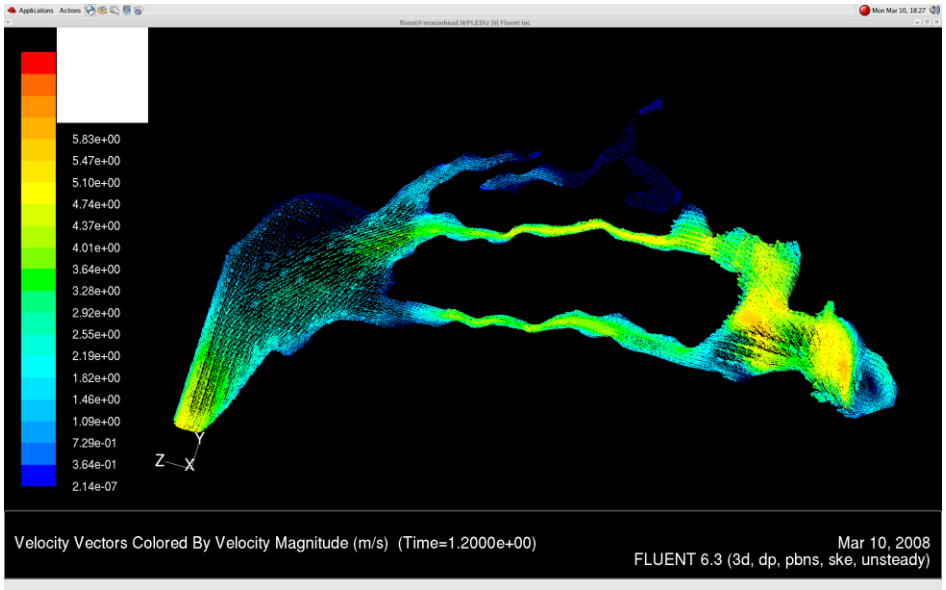

Figure 73: Velocity Vectors seen at 1.2 Seconds

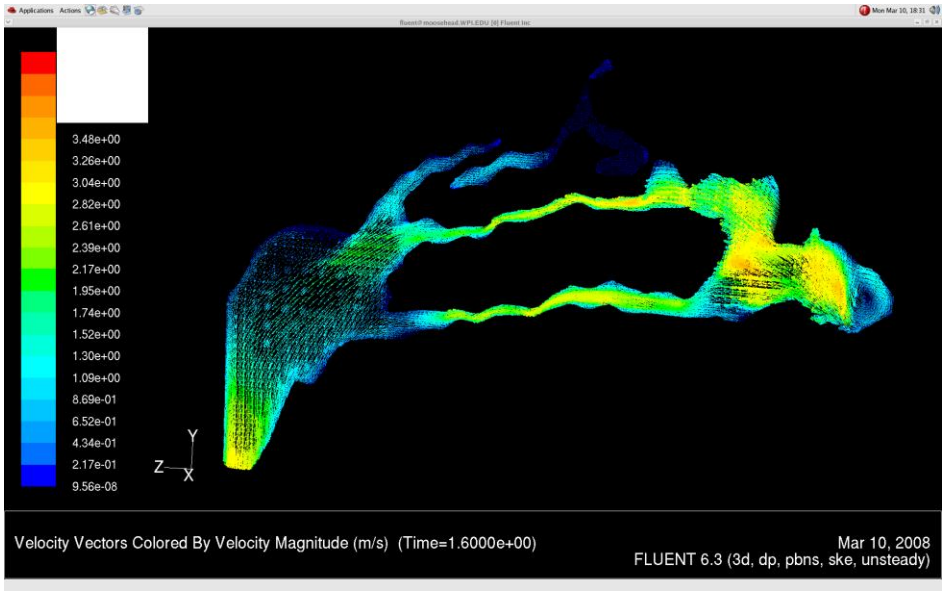

Figure 74: Velocity Vectors seen at 1.6 Seconds

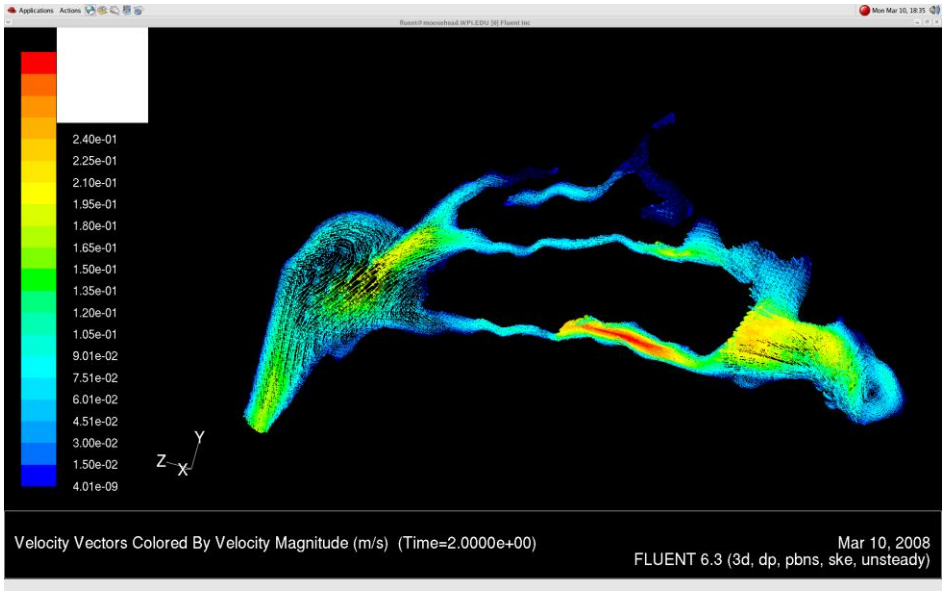

Figure 75: Velocity Vectors seen at 2.0 Seconds

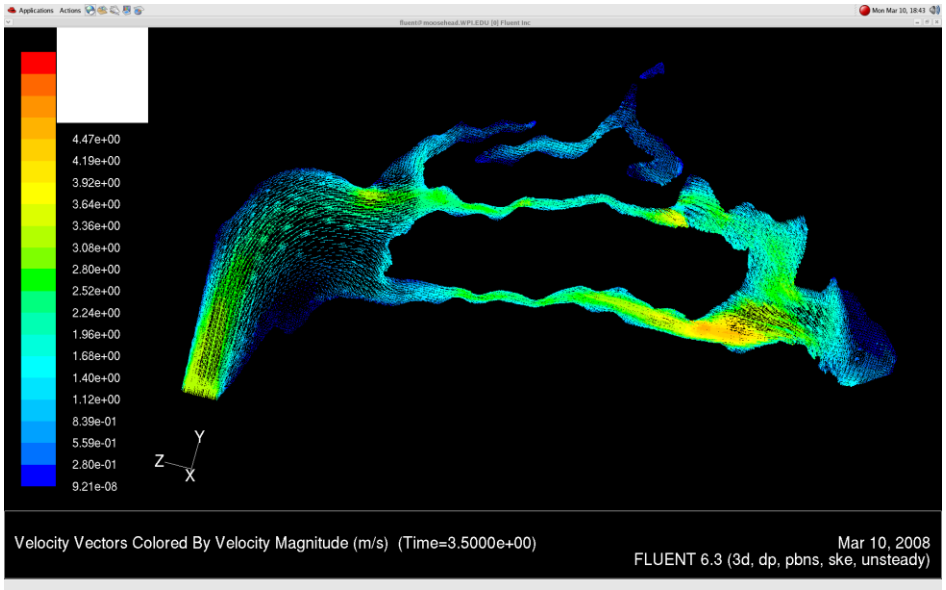

Figure 76: Velocity Vectors seen at 3.5 Seconds

Vortex graphs:

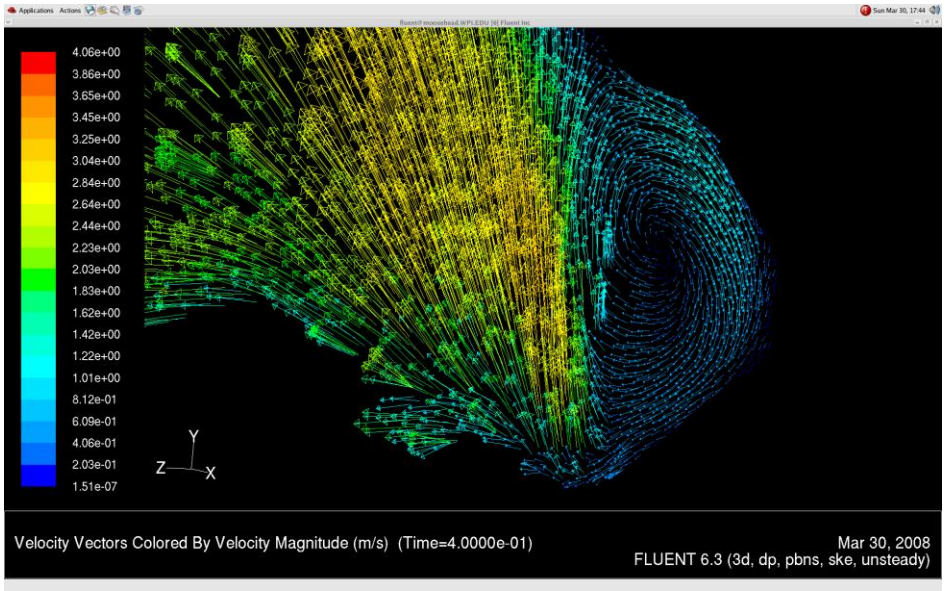

Figure 77: Vortex Vectors Seen at 0.4 Seconds

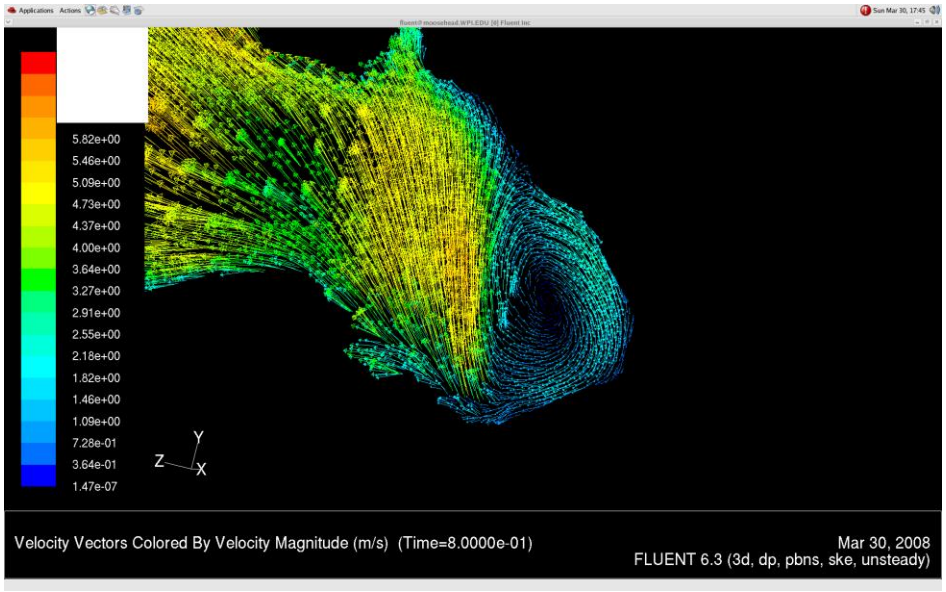

Figure 78: Vortex Vectors Seen at 0.8 Seconds

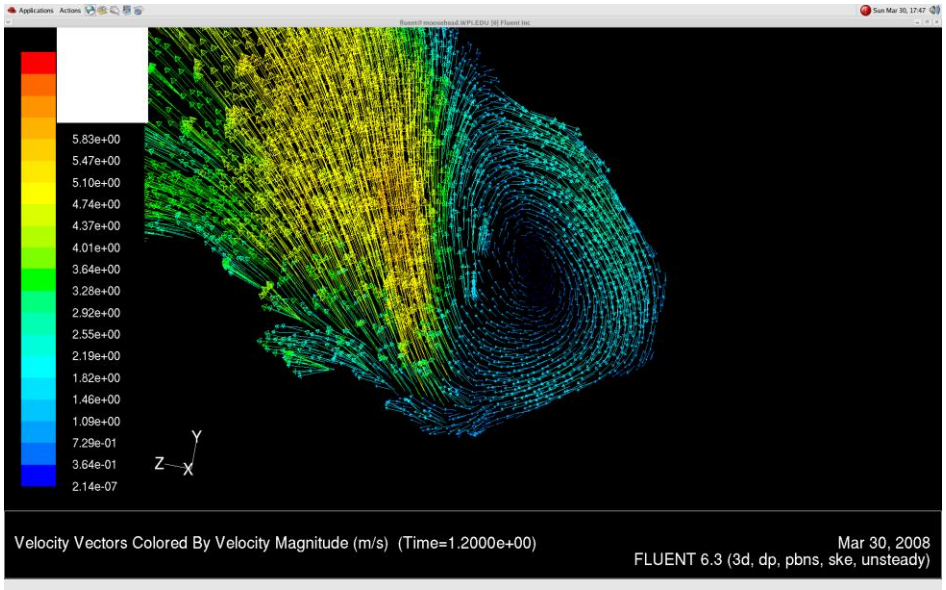

Figure 79: Vortex Vectors Seen at 1.2 Seconds

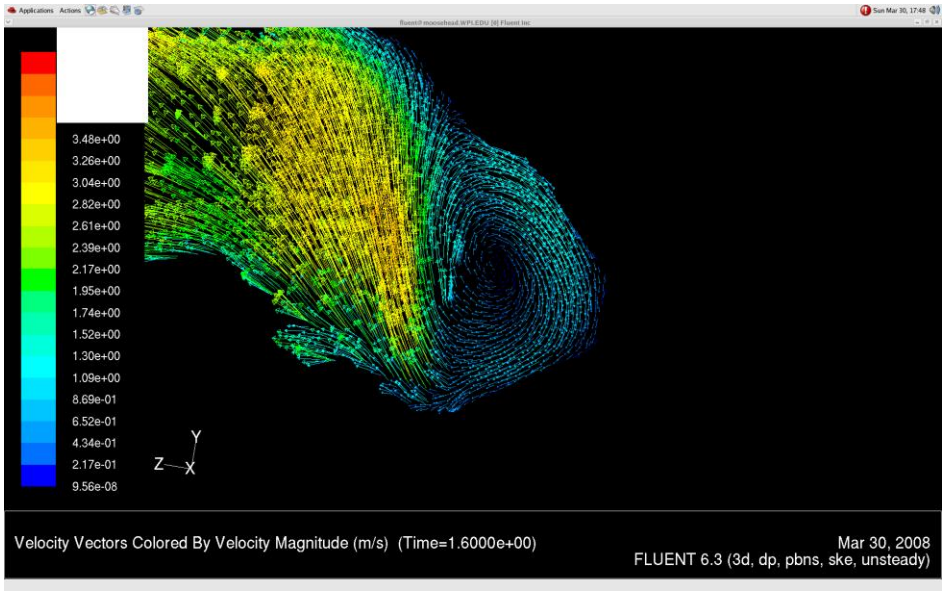

Figure 80: Vortex Vectors Seen at 1.6 Seconds

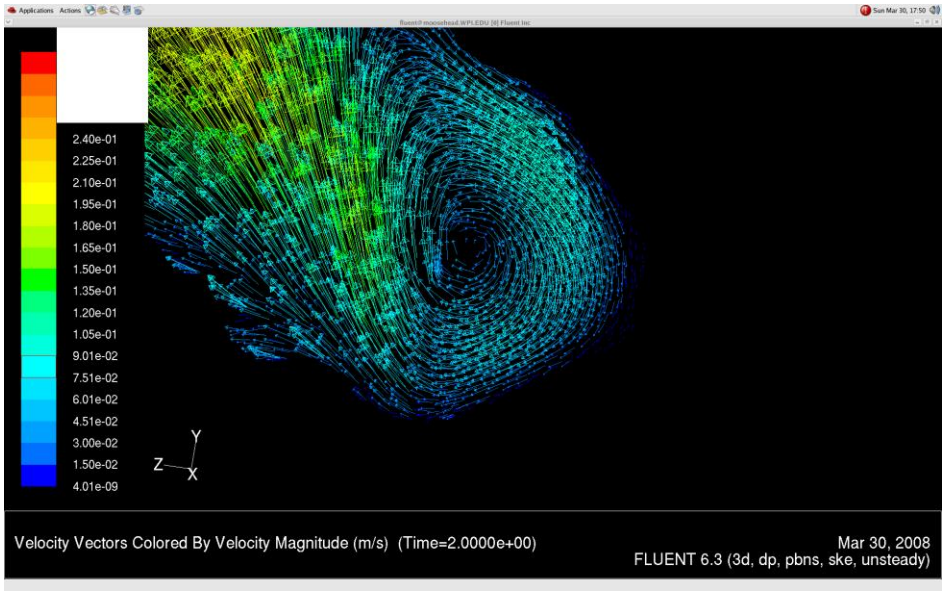

Figure 81: Vortex Vectors Seen at 2.0 Seconds

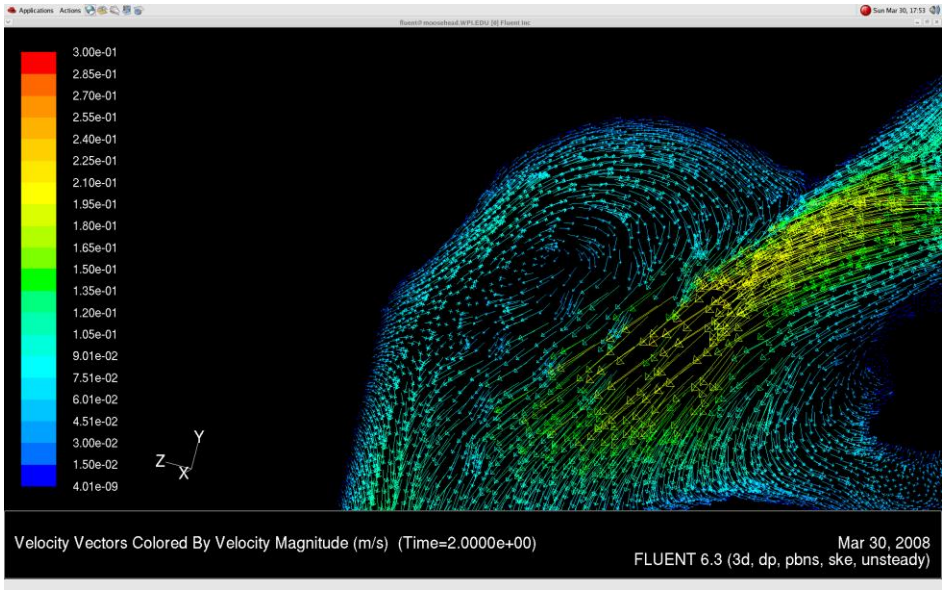

Figure 82: Vortex Vectors Seen at 2.0 Seconds

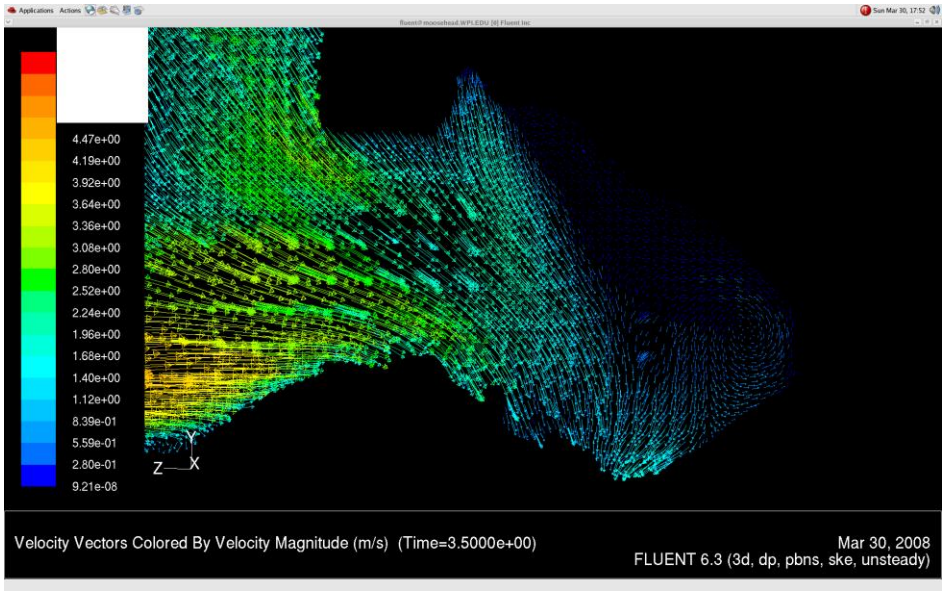

Figure 83: Vortex Vectors Seen at 3.5 Seconds

Turbulence:

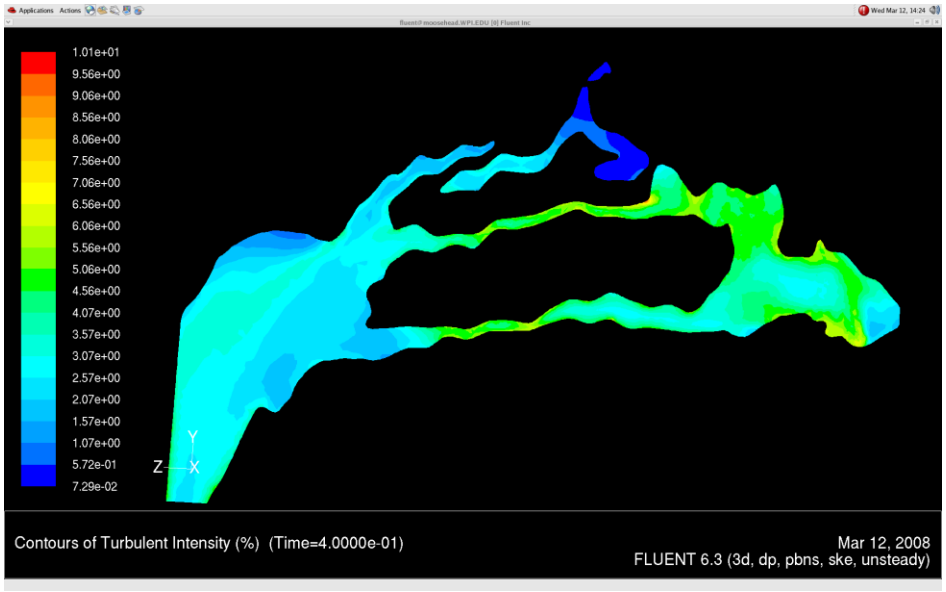

Figure 84: Turbulent Intensities at 0.4 Seconds

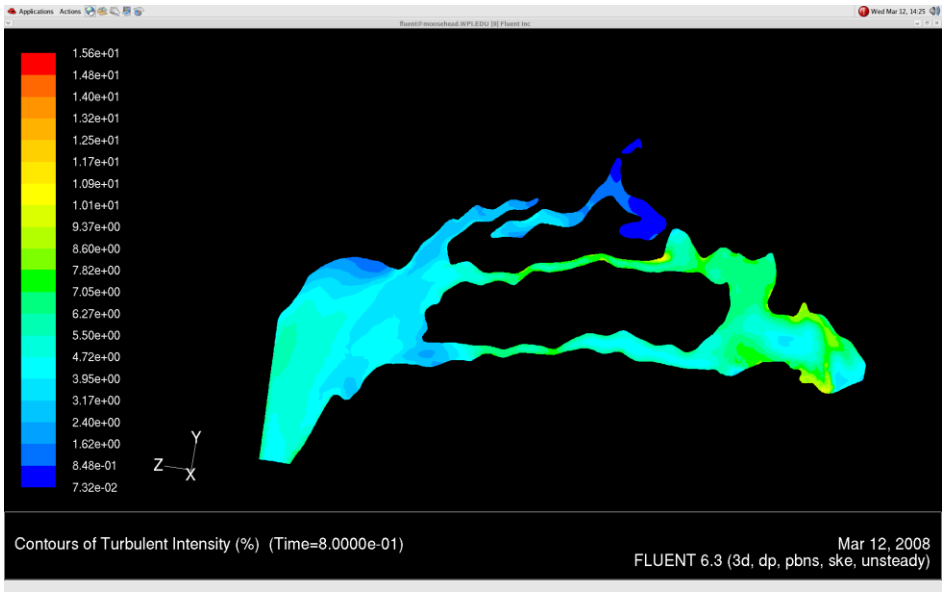

Figure 85: Turbulent Intensities at 0.8 Seconds

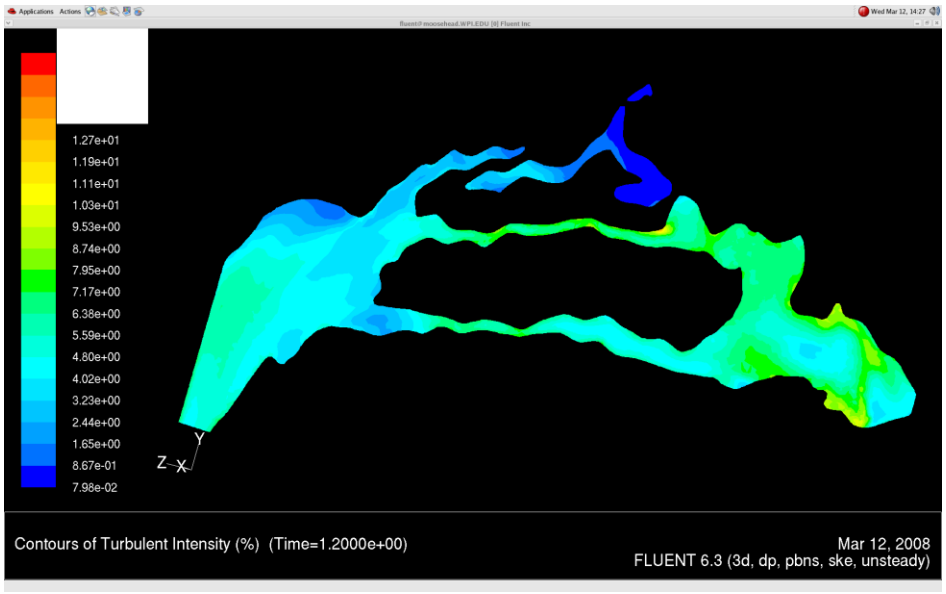

Figure 86: Turbulent Intensities at 1.2 Seconds

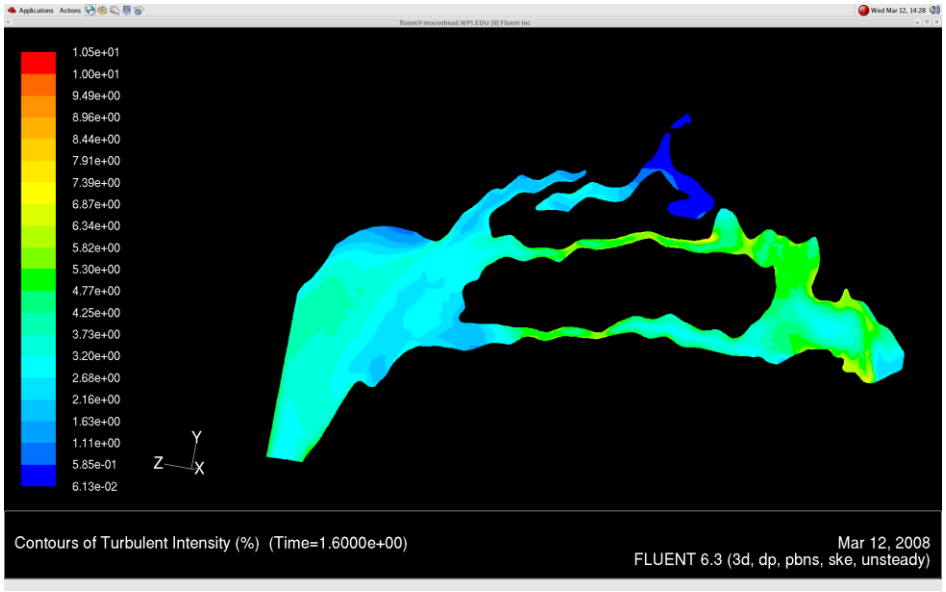

Figure 87: Turbulent Intensities at 1.6 Seconds

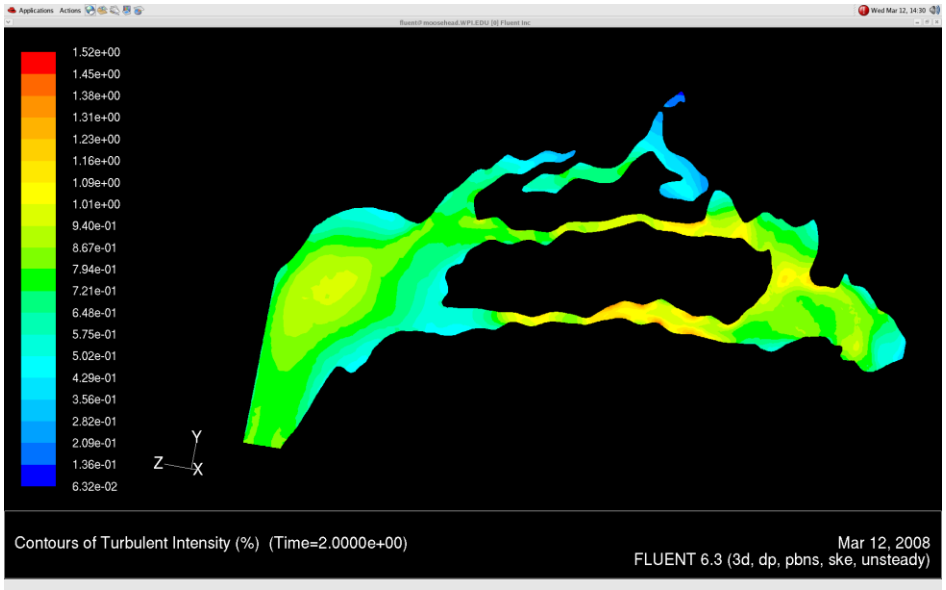

Figure 88: Turbulent Intensities at 2.0 Seconds

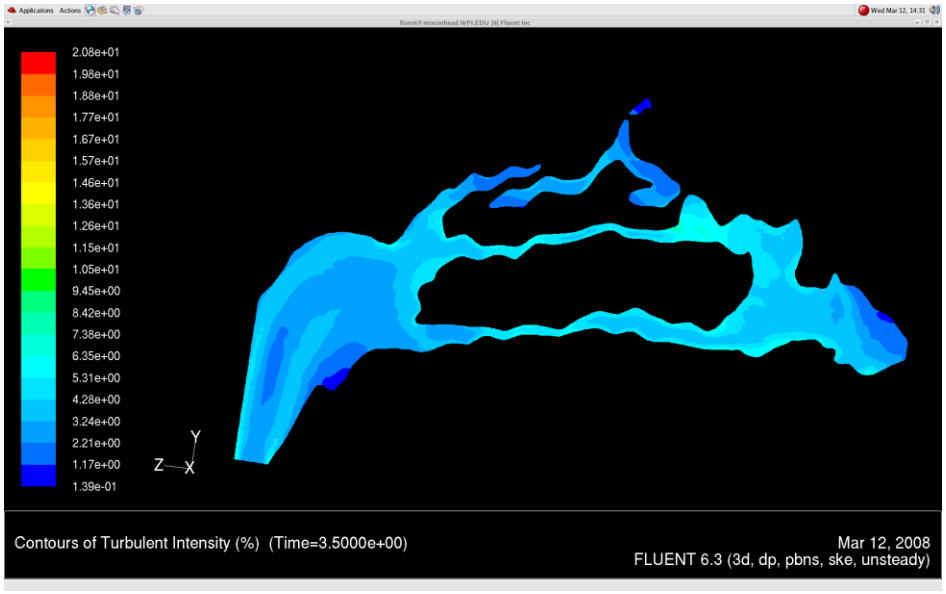

Figure 89: Turbulent Intensities at 3.5 Seconds

Corresponding Steady Plots:

Flow of 2.70 m/s (corresponds to time = 0.4 and 1.6 seconds)

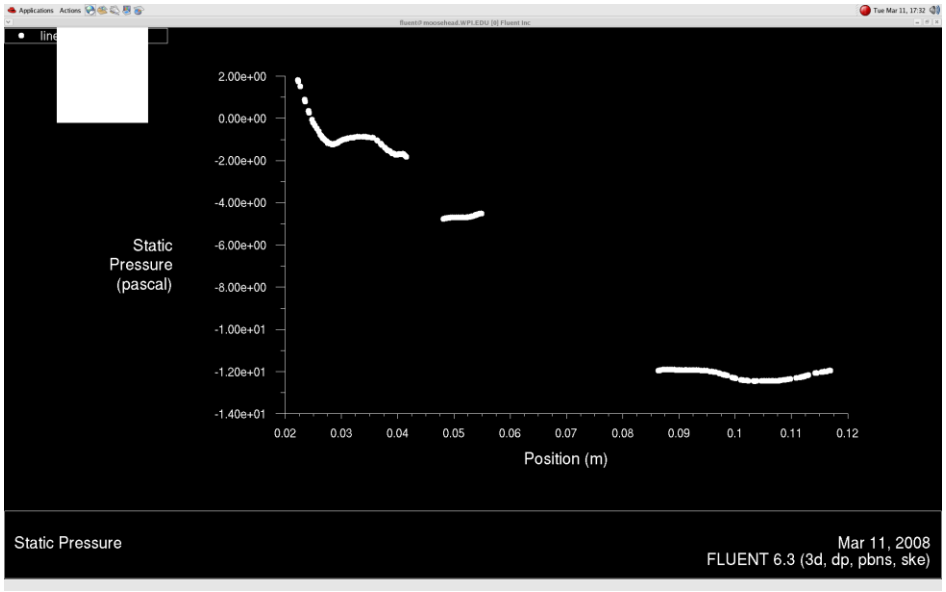

Figure 90: Steady-State Pressure drop from Nostrils to Outlet seen at 270 cc/s

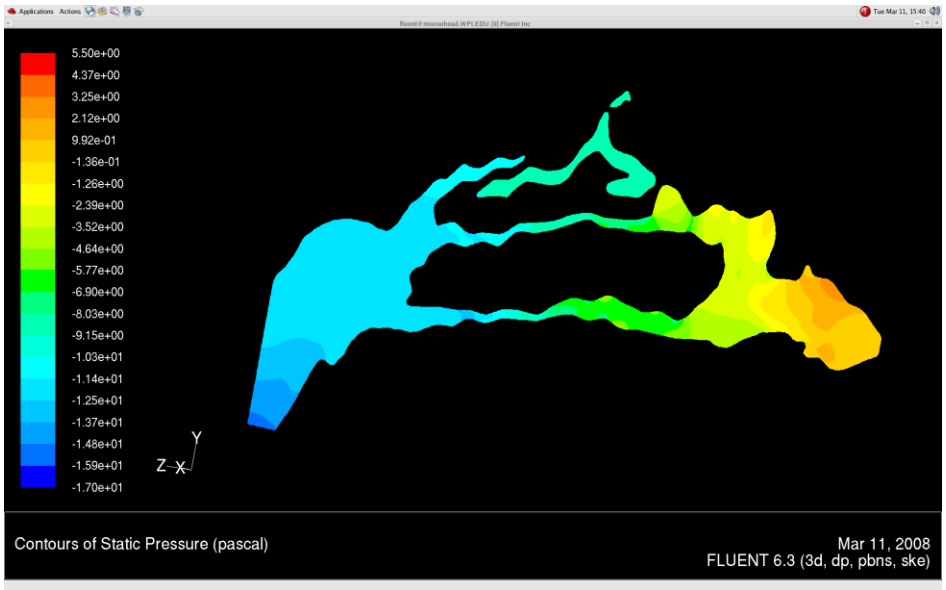

Figure 91: Steady-State Pressure Contour Seen at 270 cc/s

Velocity Profiles:

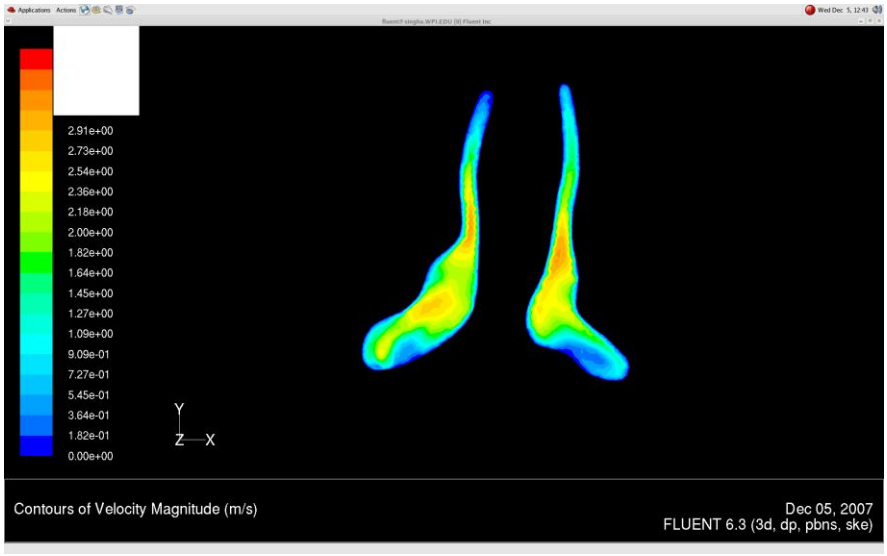

Figure 92: Steady State Entry-Region Velocity Contour Seen at 270 cc/s

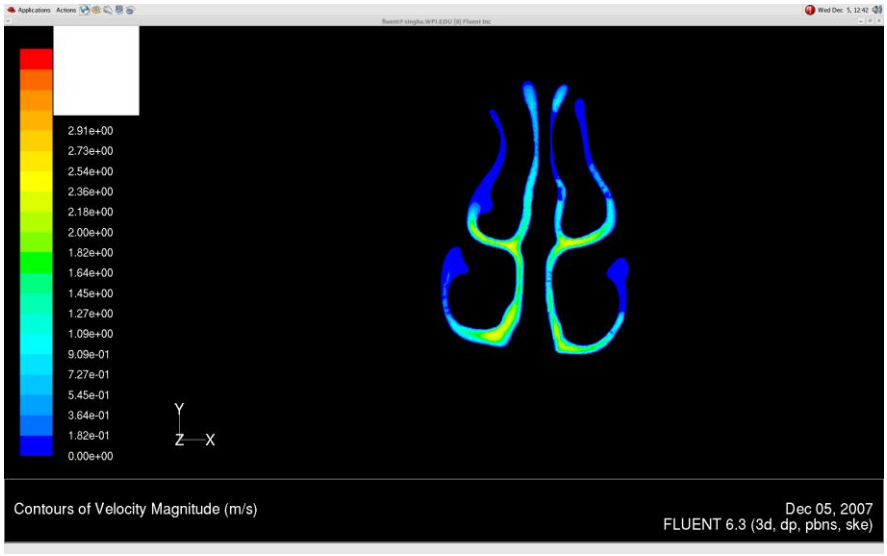

Figure 93: Steady State Velocity Contours Seen Near Turbinate for 270 cc/s

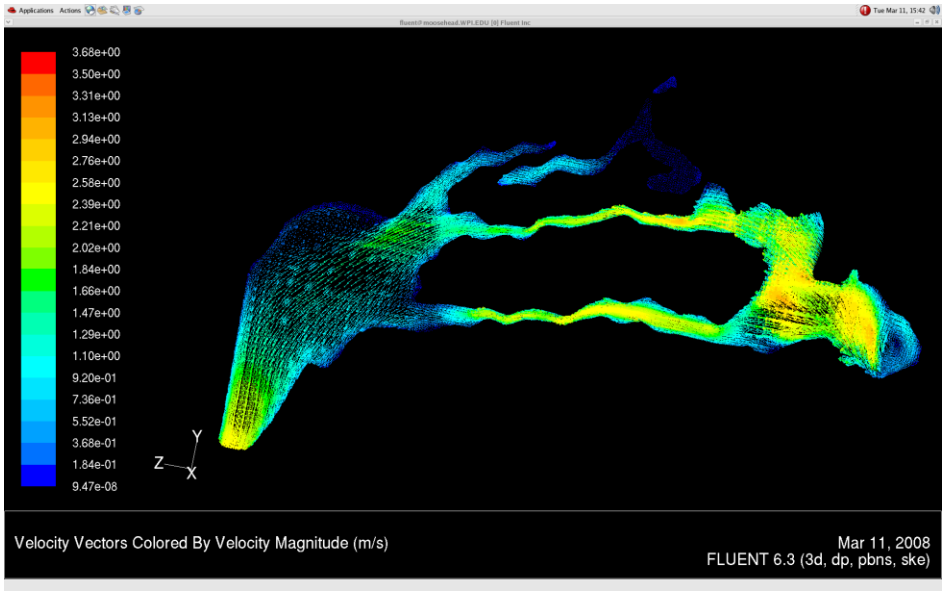

Figure 94: Steady State Velocity Vectors Seen at 270 cc/s

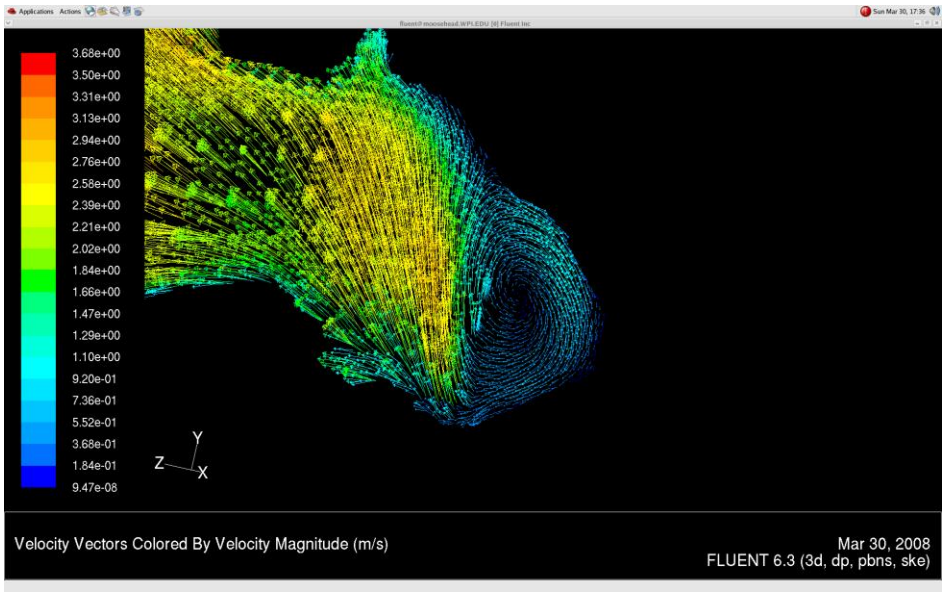

Figure 95: Steady State Vortex Vectors Seen at 270 cc/s

Turbulence:

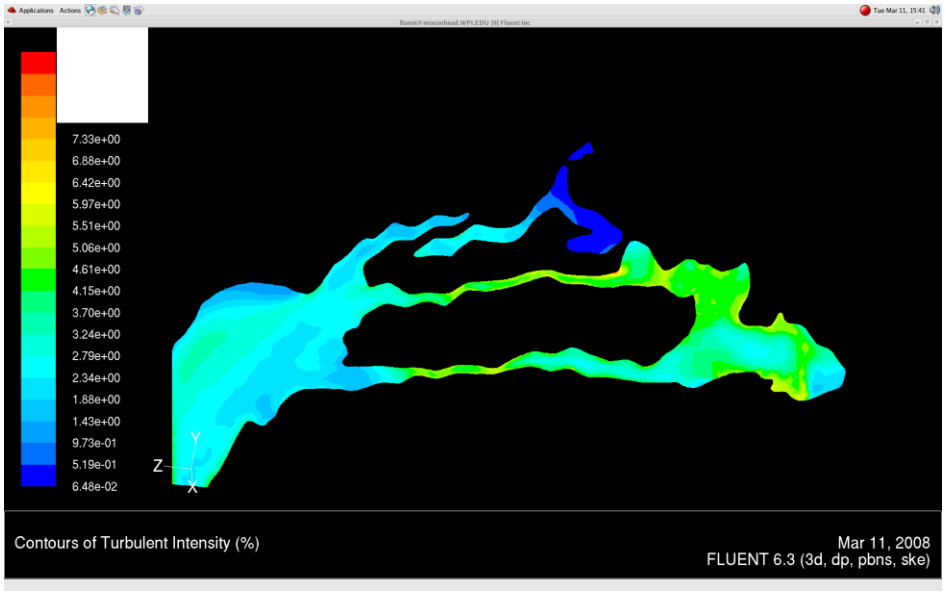

Figure 96: Steady State Turbulent Intensities Seen at 270 cc/s

Flow of 5 m/s (Corresponds to time = 0.8 and 1.2 seconds)

Pressure:

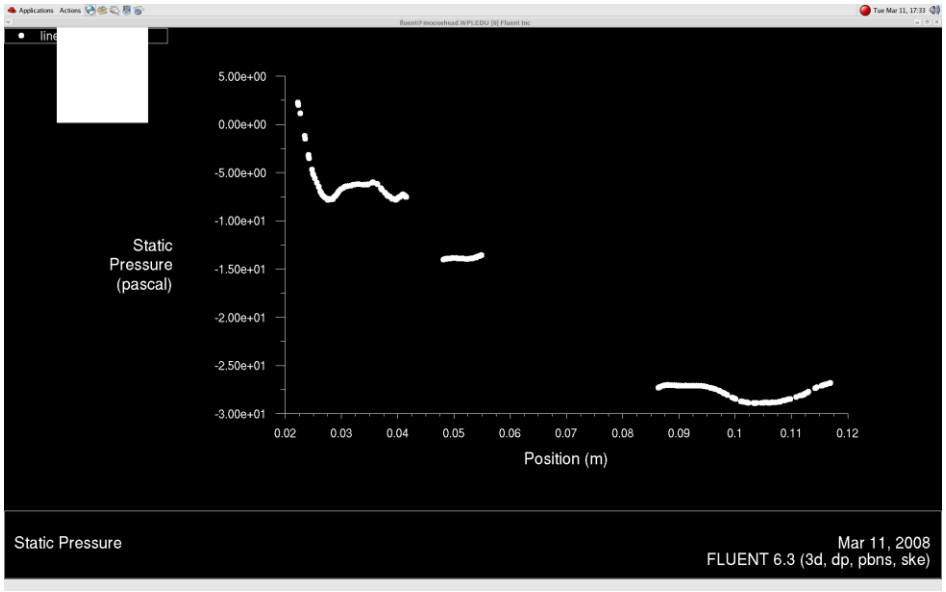

Figure 97: Steady State Pressure Drop from Nostrils to Outlet at 500 cc/s

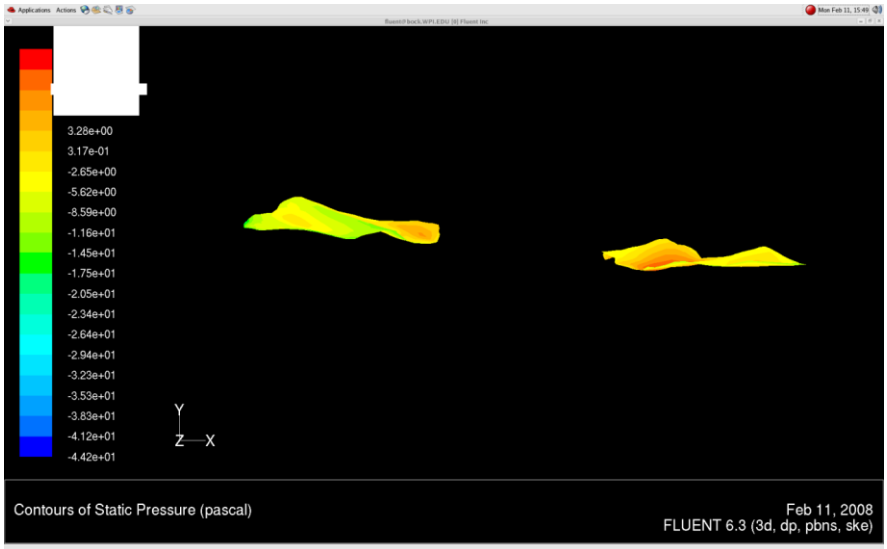

Figure 98: Steady State Pressure Contours Seen Over Nostril at 500 cc/s

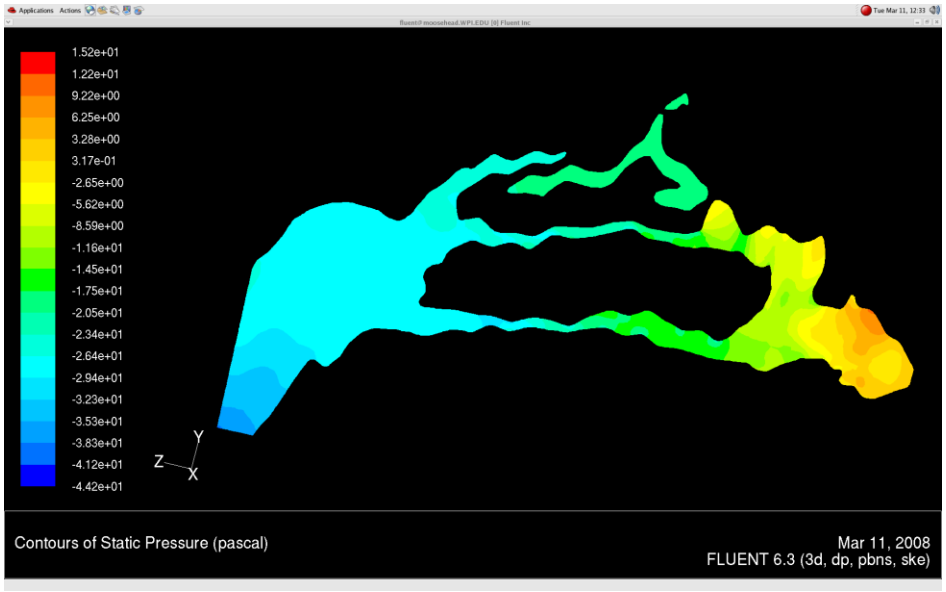

Figure 99: Steady State Pressure Contour Seen at 500 cc/s

Velocity:

Figure 100: Steady State Velocity Contours Seen Near Entry Region for 500 cc/s

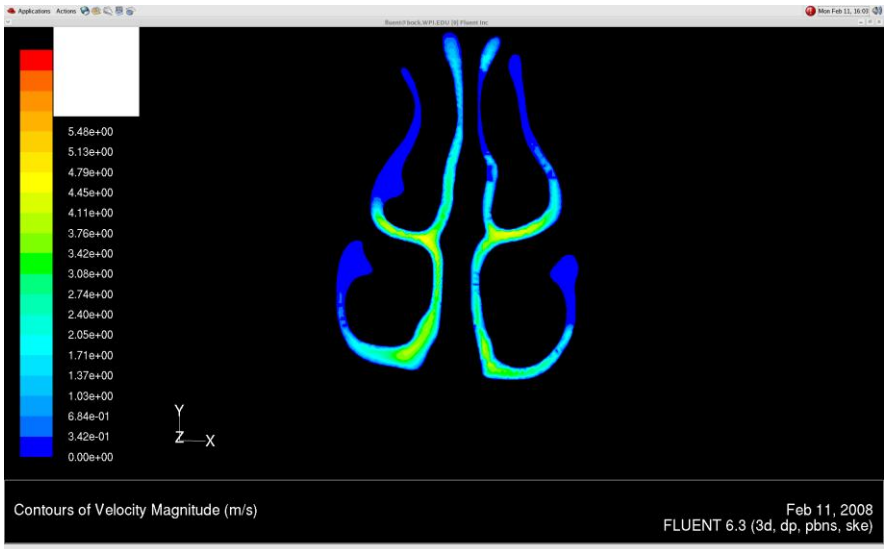

Figure 101: Steady State Velocity Contours Seen Near Turbinates for 500 cc/s

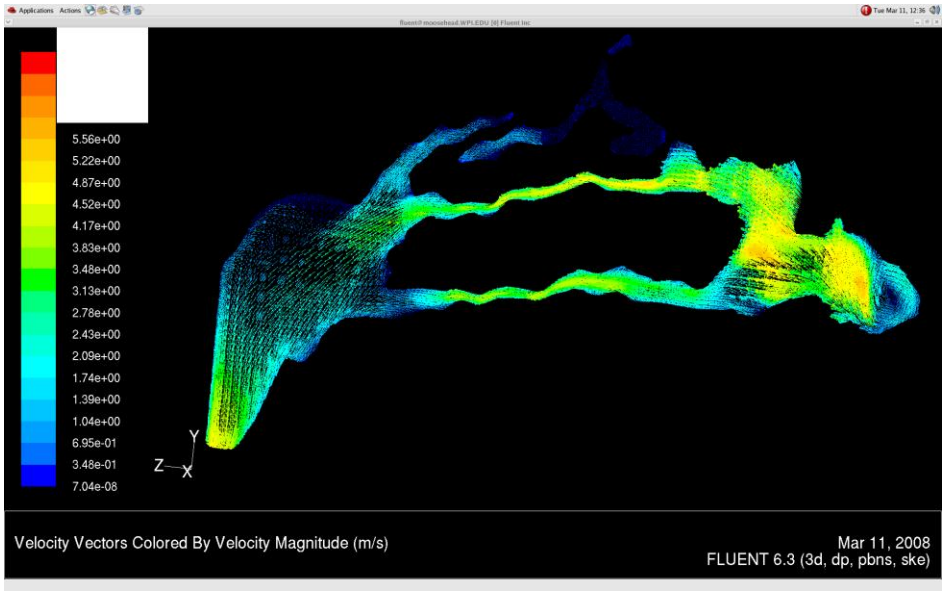

Figure 102: Steady State Velocity Vectors Seen for 500 cc/s

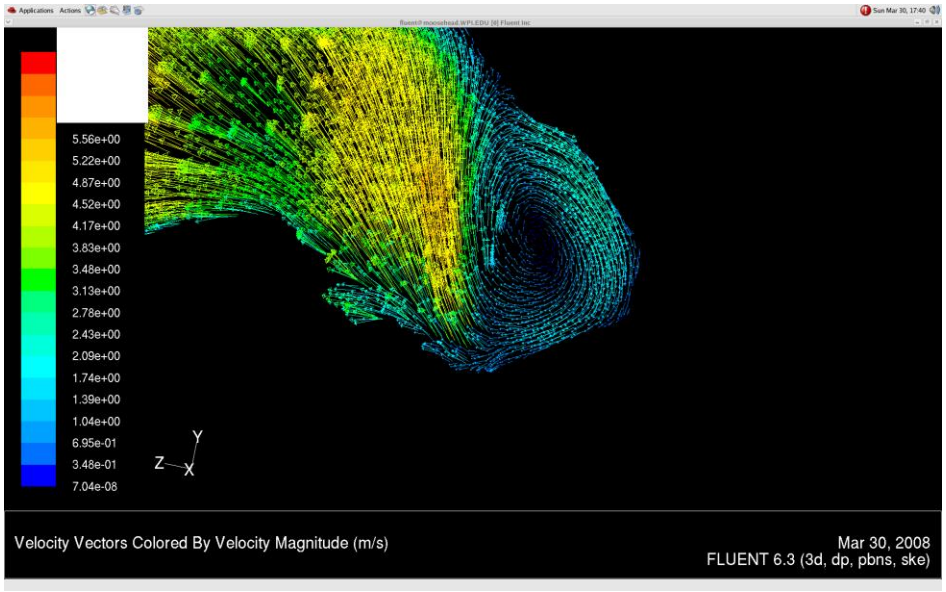

Figure 103: Steady State Vortex Vectors at 500 cc/s

Turbulence:

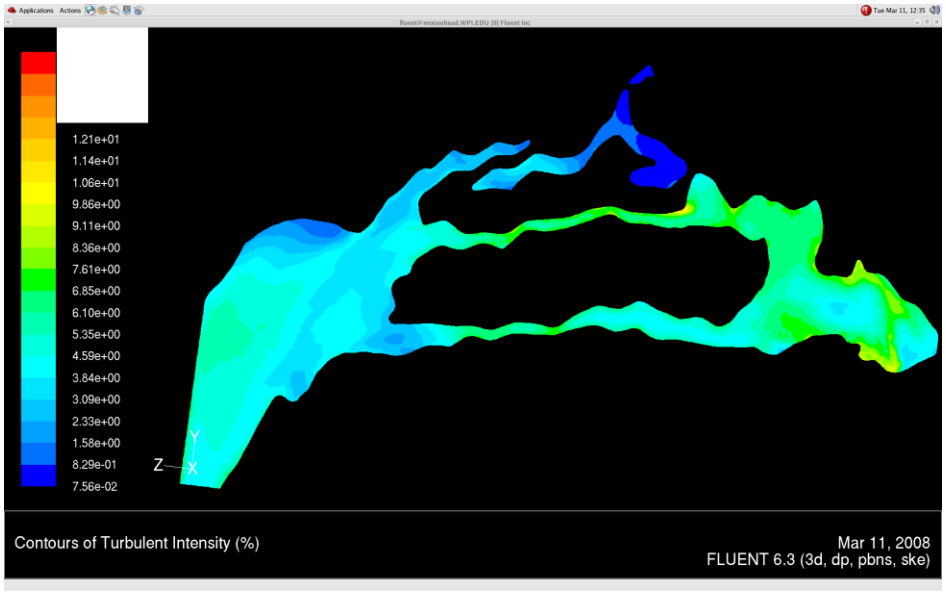

Figure 104: Steady State Turbulent Intensities for 500 cc/s

Flow of 0.13 m/s (Corresponding to time = 2.0 seconds)

Pressure:

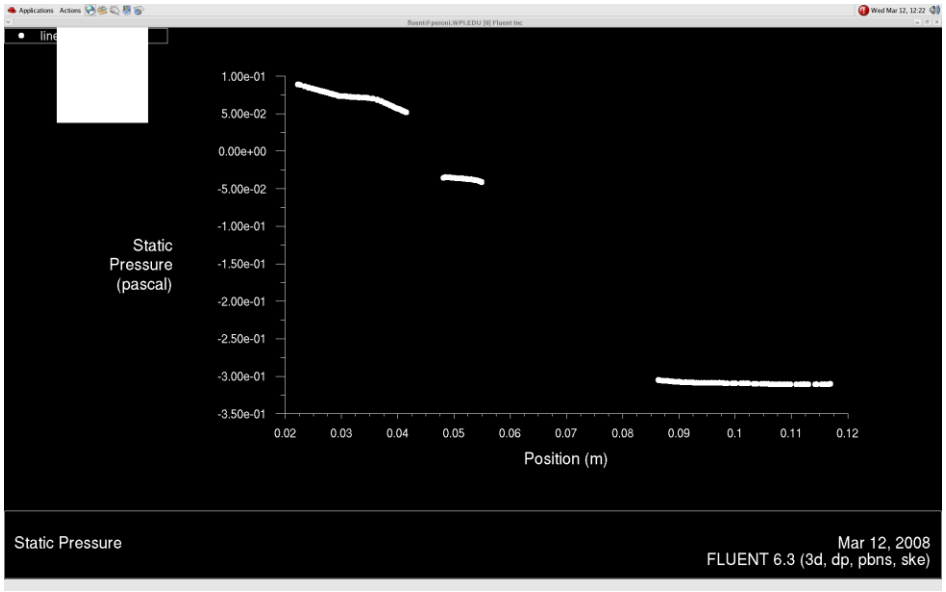

Figure 105: Steady State Pressure Drop from Nostrils to Outlet for 13 cc/s

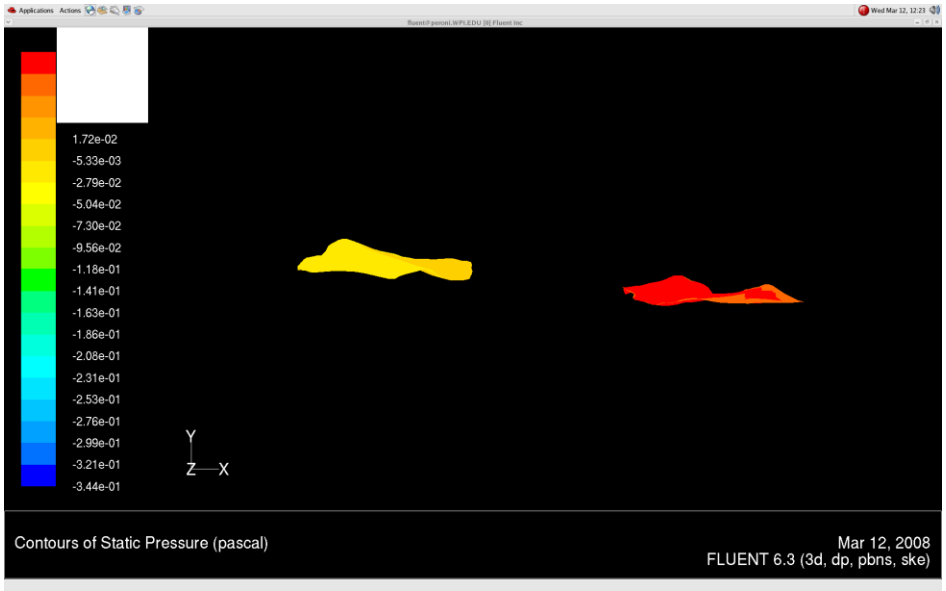

Figure 106: Steady State Pressure Contours Seen Over Nostrils for 13 cc/s

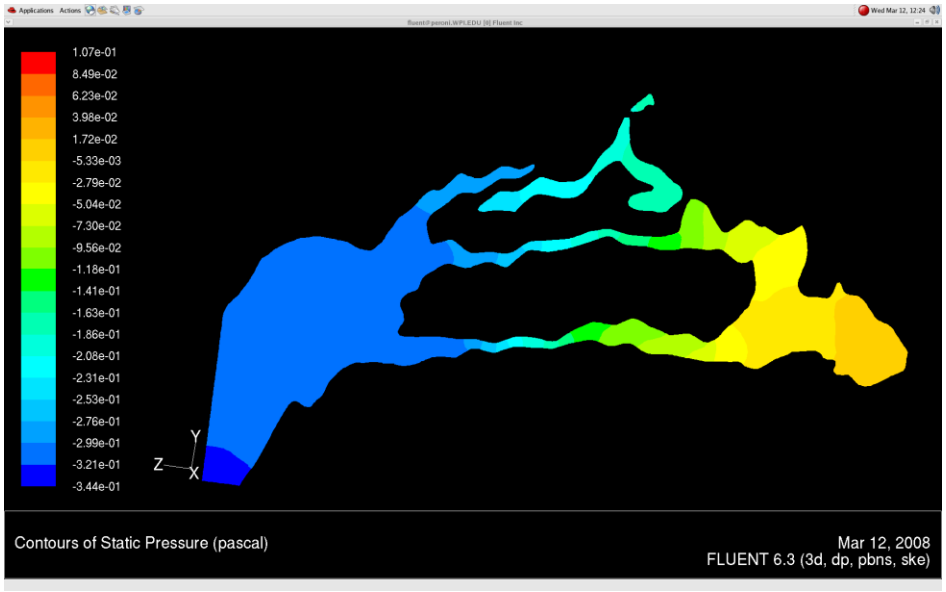

Figure 107: Steady State Pressure Contours Seen for 13 cc/s

Velocity:

Figure 108: Steady State Velocity Contours Seen Near Entry-Region for 13 cc/s

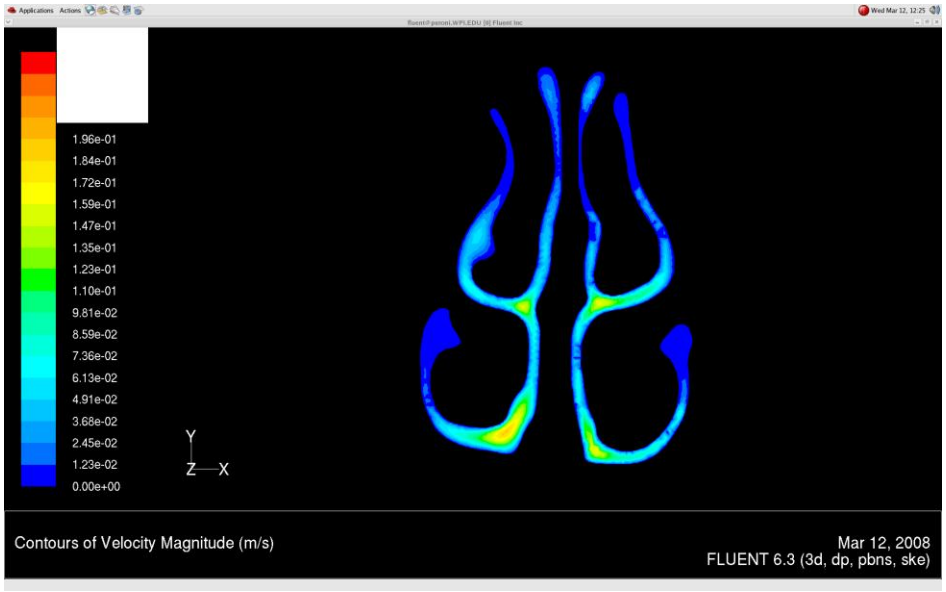

Figure 109: Steady State Velocity Contours Seen Near Turbinate Region for 13 cc/s

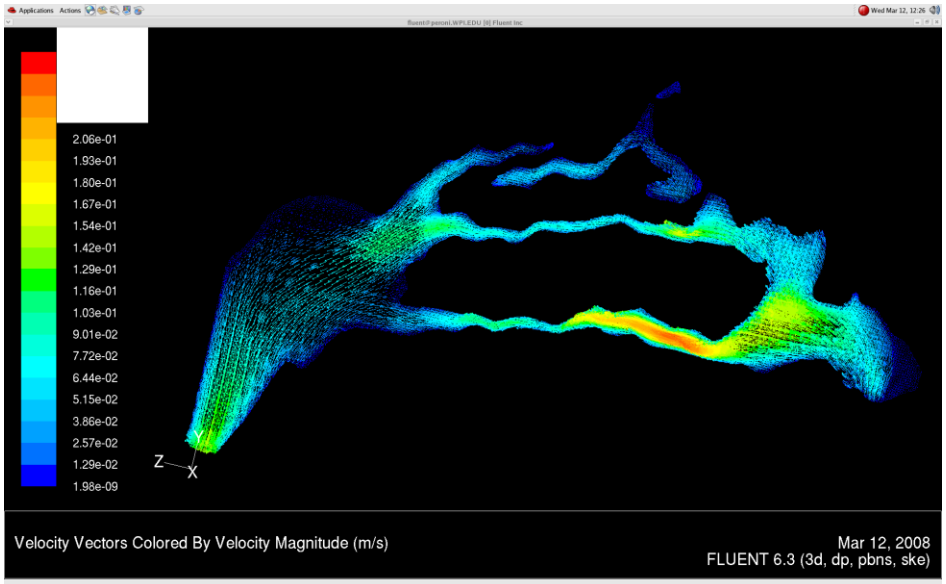

Figure 110: Steady State Velocity Vectors Seen for 13 cc/s

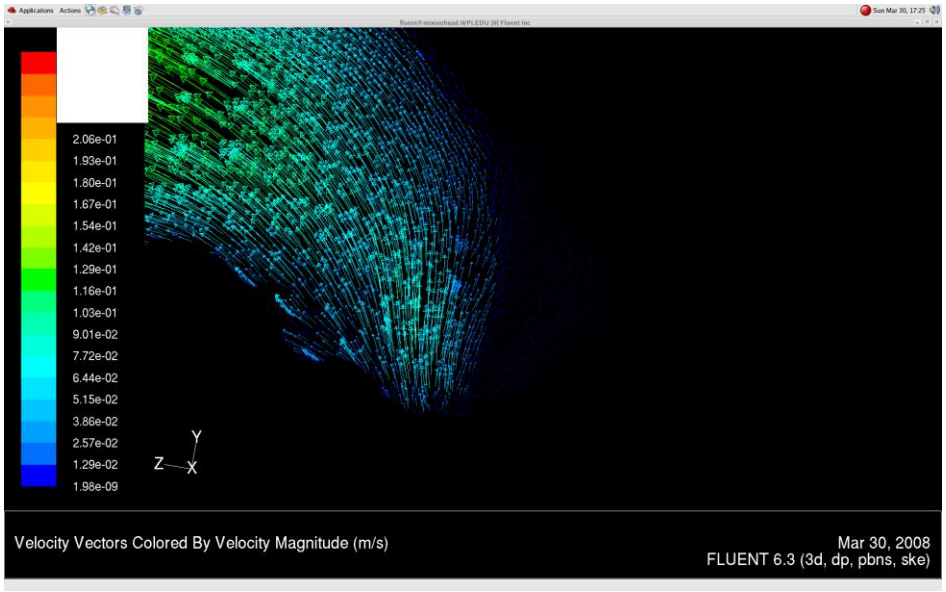

Figure 111: Steady State Vortex Vectors for 13 cc/s

Turbulence:

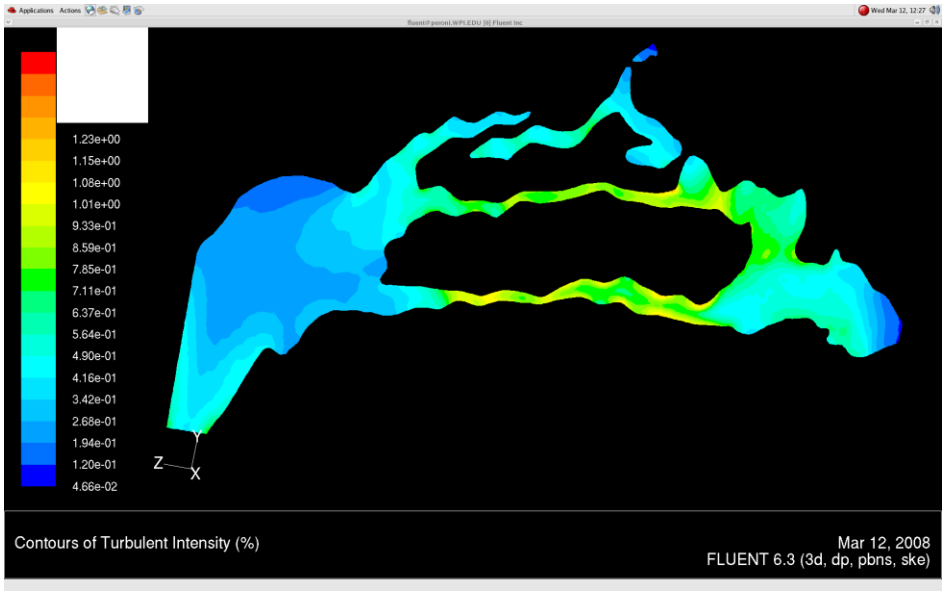

Figure 112: Steady State Turbulent Intensities for 13 cc/s

Flow of -3.7 m/s (Corresponding to time = 3.5 seconds)

Pressure:

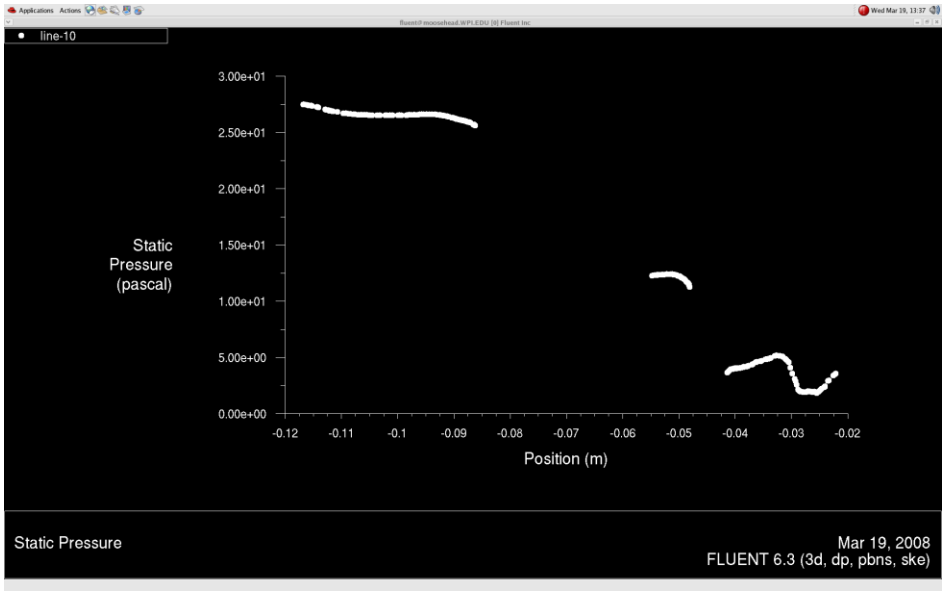

Figure 113: Steady State Pressure Drops Seen from Outlet to Nostrils for -370 cc/s(Expiration)

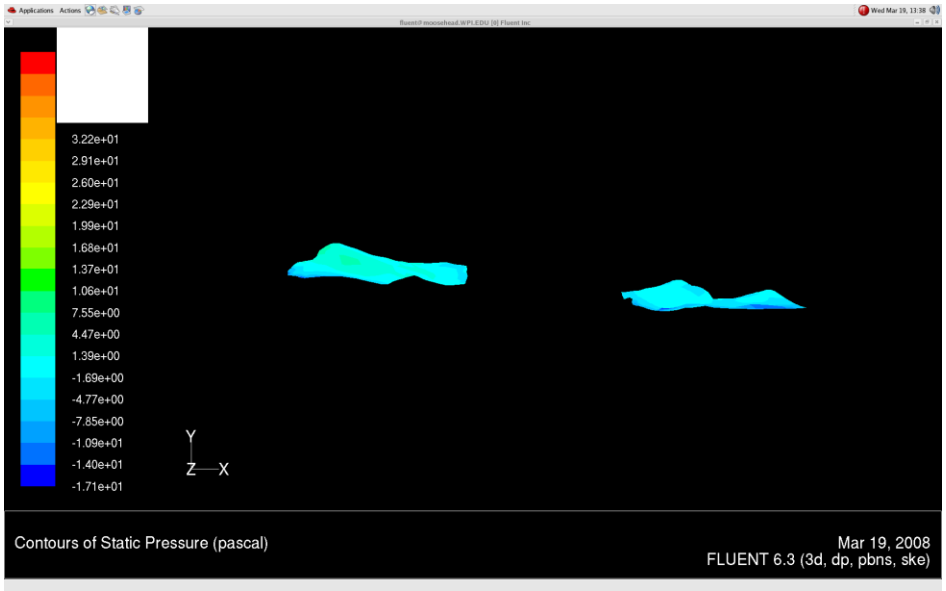

Figure 114: Steady State Pressure Contours over Nostrils for -370 cc/s(Expiration)

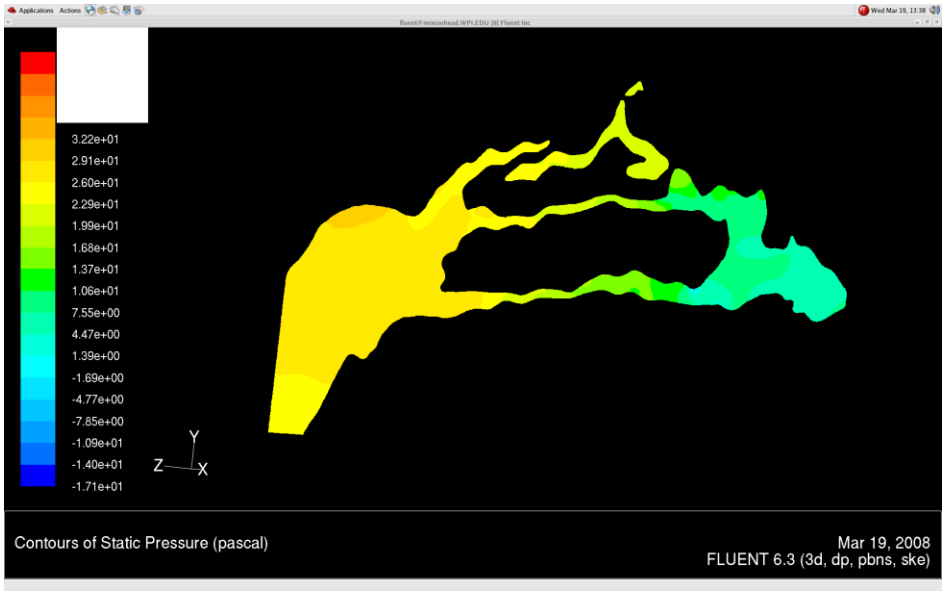

Figure 115: Steady State Pressure Contours for -370 cc/s(Expiration)

Velocity:

Figure 116: Steady State Velocity Contours Seen Near Entry Region for -370 cc/s(Expiration)

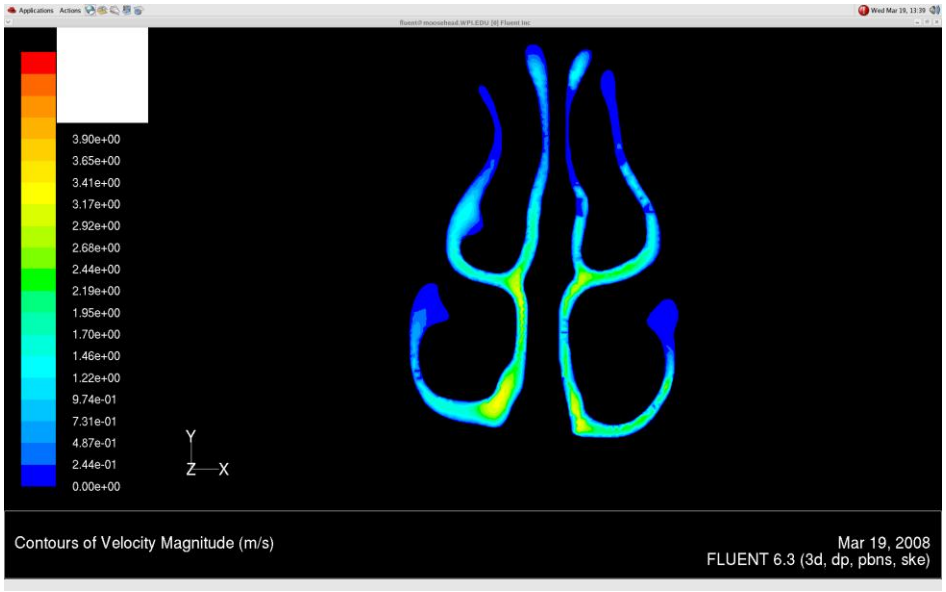

Figure 117: Steady State Velocity Contours Seen Near Turbinate Regions for -370 cc/s(Expiration)

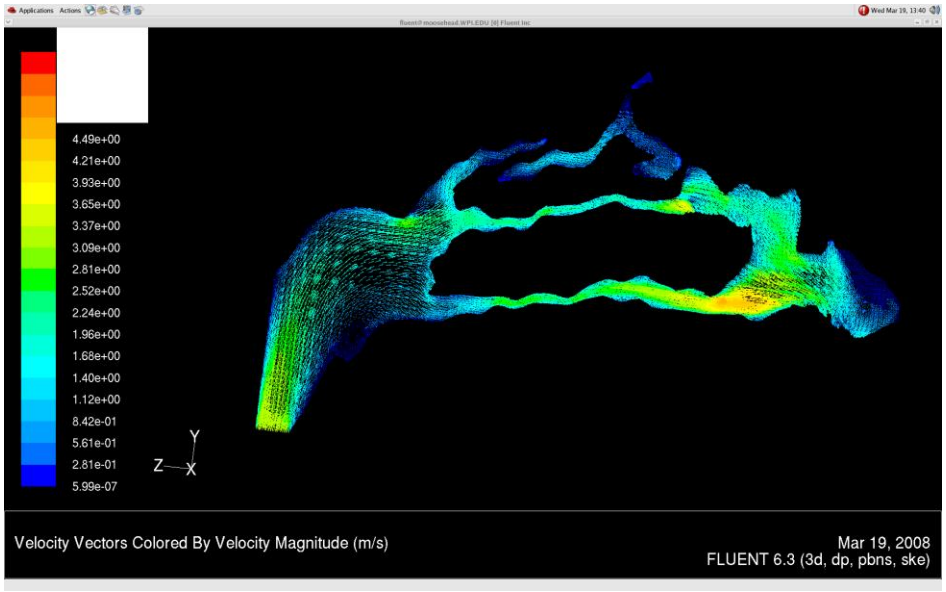

Figure 118: Steady State Velocity Vectors for -370 cc/s (Expiration)

Turbulence:

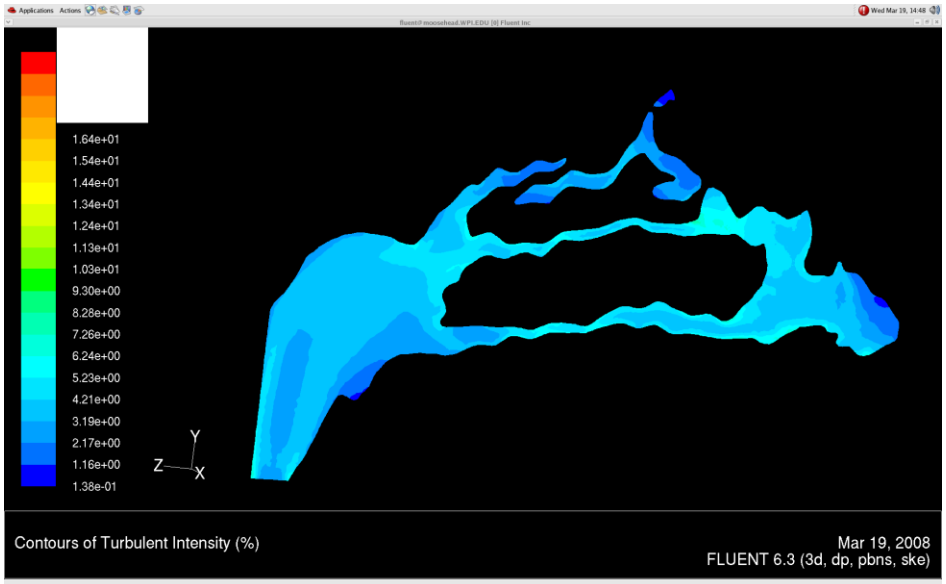

Figure 119: Steady State Turbulent Intensities for -370 cc/s (Expiration)

Chapter 6: Conclusion:

1. Comparison to Experimental Results

The following table describes the pressure drops seen at various flow rates for both the CFD analysis and the experimental simulation run by **Learned et al.**[15] Since the pressure drops derived from CFD were not affected by the time, there was no need to differentiate between steady and unsteady flow in this comparison.

Table 2: Comparison of Pressure Drops Between CFD and Experimental Results

Flow Rate(cc/s)	CFD Pressure drop (Pa)	Experimental Pressure drop (Pa)
13	Less than 0.5 Pa	About a couple hundredths of a Pa
100	3.5	5
270	12	20
500	27	55
370 (Exhale)	25	N/A

According to these data, the Pressure drops found through CFD analysis differ somewhat from those found experimentally. There are several possible reasons why this may be the case. First of all, the experimental procedures use plastinated models, which probably have a different friction factor, which would have an impact on the pressure drop. Secondly, the experimental models rely on a model about 2x as large as the actual model. Even using the scaling equations, the use of a different sized model may have a significant impact on the pressure drop. Finally, the experimental models rely on water rather than air, which can affect the calculated/measured pressure drop even when the scaling method (i.e. keeping the Reynold's numbers the same) are appropriately applied.

In this study, we only observed one exhalation flow, which had a flow rate that was not readily comparable to the results found in the experimental simulation.

2. General Observations Due to Anatomy and Physiology

After analyzing the graphs, contours and vector plots, we were able to affirm that the results found in the literature were consistent with our own findings. These findings include:

- The pressure drop seen over the left nostril is slightly higher than that seen over the right nostril. In the experiment conducted by Zhao and his team, their data suggests that the left nostril always has a higher pressure drop for both inspiratory and expiratory flow. However, it is possible that other experiments may yield different results.
- The flow is not fully developed by the time it reaches the outlet.
- The velocity of the flow is highest midway between the septum and the wall of the nose, where there is the least friction. Flow near either the septum or the wall of the nose is small because of the no-slip condition.
- There is almost no flow through the meatuses. Since the meatuses are made up of a spongy tissue, some air is allowed to pass through them. In the CFD solution, the meatuses are probably defined along with the wall, showing that, which would force the flow passing through them to be zero.
- According to the literature, it is generally expected that there will be a greater flow rate in the inferior turbinate than in the middle airway. However, our results seems to suggest that the percentage of flow passing through the middle and inferior airways depends on the flow rate. At lower flow rates, there seems to be more flow passing through the inferior airway, while at higher flows there seems to be more flow passing through the middle airways. At moderate flow rates, the flow passing through the middle and lower airways is approximately the same. The contours near the turbinate region seem to suggest that the area near the inferior airway is about twice that near the middle airway. At lower flow rates, the velocity of the flow passing through the inferior airway is higher than that in the middle airway, even though the inferior airway appears to have twice the flow area. At these rates, the percentage of flow passing through the inferior airway is about 70%. At medium and high flow rates, the flow passing through the middle airway has a higher velocity, however, since the inferior airway has a larger area, the flow through the inferior airway is about 60%.
- Vortex formation tended to take place in the entrance region, almost immediately after passing through the nostrils. However, during the transition from inspiratory flow to expiratory flow (which takes place 2 seconds into the breathing curve), there is also another vortice near the outlet. The literature indicates that there vortices may appear just before reaching the turbinates. However, there is no CFD evidence of vortices forming anywhere except near the inlet and outlet.

- Turbulence levels are very small (less than 2%) for flow rates of about 100 cc/s. At medium flow rates (250 cc/s), they become more significant (approaching values of up to about 4%). At the highest flow rates (5 cc/s), the turbulence becomes more significant (reaching orders of up to about 6 or 7%).

3. The Role of Turbulence Models

The turbulence models do not seem to make much of a contribution to the results. The only noticeable difference between the laminar and k-epsilon models is that at higher flow rates the laminar models show vortices that are not as organized, and appear to show more of a figure 8 profile than a circular profile. Other than the shape of the vortices, there are no differences between the laminar and k-epsilon models. The pressure drop curves, as well as the pressure contours and velocity vector plots are almost identical between the laminar and k-epsilon models.

4. The Role of Time: Quasi-Steady vs. Unsteady

By comparing the graphs, flow fields and contours of the steady and unsteady models, we noticed that there were no noticeable differences between the two models, except at the time corresponding to the transition between the inspiration and expiration stages of the breathing cycle. This led us to the conclusion that except for this one stage in the breathing cycle, time was not a contributing factor. Therefore, we concluded that for these tidal volumes and breathing rates, the flow was quasi-steady.

Bibliography

- 1. Tannehill, J. C., et al. (1997). *Computational Fluid Mechanics and Heat Transfer.* Levittown, PA: Taylor and Francis.
- 2. Croce, C. (May 5, 2006). In Vitro Experiments and Numerical Simulations of Airflow in Realistic Nasal Airway Geometry. (Volume 34, Number 6 / June, 2006).
- 3. Zhao, Kai. Numerical Modeling of Turbulent and Laminar Airflow and Odorant Transport during Sniffing in the Human and Rat Nose. (February 2006). *Chem Senses*, *31*, 107-118
- 4. Ishikawa, Shigeru. Visualization of Flow Resistance in Physiological Nasal Respiration: Analysis of Velocity and Vorticities Using Numerical Simulation. (November 2006). *Arch Otolaryngol Head Neck Surg*, *132*, 1203-1209
- 5. T, K. J. et. al. (July 2007). Detailed flow patterns in the nasal cavity. *J Appl Physiol*, *89*, 323
- 6. Horschler, I. (August 2006). Investigation of the impact of the geometry on the nose flow. *European Journal of Mechanics, B/Fluids*, *25*(4), 471-490
- 7. Elad, D., et al. (November 1993). Analysis of air flow patterns in the human nose. *Medical & Biological Engineering & Computing*, *31*(6), 585-592
- 8. Zhao, K., et al. (June 2004). Effect of Anatomy on Human Nasal Air Flow and Odorant Transport Patterns: Implications for Olfaction. *Chem Senses*, *29*.
- 9. Davidson, L. (November 2003). An Introduction to Turbulence Models. *Department of Thermo and Fluid Dynamics*
- 10. Kalitzin, G. & Iaccarino, G. (2002). Turbulence modeling in an immersed-boundary. *Center for Turbulence Research*
- 11. Paciorri, R., et al. (2003). VALIDATION OF THE SPALART-ALLMARAS TURBULENCE MODEL FOR. *von Karman Institute for Fluid Dynamics*
- *12. Basic study of Reynolds stress model calculations*. Retrieved 1993, from http://adsabs.harvard.edu/abs/1993JSMET.59.2111Y

- 13. Alpman, E. & Long, L. N. Unstructured Reynolds Stress Model Solutions for Turbulent. *Pennsylvania State University.* Retrieved 2003, from http://www.personal.psu.edu/lnl/papers/ahsAlpmanLong2005.pdf
- 14. Weihold, I. Numerical Simulation of Airflow Through the Human Nose. Eur Arch Otorhinolaryngol. Retrieved 2007.
- 15. Learned, Amanda et al. Alterations in Flow Patterns through Nasal Passages due to a Turbinectomy. Retrieved 2006.